National and Kapodistrian University of Athens
Physics Department - Nuclear and Particle Physics Section

# Amplification and Oscillations in the Curvature Power Spectrum from Features in the Inflaton Potential

**George Kodaxis**

PhD Thesis

Supervisor: Prof. Nikolaos Tetradis


Athens 2023

## Advisory committee

- Alexandros Kehagias – Professor, NTUA
- Vassilios Spanos – Associate Professor, NKUA
- Nikolaos Tetradis (Supervisor) – Professor, NKUA

## PhD thesis examination committee

- Fotios Diakonos – Professor, NKUA
- Georgios Diamandis – Associate Professor, NKUA
- Alexandros Kehagias – Professor, NTUA
- Christoforos Kouvaris – Professor, NTUA
- Konstantinos Sfetsos – Professor, NKUA
- Vassilios Spanos – Associate Professor, NKUA
- Nikolaos Tetradis (Supervisor) – Professor, NKUA

# Περίληψη

Οι κοσμολογικές διαταραχές που γεννιούνται στα τελευταία στάδια του πληθωρισμού και αντιστοιχούν σε μικρές κλίμακες δεν αποτυπώνονται στην κοσμική μικροκυματική ακτινοβολία υποβάθρου, αλλά μπορεί να είναι ιδιαίτερης σημασίας αν το μέγεθός τους είναι μεγάλο. Μια μεγάλη αύξηση του φάσματος των αρχέγονων βαθμωτών διακυμάνσεων μπορεί να πυροδοτήσει τη βαρυτική κατάρρευση και τη δημιουργία αρχέγονων μελανών οπών καθώς και ενός υποβάθρου στοχαστικών βαρυτικών κυμάτων που είναι πιθανόν παρατηρήσιμα από σχεδιασμένα μελλοντικά πειράματα. Ο βασικός στόχος της παρούσας διδακτορικής διατριβής είναι η όσο το δυνατόν πιο γενική και ανεξάρτητη μοντέλου ανάλυση των χαρακτηριστικών του πληθωριστικού δυναμικού που προκαλούν σημαντική ενίσχυση και ταλαντώσεις στο φάσμα διαταραχών καμπυλότητας.

Στο κεφάλαιο 2 γίνεται βιβλιογραφική ανασκόπηση των βασικών στοιχείων της σύγχρονης κοσμολογίας και του πληθωρισμού. Συγκεκριμένα στην ενότητα 2.1 γίνεται αναφορά στη μετρική Friedman-Robertson-Walker (FRW) που περιγράφει ένα ομοιογενές και ισότροπο Σύμπαν καθώς και στις εξισώσεις Friedmann, που διέπουν τη δυναμική του εν λόγω Σύμπαντος. Στην ενότητα 2.2 εισάγουμε την έννοια του πληθωρισμού και περιγράφουμε τη δυναμική που διέπει τα πιο απλά πληθωριστικά πρότυπα, τα οποία περιλαμβάνουν ένα βαθμωτό πεδίο σε ελάχιστη σύζευξη με τη βαρύτητα. Επίσης περιγράφουμε την προσέγγιση αργής κύλισης, η οποία μπορεί να εφαρμοστεί στα περισσότερα υπάρχοντα πληθωριστικά μοντέλα και απλοποιεί σημαντικά τις εξισώσεις κίνησης. Για λόγους πληρότητας, στην ενότητα 2.3 γίνεται και μια σύντομη περιγραφή της περιόδου αναθέρμανσης του Σύμπαντος.

Στο κεφάλαιο 3 γίνεται παρουσίαση της κοσμολογικής θεωρίας διαταραχών και των βασικών εννοιών που χρειάζονται στα ακόλουθα κεφάλαια. Ξεκινάμε με την περιγραφή των διαταραχών της μετρικής (ενότητα 3.1), οι οποίες διακρίνονται σε βαθμωτές, διανυσματικές και τανυστικές διαταραχές. Εστιάζοντας στους βαθμωτούς βαθμούς ελευθερίας, βλέπουμε πώς αυτοί μετασχηματίζονται κάτω από μετασχηματισμούς βαθμίδας (συντεταγμένων) και παραθέτουμε ορισμένες γνωστές βαθμίδες. Στη συνέχεια (ενότητα 3.2) γίνεται ανάλυση των διαταραχών του τανυστή ενέργειας-ορμής χρησιμοποιώντας έννοιες ρευστοδυναμικής και παρουσιάζονται βασικές έννοιες, όπως αυτή των αδιαβατικών και των εντροπικών διαταραχών καθώς, και χρήσιμα μεγέθη όπως η συγκινούμενη διαταραχή καμπυλότητας. Στην ενότητα 3.3 θεωρούμε ότι η κύρια συνεισφορά στην ενέργεια του Σύμπαντος προέρχεται από το πληθωριστικό πεδίο και μελετάμε την εξέλιξη των διακυμάνσεών του, η οποία διέπεται από την εξίσωση Mukhanov-Sasaki. Γίνεται επίσης αναφορά στην κβάντωση του πληθωριστικού πεδίου και στο κενό Bunch-Davies, καθώς και στην έννοια του φάσματος διαταραχών καμπυλότητας που αποτελεί το βασικό υπό μελέτη μέγεθος στην

παρούσα διατριβή.

Στο κεφάλαιο 4, στο οποίο ξεκινά το ερευνητικό κομμάτι της διατριβής, γίνεται μελέτη των χαρακτηριστικών του δυναμικού του πληθωριστικού πεδίου σε πληθωριστικά πρότυπα με ένα πεδίο που μπορούν να οδηγήσουν σε σημαντική ενίσχυση του φάσματος διαταραχών καμπυλότητας. Τα χαρακτηριστικά αυτά είναι τα σημεία καμπής, που έχουν μελετηθεί ευρέως στο παρελθόν, και τα σκαλοπάτια στο δυναμικό, στα οποία δίνουμε μεγαλύτερη έμφαση καθώς δεν έχουν μελετηθεί ιδιαίτερα στο πλαίσιο που μας ενδιαφέρει. Οι εξισώσεις των διακυμάνσεων είναι βολικό να γραφούν χρησιμοποιώντας τον αριθμό των εκθετικών αναδιπλώσεων $N$ ως ανεξάρτητη μεταβλητή, πράγμα που γίνεται στη ενότητα 4.1. Η ποσότητα που είναι καθοριστική για την ενίσχυση των διακυμάνσεων καμπυλότητας είναι ο όρος τριβής $f(N)$ στην εξίσωση (4.20) που ορίζεται από τη σχέση (4.25). Για ένα σκαλοπάτι στο δυναμικό, παρόλο που αυτός ο όρος είναι θετικός κατά τη διάρκεια του πρώτου μέρους της μετάβασης και μειώνει τη διαταραχή, γίνεται αρνητικός καθώς το πεδίο προσεγγίζει τη δεύτερη πεδιάδα αργής κύλισης και επομένως μπορεί να οδηγήσει σε μεγάλη αύξηση, όπως βλέπουμε στην ενότητα 4.2. Παρατηρούμε επίσης ότι η εν λόγω ενίσχυση αυξάνεται όταν το σκαλοπάτι είναι πιο απότομο, καθώς επίσης και όταν αυξάνεται ο αριθμός των σκαλοπατιών στο δυναμικό. Στην περίπτωση των σκαλοπατιών παρατηρείται επίσης και η εμφάνιση ταλαντώσεων στο φάσμα, σε αντίθεση με την περίπτωση των σημείων καμπής, όπου το προκύπτον φάσμα είναι ομαλό. Για την ανάλυση των χαρακτηριστικών που αναφέραμε χρησιμοποιούμε ένα απλοποιημένο δυναμικό (υποενότητα 4.2.1). Στην υποενότητα 4.2.2 δίνουμε βέβαια και ένα συγκεκριμένο παράδειγμα δυναμικού με σκαλοπάτια που είναι συμβατό και με τα παρατηρησιακά δεδομένα.

Το κεφάλαιο 5 είναι αφιερωμένο στον αναλυτικό υπολογισμό του φάσματος διαταραχών καμπυλότητας μέσω δύο διαφορετικών προσεγγιστικών μεθόδων σε περιπτώσεις όπου η προσέγγιση αργής κύλισης παραβιάζεται έντονα, όπως όταν υπάρχουν σκαλοπάτια στο δυναμικό. Στην ενότητα 5.1 προσεγγίζουμε την εξέλιξη της συνάρτησης $f(N)$ μέσω παλμών σταθερού ύψους και χρησιμοποιούμε κατάλληλες συνθήκες συνέχειας στην αρχή και στο τέλος κάθε ¨παλμού' προκειμένου να έχουμε μια πλήρη λύση της (5.1). Μάλιστα, πολλά χαρακτηριστικά που εμφανίζονται στα φάσματα που προκύπτουν από αυτήν τη διαδικασία μπορούν να γίνουν κατανοητά σε ένα πολύ απλούστερο πλαίσιο, όπως βλέπουμε στην υποενότητα 5.1.2, όπου μελετάται η επίδραση ενός ¨παλμού' σε ένα ελεύθερο κύμα αγνοώντας τη διαστολή του Σύμπαντος. Για παράδειγμα στο πλαίσιο αυτό φαίνεται ξεκάθαρα η προέλευση των ταλαντώσεων του πλάτους των διαταραχών καμπυλότητας. Συγκεκριμένα αυτές εμφανίζονται επειδή ο παλμός προκαλεί αλλαγή στη σχετική φάση μεταξύ του πραγματικού και του φανταστικού μέρους. Στις υποενότητες 5.1.3 και 5.1.4 εξάγονται διάφορες χρήσιμες αναλυτικές εκφράσεις οι οποίες προσεγγίζουν ικανοποιητικά τόσο τη μέγιστη α-

ύξηση του φάσματος όσο και τις συχνότητες των εμφανιζόμενων ταλαντώσεων, όπως φαίνεται και στα παραδείγματα των φασμάτων που παρουσιάζονται στην υποενότητα 5.1.5. Επίσης μία ξεκάθαρη προσεγγιστική αναλυτική έκφραση για το φάσμα διαταραχών καμπυλότητας που προκύπτει από ένα σκαλοπάτι στο δυναμικό, η οποία είναι αρκετά αξιόπιστη γύρω από την κορυφή του φάσματος, δίνεται στην υποενότητα 5.1.6, ενώ στην υποενότητα 5.1.7 φαίνεται η ενισχυτική επίδραση πολλαπλών παλμών στο φάσμα.

Στην ενότητα 5.2 εξάγονται αναλυτικές εκφράσεις για το φάσμα διαταραχών καμπυλότητας που προκύπτει αν θεωρήσουμε μια αυθαίρετη συνάρτηση τριβής $f(N)$. Συγκεκριμένα στην υποενότητα 5.2.1 μετατρέπουμε την εξίσωση (5.1) σε μία ολοκληρωτική εξίσωση (5.36) χρησιμοποιώντας συναρτήσεις Green. Μία προσεγγιστική έκφραση, που μπορεί να θεωρηθεί ως ένα πρώτο βήμα για μία επαναληπτική επίλυση αυτής της εξίσωσης είναι η (5.45), η οποία, παρόλο που είναι έγκυρη μόνο για περιπτώσεις όπου δεν έχουμε μεγάλη ενίσχυση του φάσματος, μπορεί να προβλέψει τις προκύπτουσες ταλαντώσεις για τυχαία συνάρτηση $f(N)$. Επίσης στην υποενότητα 5.2.2 μετατρέπουμε την εξίσωση (5.1) σε ένα σύστημα διαφορικών εξισώσεων πρώτης τάξης (εξίσωση (5.51) ) και δίνουμε μια προσεγγιστική λύση του συστήματος (σχέσεις (5.53) και (5.54) ), η οποία δίνει μία καλή προσέγγιση της μέγιστης τιμής του φάσματος και των χαρακτηριστικών συχνοτήτων ακόμα και για περιπτώσεις ενίσχυσης του φάσματος κατά τρεις τάξεις μεγέθους, όπως αναφέρεται στο παράρτημα Α.

Στο κεφάλαιο 6 γίνεται κατασκευή συγκεκριμένων πληθωριστικών προτύπων στο πλαίσιο των $\alpha$-attractors τα οποία περιλαμβάνουν σκαλοπάτια ή και σημεία καμπής στο πληθωριστικό δυναμικό και προβλέπουν τη σημαντική δημιουργία αρχέγονων μελανών οπών και την παραγωγή δευτερογενών βαρυτικών κυμάτων που μπορεί προσεχώς να ανιχνευθούν. Μια εισαγωγή στα μοντέλα των $\alpha$-attractors γίνεται στην ενότητα 6.1 όπου ως αφετηρία χρησιμοποιείται ένα μοντέλο δύο πεδίων που σέβεται ορισμένες συμμετρίες και καταλήγουμε στη Λαγκρανζιανή (6.5), όπου το δυναμικό καθορίζεται από την αυθαίρετη συνάρτηση $F$. Στη συνέχεια (υποενότητα 6.1.1) επιλέγεται συγκεκριμένη μορφή για τη συνάρτηση $F$ ώστε, με κατάλληλη επιλογή των παραμέτρων που περιέχει, το δυναμικό να περιλαμβάνει $n$ σκαλοπάτια ή/και ένα σημείο καμπής. Στην ενότητα 6.2 γίνεται υπολογισμός της αφθονίας των αρχέγονων μελανών οπών που δημιουργούνται στα μοντέλα που αναφέραμε. Βρίσκουμε ότι η αύξηση του φάσματος εξαιτίας της παρουσίας σκαλοπατιών συνήθως δεν είναι επαρκής για την παραγωγή σημαντικού αριθμού μελανών οπών αν το Σύμπαν κυριαρχείται από ακτινοβολία όταν αυτές δημιουργούνται. Ωστόσο μπορεί να είναι επαρκής αν το Σύμπαν κυριαρχείται από μη σχετικιστική ύλη. Για το τελευταίο μάλιστα σενάριο προκύπτει ότι το φάσμα μαζών των μελανών οπών που προκύπτει αποκλίνει κάπως από το συνηθισμένο μονοχρωματικό προφίλ (υποενότητα 6.2.2). Επιπλέον στην ενότητα 6.3 γίνεται η μελέτη του φάσματος των στοχαστικών

βαρυτικών κυμάτων που παράγονται από τα ίδια μοντέλα. Στην υποενότητα 6.3.1 παρατίθενται οι βασικές εξισώσεις που χρειάζονται, ενώ στην υποενότητα 6.3.2 γίνονται οι σχετικοί αριθμητικοί υπολογισμοί. Το βασικό συμπέρασμα που προκύπτει για τα μοντέλα μας είναι ότι το ταλαντωτικό προφίλ στο φάσμα διαταραχών καμπυλότητας κληρονομείται από το φάσμα των βαρυτικών κυμάτων.

Στο κεφάλαιο 7 γίνεται επέκταση της ανάλυσης της ενίσχυσης του φάσματος διαταραχών καμπυλότητας σε πληθωριστικά πρότυπα με δύο πεδία. Στην ενότητα 7.1 συνοψίζονται οι βασικές εξισώσεις που σχετίζονται με τον πληθωρισμό από δύο πεδία, ξεκινώντας από αυτές που περιγράφουν την εξέλιξη του υποβάθρου (υποενότητα 7.1.1). Στη συνέχεια παρατίθενται οι εξισώσεις που διέπουν την εξέλιξη της διαταραχής καμπυλότητας και της εντροπικής διαταραχής και γίνονται ορισμένες απλοποιητικές υποθέσεις προκειμένου να εστιάσουμε στα βασικά χαρακτηριστικά που σχετίζονται με την ενίσχυση του φάσματος (υποενότητα 7.1.2). Διαπιστώνεται ότι η ενίσχυση των διαταραχών καμπυλότητας καθορίζεται από την παράμετρο αργής κύλισης $\eta$, η οποία είναι βολικό να αναλυθεί σε μία παράλληλη και μία κάθετη στην τροχιά των πεδίων συνιστώσα. Η ενίσχυση λοιπόν συμβαίνει όταν κάποια από αυτές τις συνιστώσες παίρνει πολύ μεγάλες τιμές σε σύντομα χρονικά διαστήματα. Η έντονη εξέλιξη της παράλληλης συνιστώσας συνδέεται με την ύπαρξη σκαλοπατιών ή σημείων καμπής στο δυναμικό, των οποίων η ανάλυση δεν αλλάζει όταν έχουμε δύο πεδία. Αντίθετα η κάθετη συνιστώσα του $\eta$ γίνεται πολύ μεγάλη κατά τη διάρκεια απότομων στροφών στο χώρο των πεδίων οι οποίες εξετάζονται στην ενότητα 7.2. Στην υποενότητα 7.2.1 επισημαίνεται ότι για κανονικούς κινητικούς όρους των πεδίων, που είναι η περίπτωση που μελετάμε, η μέγιστη γωνία στροφής είναι $\pi$. Ωστόσο είναι δυνατόν να έχουμε αρκετές διαδοχικές στροφές με αντίθετα πρόσημα, η ενισχυτική επίδραση των οποίων στο φάσμα καμπυλότητας είναι το βασικό σημείο ενδιαφέροντος. Στην υποενότητα 7.2.2 γίνεται προσέγγιση των στροφών μέσω 'παλμών' προκειμένου να υπάρξει κάποια αναλυτική κατανόηση των ποιοτικών χαρακτηριστικών της εξέλιξης, ενώ στο παράρτημα B παρουσιάζεται μια εναλλακτική αντιμετώπιση του προβλήματος με χρήση συναρτήσεων Green. Ο αριθμητικός υπολογισμός ορισμένων φασμάτων που αντιστοιχούν στην περίπτωση των στροφών γίνεται στην υποενότητα 7.2.3, όπου βρίσκουμε ότι τρεις ή τέσσερις στροφές σε κατάλληλη χρονική απόσταση μεταξύ τους μπορούν να προκαλέσουν αύξηση του φάσματος κατά έξι ή εφτά τάξεις μεγέθους. Τέλος στην ενότητα 7.3 γίνονται οι υπολογισμοί που αφορούν στην παραγωγή στοχαστικών βαρυτικών κυμάτων και αρχέγονων μελανών οπών στα σενάρια με στροφές και γίνεται σύγκριση με τα σενάρια των σκαλοπατιών.

Τα συμπεράσματα που εξάγονται από το σύνολο του ερευνητικού μέρους της διατριβής, μερικά από τα οποία ήδη αναφέραμε, παρουσιάζονται στο κεφάλαιο 8, όπου φαίνεται ξεκάθαρα η προοπτική του ελέγχου διαφόρων υποθέσεών μας από μελλοντικές παρατηρήσεις και πειράματα.

## Abstract

In this thesis we study features of the inflaton potential that can lead to a strong enhancement of the power spectrum of curvature perturbations. In single-field inflation, which constitutes the biggest part of this work, we focus on models with steep step-like features in the potential that result in the temporary violation of the slow-roll conditions during the inflaton evolution. These features enhance the power spectrum of the curvature perturbations by several orders of magnitude at certain scales and also produce prominent oscillatory patterns. Our analysis regarding the inflationary dynamics is both analytical and numerical. We describe quantitatively the size of the enhancement, as well as the profile of the oscillations, which are shaped by the number and position of the features in the potential. The models that we use include some simplified potentials, as well as potentials that are constructed within the framework of $\alpha$-attractors in supergravity. We also demonstrate that the induced tensor power spectrum inherits the distinctive oscillatory profile of the curvature spectrum and is potentially detectable by near-future space interferometers. In addition, the enhancement of the power spectrum by several step-like features may trigger the production of a sizeable number of primordial black holes under suitable conditions.

We also extend our work on the enhancement of the curvature spectrum during inflation to the two-field case. Our emphasis here is given on sharp turns in field space, which is a clearly multi-field phenomenon that occurs when the component of the slow-roll parameter $\eta$ perpendicular to the background trajectory grows large. Our focus is mainly on the additive effect of several turns, leading to the resonant growth of the curvature spectrum. Three or four features in the evolution of $\eta_\perp$ are sufficient in order to induce an enhancement of the power spectrum by six or seven orders of magnitude, which can lead to the significant production of primordial black holes and stochastic gravitational waves, in analogy with the case of steps in the potential.

**KEY WORDS:** inflation, curvature perturbations, power spectrum, step-like features, turns in field space, primordial black holes, induced gravitational waves

## Acknowledgements

First and foremost, my sincere gratitude goes to my supervisor Prof. Nikolaos Tetradis, who introduced me to this exciting topic and whose knowledge and insightful feedback were invaluable to my education and brought my work to a higher level. Thanks also to the members of my advisory committee Assoc. Prof. Vassilis Spanos and Prof. Alexandros Kehagias for their useful comments regarding this thesis. Moreover, I would like to thank Dr. Ioannis Daliannis, who helped me understand several aspects of Cosmology with his knowledge. In addition, I would like to express my thanks to Assoc. Prof. Fotios Diakonos and Prof. Athanasios Lahanas for the useful knowledge I obtained during my Bachelor and Master thesis respectively. I also wish to thank Dr. Ioanna Stamou, Kyriaki Kefala, Andreas Tsigkas and Konstantinos Boutivas for our nice collaboration at different time periods during the last three years. Finally, the completion of this thesis would be impossible without the support of my parents.

This thesis was supported by the Hellenic Foundation for Research and Innovation (H.F.R.I.) under the "First Call for H.F.R.I. Research Projects to support Faculty members and Researchers and the procurement of high-cost research equipment grant" (Project Number: 824).

# Contents

# Chapter 1

# Introduction

In the theory of cosmic inflation the cosmological perturbations originate from the quantum fluctuations of the fields that drive inflation [1–4]. The CMB anisotropies and the large-scale structure of the Universe offer us a window to the profile of the spectrum of the primordial perturbations generated in the early stages of inflation [5]. Perturbations generated during the later stages (at small scales) are not imprinted on the CMB sky, but they might be of particular importance if their amplitude is large. A strong enhancement of the spectrum of primordial scalar perturbations can trigger the gravitational collapse and the formation of primordial black holes (PBHs), which may survive until today in significant numbers in order to be detectable [6–9]. This possibility has been studied in great detail during the last years. (For reviews with extensive lists of references, see [10–13].) In addition, a web of strong density perturbations generates a stochastic gravitational wave (GW) background, potentially observable by operating or designed experiments that cover different frequency bands, ranging from nanohertz [14–19] to milihertz and decihertz [20–26], and up to $10^3$ hertz [27, 28]. Thus, the detection prospects of induced GWs open a new window to probe the inflationary dynamics at small scales, for which cosmic microwave background (CMB) observables lack sensitivity.

A primordial scalar spectrum with a strong enhancement can be realized in various setups that may be related to single [29–35] or multi-field inflation [36–45]. Some of these setups include inflationary potentials that contain a near-inflection point [46–63] or a step-like change [64–68], modified gravity [69–74], curvaton models [75–78], sound speed modulation and parametric resonance [79–85]. It is very interesting that the enhancement profiles produced by these inflationary models may be distinguishable. Different inflationary realizations yield power spectra with a wide or narrow peak, oscillations or a multi-peak structure.

In this thesis we focus on power spectra that display, apart from a significant enhancement, oscillatory patterns that are distinctive and possibly detectable, indicating sharp features in the inflaton potential. With the term features we mean characteristics of the potential that lead to strong deviations from the minimal and smooth inflationary evolution. These can have observable consequences, such as distinctive signatures in the power spectra of perturbations, see for example refs. [86–88]. The minimal realization of a sharp feature that involves single-field inflation dynamics and a canonical kinetic term is the presence of a step in the inflaton potential [64–68, 89–95]. In this case it can be shown that oscillations in the amplitude of the spectrum appear due to the fact that the sharp drop in the potential of the inflaton field detunes the relative phase between the real and imaginary parts of the curvature perturbation. It is also important to mention that, even though the strong features in the underlying inflaton evolution may not be simple and the range of generated spectra extensive, an analytical understanding of their form is feasible if a suitable analytical approximation is performed [96–98].

From a particle-physics point of view, it is natural to expect multi-field dynamics during inflation. The phenomenology of interest in multi-field inflation models is related to the fact that the curvature perturbations can evolve even on super-Hubble scales because of the presence of isocurvature perturbations [99–105], called also entropy perturbations or non-adiabatic pressure perturbations [106–109]. In particular inflationary set-ups, the evolution of the curvature perturbations triggered by isocurvature modes can be dramatic, generating an observable GW signal and potentially a significant primordial black hole (PBH) abundance [45, 70, 110, 111]. At the same time, the isocurvature modes can be absent at the CMB scales $\gtrsim 1$ Mpc, where the curvature perturbations are effectively described by single-field results.

When more than one fields are rolling, one can define an adiabatic perturbation component along the direction tangent to the background classical trajectory, and isocurvature perturbation components along the directions orthogonal to the trajectory [104]. Curvature perturbations may be affected by the isocurvature perturbations if the background solution follows a curved trajectory in field space. Models of inflation with curved inflaton trajectories have been studied often in the past [45, 110, 112–129]. When the inflaton slow-rolls along a deep valley while the mass term perpendicular to the trajectory is large, the isocurvature perturbation can be integrated out. This introduces corrections to the effective single-field theory, which can be absorbed in the sound speed for the low-energy perturbations [130–134]. In the particular case of a sharp turn in field space [112–120], the impact of the isocurvature modes is more prominent, with the resulting curvature spectrum departing significantly from scale invariance. An oscillatory pattern

emerges at wavenumbers characteristic of the turn [115, 116]. Also, a significant amplification takes place if during the sharp turn the isocurvature modes experience a transition from heavy to light [45, 110, 128, 135]. For broader turns the amplification is still possible [126, 127], but the oscillatory patterns fade away.

As in the single-field case, when there are two fields that experience strong features in the course of the inflationary evolution, a general and model-independent analysis can be performed by encoding the dynamics behind the strong features in the background evolution in the slow-roll parameters. This becomes apparent if we decompose, along with the perturbations, the second slow-roll parameter into its tangent $\eta_{\parallel}$ and orthogonal $\eta_{\perp}$ components. Sharp steps lead to large positive values of $\eta_{\parallel}$, while sharp turns result in large values of $\eta_{\perp}$, with either sign. This phenomenological description also helps to maintain a geometrical intuition about the field space trajectory. Suggestive constructions that capture the dynamics of the subtle underlying mechanisms that produce these features can be inversely engineered. Particular setups such as those of refs. [97,129,136], just to mention a few, indicate some model building directions.

The thesis is organized as follows: In chapter 2 we present the basic theory of modern cosmology and single-field inflation. In chapter 3 we review the theory of cosmological perturbations providing the basic formulae that are needed in our calculations. In chapter 4 we study the features of the inflaton potential in single-field inflation that result in a significant enhancement of the power spectrum of curvature perturbations by working on simplified setups. In chapter 5 we perform an approximate analytical calculation of the scalar power spectrum in cases that the slow-roll approximation is strongly violated, such as when the inflaton potential features one or more steps. We use two different methods for our calculations. In chapter 6 we construct specific inflationary models within the framework of $\alpha$-attractors that involve step-like features or inflection points in the inflaton potential. For these models we calculate the curvature power spectrum as well as the abundance of the produced PBHs and the power spectrum of the induced GWs. In chapter 7 we present the formalism of two-field inflation and study the case of sharp turns in field space both analytically and numerically. In chapter 8 we present our conclusions. In appendix A we provide an assessment of the accuracy of analytical estimates of the spectrum presented in the main text. Finally, in appendix B we give some detailed expressions resulting from the application of the Green's function method to the two-field system.

# Chapter 2

# Modern Cosmology and Inflation

## 2.1 FRW spacetime and Friedmann equations

Modern cosmology is based on the "cosmological principle", which assumes that the Universe is homogeneous and isotropic on large scales, i.e. it is invariant under spatial translations and rotations. Observational evidence during the last two decades (CMB, large scale structure) confirms the homogeneity and isotropy of the Universe on scales larger than around 100 Mpc.

The most general metric in 4 spacetime dimensions that obeys the cosmological principle is the Friedman-Robertson-Walker (FRW) metric [137, 138]. It takes the form

$$ds^2 = -dt^2 + a^2(t)\left[\frac{dr^2}{1-kr^2} + r^2(d\theta^2 + \sin^2\theta d\phi^2)\right], \tag{2.1}$$

where $a(t)$ is the cosmic scale factor and $k = -1, 0, +1$ corresponds to an open, flat or closed Universe. The above metric is written in terms of comoving coordinates $(r, \theta, \phi)$. The physical distance between two spacetime points with coordinates $(t, 0, \theta, \phi)$ and $(t, r, \theta, \phi)$ is

$$d(r,t) = \int ds = a(t)\int_0^r \frac{dr}{\sqrt{1-kr^2}} = a(t) \times \begin{cases} \sinh^{-1} r, & k = -1 \\ r, & k = 0 \\ \sin^{-1} r, & k = +1 \end{cases}. \tag{2.2}$$

Thus, in a Universe that is not static ($\dot{a} \neq 0$) distances change with time as:

$$\dot{d} = \frac{\dot{a}}{a} d = Hd, \tag{2.3}$$

where $H(t) \equiv \dot{a}/a$ is the Hubble parameter. We know that $\dot{a} > 0$ today, so the Universe is expanding. The relation (2.3) is in accordance with astronomical observations and constitutes the so-called Hubble law. The current value of $H$ is $H_0 = (67.36 \pm 0.54)(\mathrm{km/s})/\mathrm{Mpc}$ [139]. Sometimes it is more convenient to use the conformal time $\tau$ instead of the cosmic time $t$, through the definition $\tau = \int dt/\alpha(t)$.

The dynamics of the Universe is governed by the Einstein's equations

$$G_{\mu\nu} = R_{\mu\nu} - \frac{1}{2} R g_{\mu\nu} = 8\pi G T_{\mu\nu}. \tag{2.4}$$

Here $R_{\mu\nu}$ is the Ricci tensor, given by the relation

$$R_{\mu\nu} = \partial_\alpha \Gamma^\alpha_{\mu\nu} - \partial_\nu \Gamma^\alpha_{\mu\alpha} + \Gamma^\alpha_{\beta\alpha}\Gamma^\beta_{\mu\nu} - \Gamma^\alpha_{\beta\nu}\Gamma^\beta_{\mu\alpha}, \tag{2.5}$$

where $\Gamma^\kappa_{\mu\nu}$ are the Christoffel symbols

$$\Gamma^\kappa_{\mu\nu} \equiv \frac{1}{2} g^{\kappa\lambda} \left[\partial_\mu g_{\lambda\nu} + \partial_\nu g_{\mu\lambda} - \partial_\lambda g_{\mu\nu}\right], \tag{2.6}$$

and $R \equiv g^{\mu\nu} R_{\mu\nu}$ is the Ricci scalar. In the following we will use units such that $M_{\mathrm{Pl}}^2 = (8\pi G)^{-1} = 1$, where $M_{\mathrm{Pl}}$ is the reduced Planck mass ($M_{\mathrm{Pl}} = 2.4 * 10^{18}\mathrm{GeV}$).

Under the assumption of isotropy and homogeneity, and in the perfect-fluid approximation, the energy-momentum tensor $T_{\mu\nu}$ takes the form

$$T^\mu_\nu = (\rho + p) u^\mu u_\nu + p \delta^\mu_\nu, \tag{2.7}$$

where $\rho$ and $p$ are the energy density and pressure in the fluid's rest frame and $u^\mu$ the four-velocity of the fluid. In a frame that is comoving with the fluid, we have $u^\mu = (1, \vec{0})$ and

$$T^\mu_\nu = \begin{pmatrix} -\rho & 0 & 0 & 0 \\ 0 & p & 0 & 0 \\ 0 & 0 & p & 0 \\ 0 & 0 & 0 & p \end{pmatrix}. \tag{2.8}$$

For the metric (2.1) the Einstein's equations give only two independent differential equations, which are called Friedmann equations:

$$H^2 = \left(\frac{\dot{a}}{a}\right)^2 = \frac{1}{3}\rho - \frac{k}{a^2} \tag{2.9}$$

and

$$H^2 + \dot{H} = \frac{\ddot{a}}{a} = -\frac{1}{6}(\rho + 3p). \tag{2.10}$$

Combining the above equations, we can derive the continuity equation

$$\dot{\rho} + 3H(\rho + p) = 0, \tag{2.11}$$

which also results from the conservation of the energy-momentum tensor: $\nabla_\mu T^{\mu\nu} = 0$ ($\nabla_\mu$ is the covariant derivative).

If we define the equation of state $w$ of the fluid as

$$w \equiv \frac{p}{\rho}, \tag{2.12}$$

equation (2.11) can be written as

$$\frac{d\ln\rho}{d\ln a} = -3(1+w), \tag{2.13}$$

from which we have [1]

$$\rho \propto a^{-3(1+w)}. \tag{2.14}$$

From (2.9), ignoring the curvature term, we have

$$a \propto \begin{cases} t^{\frac{2}{3(1+w)}}, & w \neq -1 \\ e^{Ht}, & w = -1 \end{cases}. \tag{2.15}$$

For instance, $a(t) \propto t^{2/3}$, $a(t) \propto t^{1/2}$ and $a(t) \propto e^{Ht}$ for the scale factor in a flat Universe ($k = 0$) that contains non-relativistic matter ($w = 0$), radiation ($w = 1/3$), and a cosmological constant ($w = -1$), respectively.

If more than one constituents contribute to the energy density and pressure, we have:

$$\rho = \sum_i \rho_i, \qquad p = \sum_i p_i. \tag{2.16}$$

For each species "$i$" we define the fraction of its energy density over the critical energy density $\rho_c = 3H^2$ as $\Omega_i = \rho_i/\rho_c$. Then, eq. (2.9) becomes

$$\Omega = \sum_i \Omega_i = 1 + \frac{k}{(aH)^2}. \tag{2.17}$$

From observations (CMB, large-scale structure) we have for the corresponding current values [139]:

$$\Omega - 1 \approx 0, \qquad \Omega_B \approx 0.05, \qquad \Omega_{DM} \approx 0.26, \qquad \Omega_\gamma \approx 8{*}10^{-5}, \qquad \Omega_\Lambda \approx 0.69.$$

[1] The solution (2.14) is valid only when $w$ is constant, which is not always the case (e.g. for an evolving scalar field).

## 2.2 Inflation

Cosmological inflation was introduced in order to solve some fundamental problems that arise in standard Big Bang Cosmology, such as the horizon and the flatness problem [140]. It explains why the observable Universe is so large, flat and homogeneous on large scales. In addition, it provides a framework for understanding the formation of large-scale structure, as well as the spectrum of the temperature fluctuations of the cosmic microwave background (CMB).

Inflation is a period of accelerated expansion which is defined by the following equivalent expressions:

$$\ddot{a} > 0 \Leftrightarrow \rho + 3p < 0 \Leftrightarrow \frac{d}{dt}(aH)^{-1} < 0. \tag{2.18}$$

The accelerated expansion inverts the behavior of the comoving Hubble radius $(aH)^{-1}$, which decreases with time, contrary to the case of a Universe dominated by matter or radiation, for which $(aH)^{-1}$ increases. It is also obvious that inflation requires negative pressure ($w < -1/3$) or a violation of the strong energy condition.

### 2.2.1 Inflation implemented through a scalar field

The simplest models of inflation include a scalar field $\phi$, the inflaton. The dynamics of a scalar field, which is minimally coupled to gravity, is determined by the action

$$\mathcal{S} = \mathcal{S}_{EH} + \mathcal{S}_{\phi} = \int d^4x\sqrt{-g}\left[\frac{R}{2} + \mathcal{L}_{\phi}\right] \tag{2.19}$$

with

$$\mathcal{L}_{\phi} = -\frac{1}{2}g^{\mu\nu}\partial_{\mu}\phi\partial_{\nu}\phi - V(\phi). \tag{2.20}$$

The energy-momentum tensor for the field $\phi$ is

$$T_{\mu\nu} = -\frac{2}{\sqrt{-g}}\frac{\delta\mathcal{S}_{\phi}}{\delta g^{\mu\nu}} = \partial_{\mu}\phi\partial_{\nu}\phi + g_{\mu\nu}\mathcal{L}_{\phi}, \tag{2.21}$$

while the Euler-Lagrange equations give

$$\frac{1}{\sqrt{-g}}\partial_{\mu}(\sqrt{-g}\partial^{\mu}\phi) - V_{,\phi} = 0. \tag{2.22}$$

In the above $V_{,\phi} = dV/d\phi$.

Consistency with the FRW metric (with $k = 0$), which corresponds to a homogeneous and isotropic Universe, implies that the field $\phi$ must satisfy

$\phi(t, \vec{x}) = \phi(t)$. The energy momentum tensor (2.21) takes the form of a perfect fluid (2.8) with

$$\rho = \frac{1}{2}\dot{\phi}^2 + V(\phi) \tag{2.23}$$

and

$$p = \frac{1}{2}\dot{\phi}^2 - V(\phi). \tag{2.24}$$

The equation of state $w$ is

$$w \equiv \frac{p}{\rho} = \frac{\frac{1}{2}\dot{\phi}^2 - V}{\frac{1}{2}\dot{\phi}^2 + V}, \tag{2.25}$$

from which it can be seen that a scalar field can lead to negative pressure ($w < 0$) and accelerated expansion ($w < -\frac{1}{3}$) if the potential term $V$ dominates over the kinetic term.

Finally, for a FRW spacetime equation (2.22) gives

$$\ddot{\phi} + 3H\dot{\phi} + V_{,\phi} = 0 \tag{2.26}$$

and the first Friedmann equation becomes

$$H^2 = \frac{1}{3}\left(\frac{1}{2}\dot{\phi}^2 + V(\phi)\right). \tag{2.27}$$

### 2.2.2 Slow-roll approximation

It is useful to define the Hamilton-Jacobi slow-roll parameters [2]

$$\varepsilon_H \equiv -\frac{\dot{H}}{H^2} = -\frac{d\ln H}{dN} \tag{2.28}$$

$$\eta_H \equiv \varepsilon_H - \frac{1}{2}\frac{d\ln\varepsilon_H}{dN} = \varepsilon_H - \frac{1}{2}\frac{\dot{\varepsilon}_H}{H\varepsilon_H}, \tag{2.29}$$

where $dN \equiv d\ln a = Hdt$ measures the number of efoldings $N$ of inflationary expansion. Cosmic acceleration corresponds to $\varepsilon_H < 1$, while a de Sitter phase with constant $H$ corresponds to $\varepsilon_H = 0$.

In terms of the scalar field, the above parameters are written as

$$\varepsilon_H = \frac{1}{2}\frac{\dot{\phi}^2}{H^2} \tag{2.30}$$

[2] We shall also denote these parameters simply as $\varepsilon$ and $\eta$ in the following. We use here the subscript $H$ so as not to confuse them with the potential slow-roll parameters $\varepsilon_V$ and $\eta_V$.

and

$$\eta_H = -\frac{\ddot{\phi}}{H\dot{\phi}}. \tag{2.31}$$

From (2.30), we see that inflation occurs if the kinetic energy $\frac{1}{2}\dot{\phi}^2$ contributes very little to the total energy $\rho = 3H^2$ or equivalently

$$\dot{\phi}^2 \ll V(\phi). \tag{2.32}$$

In order for inflation to last for a sufficiently long time, the acceleration of the field has to be small, so we assume that

$$|\ddot{\phi}| \ll |3H\dot{\phi}|, |V_{,\phi}|, \tag{2.33}$$

which is equivalent to $|\eta_H| \ll 1$.

We can now use these conditions to simplify the equations of motion, resulting in the slow-roll approximation:

$$3H\dot{\phi} \approx -V_{,\phi} \tag{2.34}$$

and

$$H^2 \approx \frac{V}{3}. \tag{2.35}$$

The slow-roll conditions, $\varepsilon_H, |\eta_H| < 1$, may also be expressed as conditions on the shape of the inflaton potential, through the definition of the potential slow-roll parameters [141]:

$$\varepsilon_V \equiv \frac{1}{2}\left(\frac{V_{,\phi}}{V}\right)^2 \tag{2.36}$$

$$\eta_V \equiv \frac{V_{,\phi\phi}}{V}. \tag{2.37}$$

In the slow-roll regime we have

$$\varepsilon_V, |\eta_V| \ll 1. \tag{2.38}$$

Within the slow-roll approximation, one can easily show that the Hamilton-Jacobi and potential slow-roll parameters are related as follows:

$$\varepsilon_H \approx \varepsilon_V, \quad \eta_H \approx \eta_V - \varepsilon_V. \tag{2.39}$$

Inflation ends when the slow-roll conditions are violated:

$$\varepsilon_H(t_f) \approx 1 \qquad \text{or} \qquad \varepsilon_V(t_f) \approx 1. \tag{2.40}$$

The number of efoldings between the moment $t$ and the end of inflation $t_f$ is

$$N(\phi) \equiv \ln \frac{a_f}{a} = \int_t^{t_f} H dt = \int_\phi^{\phi_f} \frac{H}{\dot{\phi}} d\phi \approx \int_{\phi_f}^{\phi} \frac{V}{V_{,\phi}} d\phi, \tag{2.41}$$

where we have used (2.34) and (2.35). A successful solution to the horizon problem requires that the total number of inflationary efoldings is $N_{\rm tot} \gtrsim 60$, with the precise value depending on the energy scale of inflation and on the details of reheating. The largest scales observed in the CMB are produced $N_* \approx 50 - 60$ efoldings before the end of inflation (the precise value again depends on the details of reheating and the post-inflationary thermal history of the Universe [141, 142]).

## 2.3 Reheating

If inflation was realized, then reheating is an important era in the history of our Universe, as it is the time when the known matter was created. Here, we will make a very brief and mainly qualitative description of the standard mechanism of reheating.

After inflation ends, the scalar field begins to oscillate around the minimum of the potential. If we assume that the potential can be approximated as $V(\phi) = \frac{1}{2}m^2\phi^2$ near its minimum, equation (2.26) becomes

$$\ddot{\phi} + 3H\dot{\phi} = -m^2\phi. \tag{2.42}$$

When the expansion time scale exceeds the oscillation period and we have $H \ll m$, the friction term can be neglected and the field oscillates with frequency $m$. Therefore, we can deduce that the quantity

$$\dot{\rho}_\phi + 3H\rho_\phi = \frac{3}{2}H\left(m^2\phi^2 - \dot{\phi}^2\right) \tag{2.43}$$

averages to zero over one oscillation period, and thus, the field behaves like pressureless matter with $\rho_\phi \propto a^{-3}$.

In order to explain the current composition of the Universe, the inflaton field has to couple to Standard Model fields so that the inflaton energy density is transferred to ordinary particles. If the inflaton can only decay into fermions, the decay is slow and its energy density obeys the equation

$$\dot{\rho}_\phi + 3H\rho_\phi = -\Gamma_\phi\rho_\phi, \tag{2.44}$$

where $\Gamma_\phi$ is the inflaton decay rate, which depends on complicated and model-dependent physical processes. If the inflaton also decays into bosons, the decay may be very rapid and is characterized as preheating.

Finally, the particles produced by the inflaton decay will interact and create other particles. The resulting gas of particles will eventually reach thermal equilibrium with a temperature $T_{\mathrm{rh}}$ that is determined by the energy density at the end of reheating. For more details about the process of reheating (and preheating), we refer the reader to [143].

# Chapter 3

# Cosmological perturbation theory

In the previous chapter, we treated the Universe as perfectly homogeneous. However, in order to understand the structure formation and the observed CMB data, we must introduce inhomogeneities. The creation of inhomogeneities is predicted in the framework of inflation that we have described. It is a result of the quantum nature of the inflaton field, as we describe in this chapter.

## 3.1 Perturbed spacetime

We consider small perturbations around the flat FRW metric $\bar{g}_{\mu\nu}$:

$$g_{\mu\nu} = \bar{g}_{\mu\nu} + \delta g_{\mu\nu}. \tag{3.1}$$

The most general perturbed metric takes the form:

$$ds^2 = a^2(\tau)\left[-(1+2A)d\tau^2 - 2B_i dx^i d\tau + ((1-2D)\delta_{ij} + 2E_{ij})dx^i dx^j\right], \tag{3.2}$$

where $A$, $B_i$, $D$ and $E_{ij}$ are functions of space and time. $A$, $D$ transform as scalars under rotations in the background spacetime, $B_i$ transforms as a 3-d vector, and $E_{ij}$ as a 3-d tensor. However, we can extract two more scalar quantities and one more vector quantity from $B_i$ and $E_{ij}$. This scalar-vector-tensor (SVT) decomposition is performed as follows:

$$B_i = -\partial_i B + \hat{B}_i \tag{3.3}$$

$$E_{ij} = \left(\partial_i\partial_j - \frac{1}{3}\delta_{ij}\nabla^2\right)E - \frac{1}{2}\left(\partial_i\hat{E}_j + \partial_j\hat{E}_i\right) + \hat{E}_{ij}, \tag{3.4}$$

The hatted quantities (vectors and tensors) are divergenceless, i.e. $\partial^i \hat{B}_i = \partial^i \hat{E}_i = \partial^i \hat{E}_{ij} = 0$. The tensor part is also traceless, $\hat{E}^i{}_i = 0$. In this way, the 10 degrees of freedom of the metric have been decomposed into 4 scalar, 4 vector and 2 tensor degrees of freedom.

What makes this division so important is that the scalar, vector, and tensor parts do not couple to each other at first order, but they evolve independently. This enables us to treat them separately. In this thesis, we will mainly focus on scalar fluctuations, which are related to density perturbations and are responsible for the structure formation in the Universe.

It is important to mention that the metric perturbations in eq. (3.2) are not uniquely defined, but they depend on the coordinate system we have chosen, or the so-called gauge choice. A different choice of coordinates leads to the change of the values of the perturbation variables. It can even introduce fictitious perturbations or remove real perturbations in some cases [141].Therefore, we need a way to identify true perturbations.

Let us now consider the following gauge (coordinate) transformation

$$\tilde{x}^\mu = x^\mu + \xi^\mu, \qquad \text{with} \qquad \xi^0 \equiv T, \quad \xi^i \equiv L^i = -\partial^i L + \hat{L}^i, \tag{3.5}$$

where $L$ is a scalar and $\hat{L}^i$ a divergenceless vector. Taking advantage of the fact that $ds^2$ is an invariant quantity, we can find how the metric transforms under this change of coordinates. In particular, for the four scalar degrees of freedom that we are interested in, we end up with the following relations:

$$A \;\rightarrow\; \tilde{A} = A - T' - \mathcal{H}T \tag{3.6}$$

$$B \;\rightarrow\; \tilde{B} = B + T + L' \tag{3.7}$$

$$D \;\rightarrow\; \tilde{D} = D + \mathcal{H}T - \frac{1}{3}\nabla^2 L \tag{3.8}$$

$$E \;\rightarrow\; \tilde{E} = E + L. \tag{3.9}$$

The primes and the Hubble parameter correspond to derivatives with respect to conformal time.

It is also useful to define the curvature perturbation $\psi$ as

$$\psi \equiv D + \frac{1}{3}\nabla^2 E \tag{3.10}$$

Then, the most general scalar metric perturbation can be written in the form [144]

$$ds^2 = a^2(\tau)\left\{-(1+2A)d\tau^2 + 2B_{,i}dx^i d\tau + \left((1-2\psi)\delta_{ij} + 2E_{,ij}\right)dx^i dx^j\right\}, \tag{3.11}$$

with $B_{,i} = \partial_i B$, $E_{,ij} = \partial_i \partial_j E$. Here $\psi$ is used as one of the scalar variables instead of $D$. Under the gauge transformation (3.5) it transforms as

$$\psi \to \tilde{\psi} = \psi + \mathcal{H}T. \tag{3.12}$$

One way to overcome the gauge problem is to create combinations of the metric perturbations that are invariant under gauge transformations. Such scalar combinations are the following:

$$\Phi \equiv A + \mathcal{H}(B - E') + (B - E')' \tag{3.13}$$

$$\Psi \equiv D - \mathcal{H}(B - E') + \frac{1}{3}\nabla^2 E = \psi - \mathcal{H}(B - E'), \tag{3.14}$$

which are called Bardeen potentials. We can regard these variables as the "true" spacetime perturbations, as they cannot be removed by a change of coordinates.

Another way to deal with the gauge problem is to fix the gauge and calculate all metric and matter perturbations in a specific coordinate system. To simplify the problem, we can use the gauge freedom stemming from the arbitrary functions $T$ and $L$ in order to reduce the scalar degrees of freedom by two. Two of the most commonly used gauges are the following:

- **Conformal-Newtonian gauge**: In this case, we use the gauge freedom to set

  $$B = E = 0. \tag{3.15}$$

  It is easy to see that this is achieved if we choose

  $$L = -E \qquad \text{and} \qquad T = -B + E'. \tag{3.16}$$

  Moreover, we can easily see that for this choice of coordinates we have $A = \Phi$ and $D = \psi = \Psi$. Thus, the metric takes the simpler form

  $$ds^2 = a^2(\tau)[-(1 + 2\Phi)d\tau^2 + (1 - 2\Psi)\delta_{ij}dx^i dx^j]. \tag{3.17}$$

- **Spatially-flat gauge**: In this case, we make an appropriate gauge transformation to set

  $$D = E = 0 \qquad \text{or} \qquad \psi = E = 0. \tag{3.18}$$

  This is a convenient gauge for computing the fluctuations of the inflaton field.

There are also several other known gauges, such as the comoving gauge, the uniform energy-density gauge, the synchronous gauge and so on, but we do not need to analyse them in this thesis.

## 3.2 Perturbed matter

As we have mentioned in the previous chapter, the background energy tensor, which corresponds to a homogeneous and isotropic Universe, is assumed to be of the perfect fluid form

$$\bar{T}^{\mu}_{\nu} = (\bar{\rho} + \bar{p})\bar{u}^{\mu}\bar{u}_{\nu} + \bar{p}\delta^{\mu}_{\nu}, \tag{3.19}$$

where $\bar{u}^{\mu} = \frac{1}{a}(1, \vec{0})$, $\bar{u}_{\mu} = a(-1, \vec{0})$ for a comoving observer [1]. The energy tensor of the perturbed Universe can be written as

$$T^{\mu}_{\nu} = \bar{T}^{\mu}_{\nu} + \delta T^{\mu}_{\nu}. \tag{3.20}$$

After a short analysis (see e.g. [141]), we find the following relations for the components of $\delta T^{\mu}_{\nu}$:

$$\begin{aligned}
\delta T^{0}_{0} &= -\delta\rho, && (3.21)\\
\delta T^{0}_{i} &= (\bar{\rho} + \bar{p})(\upsilon_i - B_i), && (3.22)\\
\delta T^{i}_{0} &= -(\bar{\rho} + \bar{p})\upsilon^i, && (3.23)\\
\delta T^{i}_{j} &= \delta p\delta^{i}_{j} + \Pi^{i}_{j}, && (3.24)
\end{aligned}$$

where $\delta\rho$ is the density perturbation, $\delta p$ the pressure perturbation, $\upsilon_i$ the velocity perturbation that is connected to the four-velocity through the relation $\upsilon^i \equiv au^i$, and $\Pi^{i}_{j}$ the anisotropic stress tensor. The tensor $\Pi_{ij}$ is symmetric and traceless, and for a perfect fluid we have $\Pi_{ij} = 0$. If more than one fluids contribute to the energy tensor, we have:

$$\delta\rho = \sum_i \delta\rho_i, \qquad \delta p = \sum_i \delta p_i, \qquad (\bar{\rho} + \bar{p})\vec{\upsilon} = \sum_i (\bar{\rho}_i + \bar{p}_i)\vec{\upsilon}_i \tag{3.25}$$

Just like for the metric perturbations, the SVT decomposition can be applied to the energy-tensor perturbations. $\delta\rho$ and $\delta p$ are purely scalar quantities, $\vec{\upsilon}$ can be divided into scalar and vector parts:

$$\upsilon_i = -\partial_i\upsilon + \hat{\upsilon}_i, \tag{3.26}$$

while $\Pi_{ij}$ can be decomposed into scalar, vector and tensor parts:

$$\Pi_{ij} = \left(\partial_i\partial_j - \frac{1}{3}\delta_{ij}\nabla^2\right)\Pi - \frac{1}{2}\left(\partial_i\hat{\Pi}_j + \partial_j\hat{\Pi}_i\right) + \hat{\Pi}_{ij}. \tag{3.27}$$

[1] Here the factors $1/a$, $a$ are needed in the velocities, because the metric is written in terms of conformal time.

Now, under the gauge transformation (3.5), we can find the following relations for the scalar components that we are interested in:

$$\delta\rho \rightarrow \tilde{\delta\rho} = \delta\rho - T\bar{\rho}', \tag{3.28}$$
$$\delta p \rightarrow \tilde{\delta p} = \delta p - T\bar{p}', \tag{3.29}$$
$$\upsilon \rightarrow \tilde{\upsilon} = \upsilon + L', \tag{3.30}$$
$$\Pi \rightarrow \tilde{\Pi} = \Pi. \tag{3.31}$$

We can see that the anisotropic stress $\Pi_{ij}$ is gauge-invariant (not only its scalar part $\Pi$).

Having written the metric and matter perturbations, one can write the Einstein equations $\delta G^{\mu}_{\nu} = \delta T^{\mu}_{\nu}$ in the general form, after expressing the perturbed Einstein tensor in terms of the metric perturbations. However, we are not going to present these equations here, but we will focus on the specific case that the matter sector consists of a scalar field in the next section.

### 3.2.1 Adiabatic and isocurvature fluctuations

It is useful to define the total entropy perturbation as [145]:

$$\mathcal{S} \equiv \mathcal{H}\left(\frac{\delta p}{\bar{p}'} - \frac{\delta\rho}{\bar{\rho}'}\right) \equiv H\left(\frac{\delta p}{\dot{\bar{p}}} - \frac{\delta\rho}{\dot{\bar{\rho}}}\right), \tag{3.32}$$

which is a gauge invariant quantity. If we also define the speed of sound parameter $c_s^2 \equiv \dot{\bar{p}}/\dot{\bar{\rho}} \equiv \bar{p}'/\bar{\rho}'$ and use the continuity equation, we can write the above equation in the form

$$\mathcal{S} = \frac{1}{3(1+w)}\left(\frac{\delta\rho}{\bar{\rho}} - \frac{1}{c_s^2}\frac{\delta p}{\bar{\rho}}\right). \tag{3.33}$$

Perturbations for which

$$\mathcal{S} = 0 \Leftrightarrow \delta p = c_s^2 \delta\rho, \tag{3.34}$$

are called adiabatic perturbations. On the other hand, isocurvature perturbations violate the adiabaticity condition and are the complement of adiabatic perturbations. If more than one fluids are present in the Universe, adiabatic fluctuations correspond to a change in the total energy density or pressure, whereas isocurvature fluctuations correspond to perturbations between different components [141]. Single-field inflation produces purely adiabatic primordial perturbations. In multi-field inflationary models, the field fluctuations that are tangent to the background inflaton trajectory are adiabatic, while those that are perpendicular to this trajectory can be characterized as isocurvature, as we shall see later.

### 3.2.2 Comoving Curvature Perturbation

An important gauge-invariant quantity that is constructed by both metric and matter perturbations is the comoving curvature perturbation. It is defined as

$$\mathcal{R} = -\psi - \mathcal{H}(v - B). \tag{3.35}$$

It is easy to see that in the comoving gauge, where we choose $B = v = 0$, this quantity is analogous to the curvature perturbation $\psi$ that is directly related to the spatial curvature of the Universe. It can also be shown that the comoving curvature perturbation is conserved on super-Hubble scales ($k \ll \mathcal{H}$) for adiabatic fluctuations [141, 145]. This means that $\mathcal{R}$ does not change with time outside the horizon.

## 3.3 Inflaton fluctuations and their evolution

During inflation the main contribution to the energy tensor comes from the inflaton field, which governs the dynamics of the Universe, as we saw in the previous chapter. As we have done for all the other quantities, we divide the inflaton into a background and a perturbation part:

$$\phi(\tau, \vec{x}) = \bar{\phi}(\tau) + \delta\phi(\tau, \vec{x}). \tag{3.36}$$

Using the metric (3.11), which includes only the scalar parts of the perturbations, we can easily find that the perturbation of the energy-momentum tensor for the field $\phi$

$$T^{\mu}_{\nu} = \partial^{\mu}\phi\partial_{\nu}\phi - \delta^{\mu}_{\nu}\left(\frac{1}{2}g^{\rho\sigma}\partial_{\rho}\phi\partial_{\sigma}\phi + V(\phi)\right), \tag{3.37}$$

has the following components:

$$\begin{aligned}
\delta T^0_0 &= -a^{-2}\left(\bar{\phi}'\delta\phi' - A\bar{\phi}'^2\right) - V_{,\phi}\delta\phi = -\delta\rho, && (3.38)\\
\delta T^0_i &= -a^{-2}\bar{\phi}'\partial_i(\delta\phi), && (3.39)\\
\delta T^i_0 &= a^{-2}\left[\bar{\phi}'\partial^i(\delta\phi) + \bar{\phi}'^2\partial^i B\right], && (3.40)\\
\delta T^i_j &= \delta^i_j\left[a^{-2}\left(\bar{\phi}'\delta\phi' - \bar{\phi}'^2 A\right) - V_{,\phi}\delta\phi\right] = \delta^i_j\delta p. && (3.41)
\end{aligned}$$

We see that scalar fields do not have anisotropic stress. Moreover, using the above form of the energy tensor, we find that, under a gauge transformation (3.5), the field perturbation changes as

$$\delta\phi \to \tilde{\delta\phi} = \delta\phi - T\bar{\phi}'. \tag{3.42}$$

The expansion of the Einstein equations $\delta G^{\mu}_{\nu} = \delta T^{\mu}_{\nu}$ to first order in perturbations for the case of a scalar field is straightforward. The calculation results in three independent equations, which we gather here:

$$3\mathcal{H}(\mathcal{H}A + D') - \nabla^2(\psi + \mathcal{H}B) = -\frac{1}{2}\left[\bar{\phi}'\delta\phi' - A\bar{\phi}'^2 + a^2 V_{,\phi}\delta\phi\right], \quad (3.43)$$

$$\psi' + \mathcal{H}A + (-\mathcal{H}' + \mathcal{H}^2)B = \frac{1}{2}(\bar{\phi}'\delta\phi + \bar{\phi}'^2 B), \quad (3.44)$$

$$(2\mathcal{H}' + \mathcal{H}^2)A + \mathcal{H}A' + \psi'' + 2\mathcal{H}\psi' = \frac{1}{2}\left[(\bar{\phi}'\delta\phi' - \bar{\phi}'^2 A) - a^2 V_{,\phi}\delta\phi\right]. \quad (3.45)$$

The equation of motion for the field $\phi$ (see the previous chapter) gives the well-known background (Klein-Gordon) equation:

$$\bar{\phi}'' + 2\mathcal{H}\bar{\phi}' = -a^2 V_{,\phi} \quad (3.46)$$

and the field perturbation equation

$$\delta\phi'' + 2\mathcal{H}\delta\phi' - \nabla^2\delta\phi + a^2 V_{,\phi\phi}\delta\phi = -2a^2 A V_{,\phi} + (A' + 3D' + \nabla^2 B)\bar{\phi}'. \quad (3.47)$$

Now we would like to use the Einstein equations in order to eliminate the metric perturbations from eq. (3.47) and obtain a differential equation that contains only the inflaton perturbation. To achieve this, it is more convenient to go to the spatially flat gauge where $\psi = 0$. In this way, we end up with the following equation:

$$Q'' + 2\mathcal{H}Q' - \nabla^2 Q + \left[a^2 V_{,\phi\phi} - \frac{1}{a^2}\left(\frac{a^2}{\mathcal{H}}\bar{\phi}'^2\right)'\right] Q = 0, \quad (3.48)$$

where $Q \equiv \left(\delta\phi + \frac{\bar{\phi}'}{\mathcal{H}}\psi\right)$ is the so-called Sasaki or Mukhanov variable that in the spatially flat gauge is simply $Q = \delta\phi$. It can be easily checked that the quantity $Q$ is gauge invariant. Equation (3.48) is in fact the Mukhanov-Sasaki equation, which is better known in its equivalent form [146, 147]

$$v'' - \nabla^2 v - \frac{z''}{z}v = 0, \quad (3.49)$$

where[2] $v \equiv aQ$ and $z \equiv a\bar{\phi}'/\mathcal{H}$.

[2]It is apparent that this quantity is different from the velocity perturbation $v$, although we have used the same symbol.

### 3.3.1 Quantization and initial conditions

Equation (3.49) can also arise from the variation of the second order action

$$\mathcal{S}_{(2)} = \frac{1}{2}\int d^4x \left[(v')^2 - (\partial_i v)^2 + \frac{z''}{z}v^2\right]. \tag{3.50}$$

Now we can easily perform the quantization of the field $v$. We promote the field $v$ and its conjugate momentum $\pi = v'$ to quantum operators so that

$$[\hat{v}(\tau,\vec{x}),\hat{\pi}(\tau,\vec{x}')] = i\delta(\vec{x}-\vec{x}'). \tag{3.51}$$

Performing a Fourier expansion of the field $v$, we have

$$\hat{v}(\tau,\vec{x}) = \int \frac{d^3k}{(2\pi)^{3/2}}\hat{v}_{\vec{k}}(\tau)e^{i\vec{k}\cdot\vec{x}}, \tag{3.52}$$

where the Fourier components $\hat{v}_{\vec{k}}$ can be expressed in terms of annihilation and creation operators ($\hat{a}_{\vec{k}}$ and $\hat{a}^\dagger_{\vec{k}}$) as follows:

$$\hat{v}_{\vec{k}}(\tau) = v_k(\tau)\hat{a}_{\vec{k}} + v_k^*(\tau)\hat{a}^\dagger_{\vec{k}}. \tag{3.53}$$

The mode functions $v_k(\tau)$, $v_k^*(\tau)$ satisfy the Mukhanov-Sasaki equation (3.49) (if we write it in Fourier space). If they are suitably normalized, we can have the well-known canonical commutation relations

$$[\hat{a}_{\vec{k}},\hat{a}^\dagger_{\vec{k}'}] = \delta(\vec{k}+\vec{k}'). \tag{3.54}$$

The vacuum of the theory is defined via

$$\hat{a}_{\vec{k}}|0\rangle = 0. \tag{3.55}$$

However, in order to specify precisely the vacuum state, we need to choose appropriate initial conditions for the mode function. We know that at the beginning of inflation ($\tau \to -\infty$) all modes of interest were deep inside the horizon, i.e. $k \gg \mathcal{H}$. In this limit, it can be seen that the Mukhanov-Sasaki equation reduces to

$$v_k'' + k^2 v_k \approx 0, \tag{3.56}$$

whose two independent solutions are $\sim e^{\pm ik\tau}$. Nevertheless, only the positive frequency mode corresponds to the minimal energy state [141]. Thus, we must choose the initial condition

$$\lim_{\tau\to-\infty} v_k(\tau) = \frac{1}{\sqrt{2k}}e^{-ik\tau}, \tag{3.57}$$

which defines the so-called Bunch-Davies vacuum.

If we consider the de-Sitter limit ($H$ = const.), which is a good first approximation in order to describe slow-roll inflation, we have $z''/z = a''/a = 2/\tau^2$. In this case, the solution of the Mukhanov-Sasaki equation that obeys the initial condition (3.57) turns out to be

$$v_k(\tau) = \frac{1}{\sqrt{2k}} e^{-ik\tau} \left(1 - \frac{i}{k\tau}\right). \tag{3.58}$$

### 3.3.2 Power spectrum

It is straightforward to show that the variance of the inflaton fluctuations (the variance of the field operator $\hat{v}(\tau, \vec{x})$) is

$$\langle |\hat{v}|^2 \rangle = \langle 0|\hat{v}^\dagger(\tau, \vec{0})\hat{v}(\tau, \vec{0})|0\rangle = \int d\ln k \frac{k^3}{2\pi^2} |v_k(\tau)|^2. \tag{3.59}$$

We define the power spectrum of $v$ as

$$\Delta_v^2 \equiv \frac{k^3}{2\pi^2} |v_k(\tau)|^2. \tag{3.60}$$

After horizon crossing, it is convenient to switch from the inflaton fluctuation $v$ to the comoving curvature perturbation $\mathcal{R}$, which stays constant outside the horizon. Using the relation (3.35), it is easy to show that the gauge invariant quantities $v$ and $\mathcal{R}$ are related via

$$\mathcal{R} = -\frac{v}{z}. \tag{3.61}$$

Thus, the power spectrum of $\mathcal{R}$ is given by

$$\Delta_{\mathcal{R}}^2 = \frac{1}{z^2} \Delta_v^2. \tag{3.62}$$

If $\Delta_{\mathcal{R}}^2$ is $k$-independent, the spectrum is called scale-invariant. An important quantity that specifies the deviation from scale-invariance is the scalar spectral index $n_s$, which is defined by

$$n_s - 1 \equiv \frac{d\ln \Delta_{\mathcal{R}}^2}{d\ln k}, \tag{3.63}$$

where $n_s = 1$ corresponds to exact scale invariance. For slow-roll inflation, $n_s$ can be approximated as [142]

$$n_s - 1 \approx -6\varepsilon_V + 2\eta_V. \tag{3.64}$$

The power spectrum around a reference scale $k_*$ can therefore be approximated through the power law form

$$\Delta^2_{\mathcal{R}}(k) = A_s \left(\frac{k}{k_*}\right)^{n_s - 1}, \tag{3.65}$$

where $A_s$ is the amplitude of the scalar spectrum. For the pivot scale $k_* = 0.05\,\mathrm{Mpc}^{-1}$, the measured values for $A_s$ and $n_s$ are [139]

$$A_s = (2.101^{+0.031}_{-0.034}) \times 10^{-9} \tag{3.66}$$

$$n_s = 0.9649 \pm 0.0042. \tag{3.67}$$

Finally, another quantity whose calculation is important in order to check the viability of an inflationary model is the tensor-to-scalar ratio $r$, defined as

$$r \equiv \frac{A_t}{A_s}, \tag{3.68}$$

where $A_t$ is the amplitude of the tensor power spectrum (see e.g. [141]). When the slow-roll approximation applies, $r$ can be approximately calculated as

$$r \approx 16\varepsilon_V. \tag{3.69}$$

Observational constraints for $r$ refer to its upper bound. The most restrictive constraint that can be found in [139] is

$$r < 0.058. \tag{3.70}$$

# Chapter 4

# Steps and inflection points

Having presented the basic theory of inflation and cosmological perturbations, we can now study in more depth the power spectrum of curvature perturbations and the features of the potential in single-field inflation that have a significant impact on it. This chapter is essentially based on [148].

## 4.1 Dynamics in terms of the number of efoldings

In this section we collect the dynamical equations that are needed for the study of the curvature perturbations and their spectrum.

We recall that the most general scalar metric perturbation around the Friedmann-Robertson-Walker (FRW) background takes the form [144]

$$ds^2 = a^2(\tau)\left\{-(1+2A)d\tau^2 + 2B_{,i}\,dx^i d\tau + ((1-2\psi)\delta_{ij} + 2E_{,ij})\,dx^i dx^j\right\}, \tag{4.1}$$

with $B_{,i} = \partial_i B$, $E_{,ij} = \partial_i\partial_j E$. As we have mentioned in the previous chapter, on this background one can parametrize the inflaton field as $\varphi(\tau) + \delta\varphi(\tau, x)$[1] and define a gauge-invariant perturbation as

$$v = a\left(\delta\varphi + \frac{\varphi'}{\mathcal{H}}\psi\right), \tag{4.2}$$

which satisfies the Mukhanov-Sasaki equation [146, 147]

$$v'' - \nabla^2 v - \frac{z''}{z}\,v = 0, \tag{4.3}$$

[1] From now on, we omit overbars in background quantities and we often use the symbol $\varphi$ instead of $\phi$ for the inflaton.

with $z = a\varphi'/\mathcal{H}$. The Fourier modes of $v$ satisfy

$$v_k''(\tau) + \left(k^2 - \frac{z''}{z}\right) v_k(\tau) = 0. \tag{4.4}$$

The standard assumption, which we adopt, is that at early times the field is in the Bunch-Davies vacuum. The strong features of the potential have not become relevant yet, so that the background field is in the slow-roll regime. All the modes that are phenomenologically interesting today were deeply subhorizon at such early times. They are described by the standard expression $v_k = e^{-ik\tau}/\sqrt{2k}$, which we use in order to set the initial conditions for their subsequent evolution. The spectrum of perturbations becomes more transparent through the use of the gauge-invariant comoving curvature perturbation $R = -v/z$ [2], which satisfies

$$R_k'' + 2\frac{z'}{z}R_k' + k^2 R_k = 0 \tag{4.5}$$

in Fourier space.

As we are mainly interested in the amplitude of the complex variables $v$ and $R$, we introduce polar coordinates, such that $v_k(\tau) = \mathcal{V}_k(\tau)\exp(-i\theta_k(\tau))$, with $\mathcal{V}_k$ and $\theta_k$ real. From eq. (4.4) we obtain

$$\mathcal{V}_k'' + \left(k^2 - \frac{z''}{z} - \theta_k'^2\right)\mathcal{V}_k = 0 \tag{4.6}$$

$$\frac{\theta_k''}{\theta_k'} + 2\frac{\mathcal{V}_k'}{\mathcal{V}_k} = 0. \tag{4.7}$$

The second equation can be integrated, with the solution $\theta_k'\,\mathcal{V}_k^2 = \text{constant}$. At early times we have $\mathcal{V}_k = 1/\sqrt{2k}$ and $\theta_k = k\tau$. This fixes the constant of integration to $1/2$, so that we can set

$$\theta_k' = \frac{1}{2\mathcal{V}_k^2} \tag{4.8}$$

in eq. (4.6). In this way we obtain

$$\mathcal{V}_k'' + \left(k^2 - \frac{z''}{z} - \frac{1}{4\mathcal{V}_k^4}\right)\mathcal{V}_k = 0, \tag{4.9}$$

[2] In this and the following chapter we symbolise the comoving curvature perturbation with $R$ and its amplitude with $\mathcal{R}$.

which must be solved with initial conditions $\mathcal{V}_k \to 1/\sqrt{2k}$, $\mathcal{V}_k' \to 0$, for $\tau \to -\infty$. The curvature perturbation is parametrized as $R_k(\tau) = -\mathcal{R}_k(\tau)\exp(-i\theta_k(\tau))$, with $\mathcal{R}_k = \mathcal{V}_k/z$. Its amplitude satisfies

$$\mathcal{R}_k'' + 2\frac{z'}{z}\mathcal{R}_k' + \left(k^2 - \frac{1}{4z^4\mathcal{R}_k^4}\right)\mathcal{R}_k = 0. \tag{4.10}$$

It is convenient for the numerical analysis to use the number of efoldings $N$ as the independent variable for the evolution of the perturbations. Then the Hubble parameter and the Hamilton-Jacobi slow-roll parameters are given by the relations

$$H^2 = \frac{V(\varphi)}{3 - \frac{1}{2}\varphi_{,N}^2} \tag{4.11}$$

$$\varepsilon_H = -\frac{d\ln H}{dN} = \frac{\varphi_{,N}^2}{2} \tag{4.12}$$

$$\eta_H = \varepsilon_H - \frac{1}{2}\frac{d\ln\varepsilon_H}{dN} = \frac{\varphi_{,N}^2}{2} - \frac{\varphi_{,NN}}{\varphi_{,N}}, \tag{4.13}$$

where subscripts denote derivatives with respect to $N$. The parameter $z$ is given by

$$z = e^N\,\varphi_{,N}, \tag{4.14}$$

while the effective equation of state for the background is $w = -1 + 2\varepsilon_H/3$.

The evolution of the background field is governed by the equation

$$\varphi_{,NN} + 3\varphi_{,N} - \frac{1}{2}\varphi_{,N}^3 + \left(3 - \frac{1}{2}\varphi_{,N}^2\right)\frac{V_{,\varphi}}{V} = 0, \tag{4.15}$$

with $V(\varphi)$ the inflaton potential. The inflaton fluctuation obeys the equation

$$v_{k,NN} + (1-\varepsilon_H)v_{k,N} + \left(\frac{k^2}{e^{2N}H^2} + (1+\varepsilon_H-\eta_H)(\eta_H-2) - (\varepsilon_H-\eta_H)_{,N}\right)v_k = 0, \tag{4.16}$$

and its amplitude

$$\mathcal{V}_{k,NN} + (1-\varepsilon_H)\mathcal{V}_{k,N} + \left[\frac{k^2}{e^{2N}H^2}\left(1 - \frac{1}{4k^2\mathcal{V}_k^4}\right) + (1+\varepsilon_H-\eta_H)\cdot (\eta_H-2) - (\varepsilon_H-\eta_H)_{,N}\right]\mathcal{V}_k = 0. \tag{4.17}$$

In the above differential equations we can express the coefficients as

$$1 - \varepsilon_H = 1 - \frac{\varphi_{,N}^2}{2} \tag{4.18}$$

$$(1+\varepsilon_H-\eta_H)(\eta_H-2)-(\varepsilon_H-\eta_H)_{,N} = -2-3\frac{\varphi_{,NN}}{\varphi_{,N}}-\frac{\varphi_{,NNN}}{\varphi_{,N}}+\frac{\varphi_{,N}^2}{2}+\frac{1}{2}\varphi_{,N}\,\varphi_{,NN}. \tag{4.19}$$

We can also write equivalent equations for the curvature perturbation, which take the form

$$R_{k,NN}+\left(3+\frac{2\varphi_{,NN}}{\varphi_{,N}}-\frac{\varphi_{,N}^2}{2}\right)R_{k,N}+\frac{k^2}{e^{2N}H^2}R_k=0 \tag{4.20}$$

and

$$\mathcal{R}_{k,NN}+\left(3+\frac{2\varphi_{,NN}}{\varphi_{,N}}-\frac{\varphi_{,N}^2}{2}\right)\mathcal{R}_{k,N}+\frac{k^2}{e^{2N}H^2}\left(1-\frac{1}{4k^2e^{4N}\varphi_{,N}^4\mathcal{R}_k^4}\right)\mathcal{R}_k=0, \tag{4.21}$$

for the perturbation and its amplitude, respectively.

The spectrum of curvature perturbations is

$$\Delta_R^2=\frac{k^3}{2\pi^2}\frac{\mathcal{V}_k^2}{e^{2N}\varphi_{,N}^2}=\frac{k^3}{2\pi^2}\mathcal{R}_k^2. \tag{4.22}$$

The normalization of the spectrum can be set in terms of a pivot scale $k_*$ and the number of efoldings $N_*$ at which it crosses the horizon: $k_*=e^{N_*}H_*$. By defining dimensionless variables $\tilde{k}=k/k_*$, $\tilde{v}_k=\sqrt{k_*}\,v_k$, $\tilde{\mathcal{V}}_k=\sqrt{k_*}\,\mathcal{V}_k$, $\tilde{R}_k=\sqrt{k_*}\,R_k$, $\tilde{\mathcal{R}}_k=\sqrt{k_*}\,\mathcal{R}_k$, as well as $\delta N=N-N_*$, we obtain

$$\Delta_R^2=A_s\frac{\tilde{k}^3\,2\tilde{\mathcal{V}}_k^2}{e^{2\,\delta N}}\frac{\varphi_{,N*}^2}{\varphi_{,N}^2}. \tag{4.23}$$

where

$$A_s=\frac{1}{4\pi^2}\frac{H_*^2}{\varphi_{,N*}^2} \tag{4.24}$$

sets the scale for the amplitude.

For a given inflaton potential, one can integrate numerically eq. (4.15) in order to derive the inflaton background, and then integrate one of eqs. (4.16), (4.17), (4.20), (4.21) for the field or curvature perturbation, in order to deduce the spectrum. The real and imaginary parts of $v_k$ and $R_k$ oscillate very rapidly for subhorizon perturbations, as can be deduced from eqs. (4.16), (4.20). This makes the numerical integration of these equations more demanding. On the other hand, the amplitudes $\mathcal{V}_k$ and $\mathcal{R}_k$ have a smoother evolution. It is possible for these quantities to become oscillatory also, as we shall see in the following. However, the presence of the terms $\sim\mathcal{V}_k^{-4}$ in eq. (4.17) and $\sim\mathcal{R}_k^{-4}$ in eq. (4.21) guarantees that these amplitudes remain

always positive. For the numerical analysis of the following section, we solve the evolution equations both for the field perturbation $v_k$ and its amplitude $\mathcal{V}_k$ in order to cross-check the results.

A quantity that plays a crucial role in determining the qualitative behaviour of the solutions is the one in the first parenthesis of eqs. (4.20), (4.21), which we denote by

$$f(N) = 3 + \frac{2\varphi_{,NN}}{\varphi_{,N}} - \frac{\varphi_{,N}^2}{2} \tag{4.25}$$

as a function of $N$. In the slow-roll regime, this quantity acts as a generalized friction term. However, for the more general evolution that we are considering, it may become negative and lead to a dramatic enhancement of the perturbations. We also define the function

$$g(N) = 1 - \frac{1}{4k^2 e^{4N} \varphi_{,N}^4 \mathcal{R}_k^4}, \tag{4.26}$$

appearing in the second parenthesis, evaluated on a given solution for the perturbation. This function diverges whenever the amplitude $\mathcal{R}_k$ approaches zero, thus preventing it from turning negative. An alternative way to view this point is to notice that eq. (4.21) is equivalent to eq. (4.20), while the amplitude of $R_k$ cannot turn negative. The fact that $\mathcal{R}_k$ can approach zero at certain times during the later stages of the evolution, as we shall see in the following, indicates that during these stages the real and the imaginary part of $R_k$ are in phase and can cross zero almost simultaneously.

## 4.2 Features of the inflaton potential

We would like to explore features of the inflaton potential that can result in an amplification of the spectrum of curvature perturbations by several orders of magnitude. Our underlying motivation is to determine the appropriate conditions for the creation of primordial black holes. This is possible in a range of scales in which perturbations become of order one. Significant deviations from the scale-invariant spectrum can occur only at small length scales (large wavenumbers), for which the evolution of the spectrum is highly nonlinear, so that current observations do not constrain its form severely. Such scales correspond to comoving wavenumbers larger than $\mathcal{O}(1)$ in units of $\mathrm{Mpc}^{-1}$.

### 4.2.1 Minimal framework

Instead of considering a specific model, we keep only the minimal number of elements required for addressing the problem. We focus on only a limited range of scales, and the corresponding values of the inflaton background when these exit the horizon. We approximate the inflaton potential by the smallest number of relevant terms. The features of interest are:

1. an inflection point, at which the first and second derivatives of the potential vanish,

2. one or more points at which the potential decreases sharply.

Both these features can appear in a potential with the simple parameterization

$$V(\varphi) = V_0 \left( 1 + \frac{1}{2} \sum_i A_i \left( 1 + \tanh(c_i(\varphi - \varphi_i)) \right) + B\varphi \right), \tag{4.27}$$

where $i$ is a positive integer counting certain special field values. The first terms in the parenthesis can be identified with the vacuum energy that drives inflation. The crucial assumption that we have made is that the vacuum energy can have one or more transition points at which it jumps from one constant value to another. One could speculate that these points correspond to values of the inflaton background associated with some kind of decoupling of modes whose quantum fluctuations contribute to the vacuum energy. However, such a speculation cannot be put easily on formal ground because of our lack of understanding of the nature of the cosmological constant. Sharp changes in the vacuum energy can also occur during transitions from one region of a multi-field potential to another. The analysis of such a system would require the inclusion of entropy perturbations. The current work can be regarded as simplified first step towards understanding the features that could appear in the spectrum of curvature perturbations for a multi-field system. The linear term in the potential (4.27) is the only term in a field expansion that is indispensable for our discussion. In this subsection we neglect the effect of higher powers of the inflaton field that would make the analysis model dependent. We assume, without loss of generality, that $B < 0$. An inflection point can appear at $\phi_1 = 0$ if $A_1 = -2B/c$, $A_i = 0$ for $i > 1$. Negative values of $A_i$ result in a series of steps in the potential.

A drawback of the potential (4.27) is that it is not possible to make a connection with the range of the spectrum that is relevant for the cosmic-microwave-background (CMB). The slope $B$ of the potential required for agreement with the measured spectral index is too steep for obtaining a large

number of efoldings. As a result, contact with the observations is not possible and we treat the pivot scale $k_*$, the amplitude $A_s$ and the spectral index $n_s$, introduced in the previous section, as free parameters. In particular, we assume that $k_*$ is located deep in the nonlinear part of the spectrum and the spectral index is sufficiently close to 1 for a large number of efoldings to be produced. We present our results for the spectrum in units of $A_s$, which is equivalent to setting $A_s = 1$. It is also obvious from eq. (4.15) that the absolute scale $V_0$ of the potential does not play any role for our considerations. In practice, we set $V_0 = 1$ for the numerical analysis. Finally, the inflaton field and the constants $c_i$, $B$ are given in units of $M_{\rm Pl}$ (we remind that we have set $M_{\rm Pl} = 1$ in our equations).

Before computing the spectrum, it is instructive to understand which type of background evolution leads to its enhancement. The perusal of eq. (4.21) leads to the conclusion that the sign of the function $f(N)$ defined in eq. (4.25) is crucial. For $f(N) > 0$ the second term of eq. (4.21) acts as a friction term, suppressing the growth of the curvature perturbation. The opposite happens for $f(N) < 0$. It is known that the presence of an inflection point in the potential enhances the spectrum. For this reason, we examine first the form of $f(N)$ for such a case. Then we analyse the conditions under which a similar enhancement of the spectrum can occur for a potential with a step-like structure. It must be emphasized that the two cases are distinct. The rolling of the inflaton through an inflection point does not stop inflation, even though the standard slow-roll conditions are not satisfied because of the large value of $\eta_H$. On the other hand, the transition through a sharp drop in the potential leads to a fast increase of the time-derivative of the inflaton, and in many cases to a brief interruption of inflation. This is apparent from the effect of a large value of $\varepsilon_H$ on the effective equation-of-state parameter $w = 2\varepsilon_H/3 - 1$.

In fig. 4.1 we present various elements of the calculation of the power spectrum for different potentials. We have used the same scale for all related plots in order to make the comparison easy. The first plot in each row depicts the inflaton potential. The potential at the top has an inflection point at $\varphi = 0$, even though this is not clearly visible. The potentials in the next three rows display a step at $\varphi = 0$, whose steepness is increased from top to bottom by choosing larger values of the parameter $c_1$. The form of the potential is reflected in the field evolution. In the second plot of the first row, the field stays almost constant near zero for several efoldings. In the following rows it evolves very quickly, within 2-3 efoldings, from one plateau

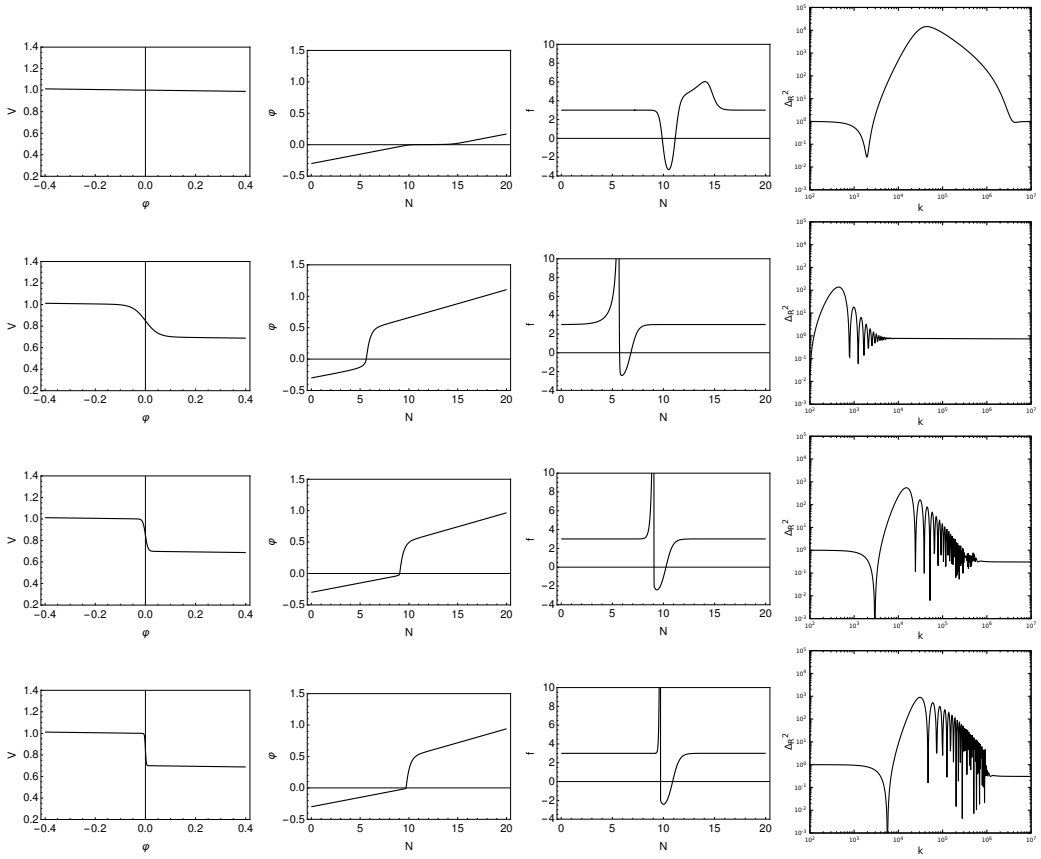


Figure 4.1: The inflaton potential $V(\varphi)$ of eq. (4.27), the evolution of the inflaton $\varphi$, the function $f(N)$ defined in eq. (4.25), and the power spectrum of curvature perturbations with wavenumber $k$, for various choices of the parameters of the potential: First row: $A_1 = 0.000605$, $c_1 = 100$, $B = -0.03$. Second row: $A_1 = -0.3$, $c_1 = 20$, $B = -0.03$. Third row: $A_1 = -0.3$, $c_1 = 100$, $B = -0.03$. Fourth row: $A_1 = -0.3$, $c_1 = 300$, $B = -0.03$. The scales of $k$ and $V$ are arbitrary.

of the potential to the next. The third plot in each row depicts the "effective friction" $f(N)$. In all cases this function becomes negative during part of the evolution, thus leading to a strong enhancement of the fluctuations. For an inflection point it starts with the standard value 3, then becomes negative, returns to positive values larger than 3, and eventually becomes equal to 3 again. For a step in the potential, there is a strong increase to very large positive values before the function becomes negative. This increase is confined within a period of efoldings that shrinks with increasing steepness (and $c_1$). On the other hand, the form of $f(N)$ in the interval where it is negative

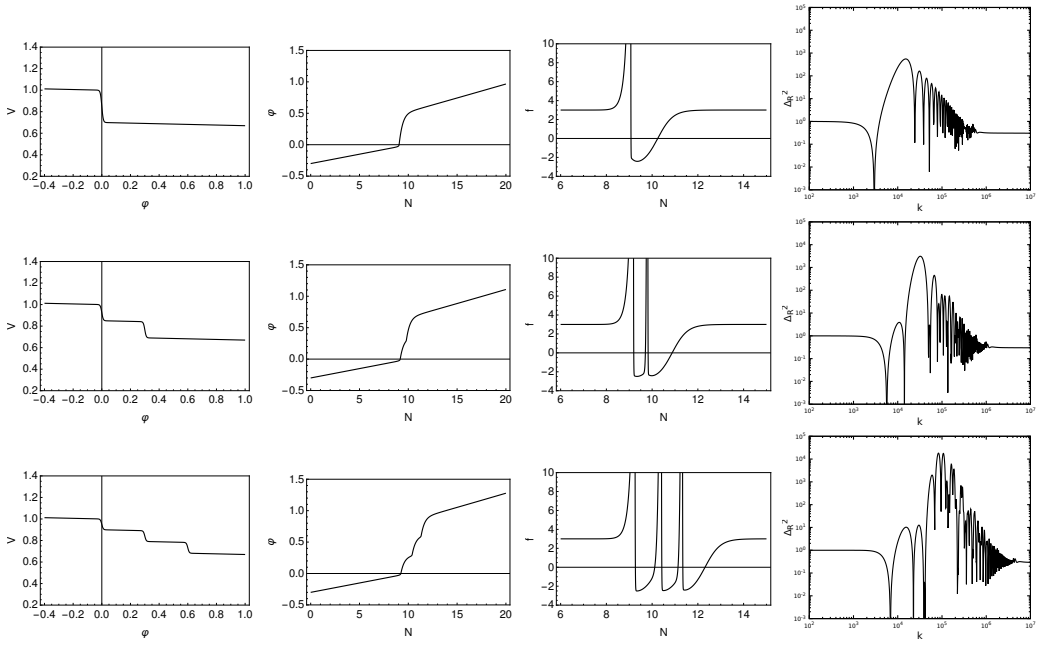


Figure 4.2: The inflaton potential $V(\varphi)$ of eq. (4.27), the evolution of the inflaton $\varphi$, the function $f(N)$ defined in eq. (4.25), and the power spectrum of curvature perturbations with wavenumber $k$, for various choices of the parameters of the potential: First row: $A_1 = -0.3$, $c_1 = 100$, $B = -0.03$. Second row: $A_1 = A_2 = -0.15$, $\varphi_2 = 0.3$, $c_1 = c_2 = 100$, $B = -0.03$. Third row: $A_1 = A_2 = A_3 = -0.1$, $\varphi_2 = 0.3$, $\varphi_3 = 0.6$, $c_1 = c_2 = c_3 = 100$, $B = -0.03$. The scales of $k$ and $V$ are arbitrary.

is largely independent of $c_1$, because it is determined by the approach of the field to slow roll on the second plateau. It seems reasonable to expect that, for steeper steps, the suppression of the perturbation during the strong increase of $f(N)$ is a subleading effect relative to the subsequent enhancement. This expectation is confirmed by the spectrum depicted in the last plot of each row. In the first row we observe the strong and broad enhancement of the spectrum associated with an inflection point. After an initial dip, the spectrum grows rather steeply towards a maximum, beyond which it decays smoothly towards its almost scale-invariant form. This behavior is consistent with the general analysis of ref. [149]. The spectra of the next three rows display a strong oscillatory behaviour, which will be discussed in the following. The largest enhancement is achieved for a band of wavenumbers during the first oscillation. It is clear that the magnitude of this enhancement increases with $c_1$.

The maxima of the spectra in fig. 4.1 are larger by up to three orders

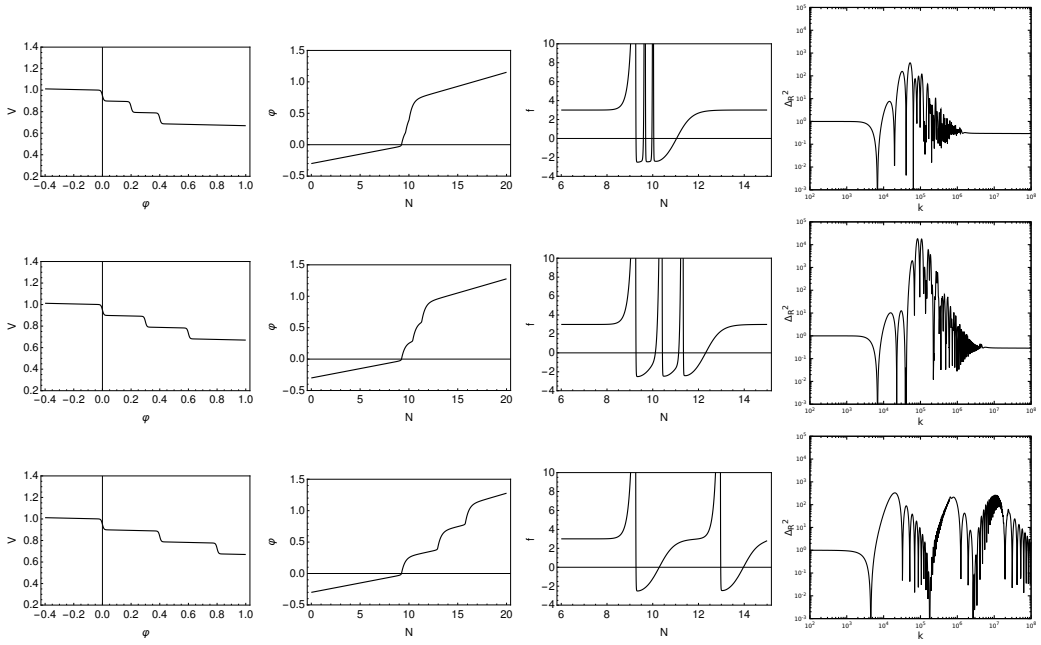


Figure 4.3: The inflaton potential $V(\varphi)$ of eq. (4.27), the evolution of the inflaton $\varphi$, the function $f(N)$ defined in eq. (4.25), and the power spectrum of curvature perturbations with wavenumber $k$, for various choices of the parameters of the potential: First row: $\varphi_2 = 0.2$, $\varphi_3 = 0.4$. Second row: $\varphi_2 = 0.3$, $\varphi_3 = 0.6$. Third row: $\varphi_2 = 0.4$, $\varphi_3 = 0.8$. In all cases: $A_1 = A_2 = A_3 = -0.1$, $c_1 = c_2 = c_3 = 100$, $B = -0.03$. The scales of $k$ and $V$ are arbitrary.

of magnitude relative to the standard value for the scale-invariant case. The enhancement is restricted by the fact that the maximal "velocity" achieved by the rolling field is limited by the size of the step. It is possible, however, that the potential includes several step-like features. We examine their effect in fig. 4.2, where we compare potentials with one, two or three steps. The total drop in the potential is the same in all three cases. It is apparent from the last column that the presence of several features in the potential can lead to the increase of the spectrum by several orders of magnitude. The reason can be traced to the "effective friction" $f(N)$, displayed in the third column. The presence of several steps increases the total number of efoldings over which this function takes negative values. This is reflected in the larger enhancement of the perturbations.

The field values at which the features of the potential appear play a crucial role for the form of the resulting spectrum. This feature is demonstrated in fig. 4.3 in which we consider potentials with three steps, at field values with

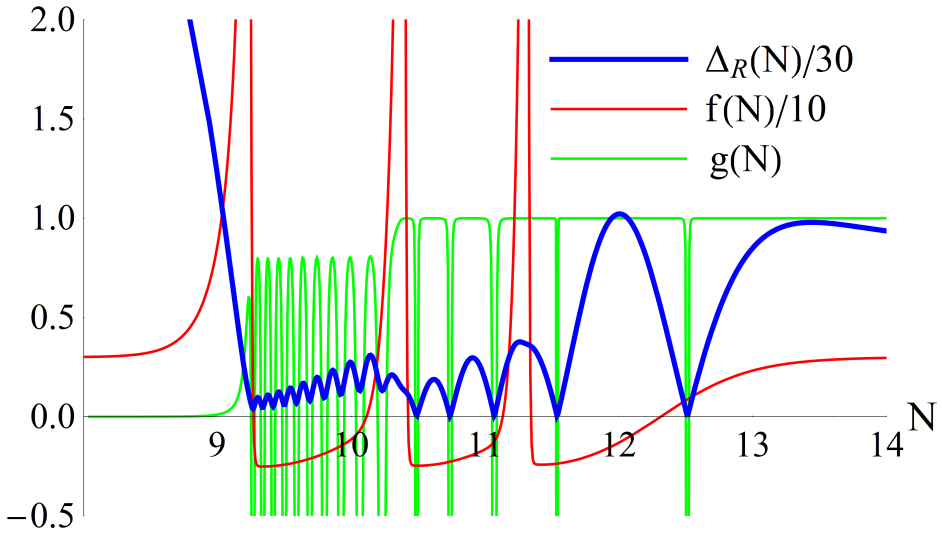


Figure 4.4: The curvature perturbation as a function of the number of efoldings $N$, and the functions $f(N)$, $g(N)$, for the potential (4.27) with $A_1 = A_2 = A_3 = -0.1$, $\varphi_2 = 0.3$, $\varphi_3 = 0.6$, $c_1 = c_2 = c_3 = 100$, $B = -0.03$. Blue line: $\frac{1}{30}\sqrt{\Delta^2_R(k,N)}$ for $k = 2.66 \times 10^5$. Red line: The function $\frac{1}{10}f(N)$ defined in (4.25). Green line: The function $g(N)$ defined in (4.26).

increasing distance from each other. It is apparent from the first row that when the steps are very close to each other the function $f(N)$ stays negative for a small number of efoldings and the enhancement is comparable to the one-step case. Increasing the distance leads to spectrum enhancement, as $f(N)$ stays negative longer. However, the enhancement persists up to a certain distance between the features of the potential, beyond which each step acts independently on the spectrum. This beaviour is apparent in the second and third rows of fig. 4.3.

A prominent feature of the spectra resulting from sharp drops in the inflaton potential is the appearance of strong oscillations, whose origin we would like to understand. One can speculate that the oscillatory pattern arises when modes within a wavenumber range exit the horizon, but then reenter during the period when inflation stops and the comoving horizon grows. Upon reentry they start oscillating again, until they exit for a second time during a subsequent period of inflation [85, 144]. However, the onset or

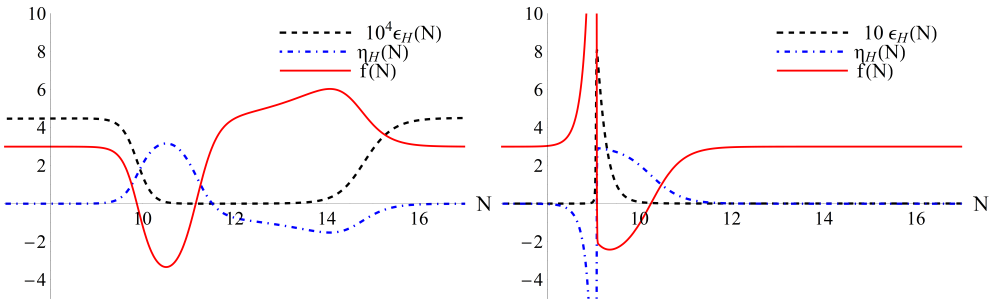


Figure 4.5: The Hamilton-Jacobi slow-roll parameters $\epsilon_H$ and $\eta_H$, defined in eqs. (4.12) and (4.13) respectively, and the "effective-friction" term $f(N)$ defined in eq. (4.25), as a function of the number of efoldings, for two choices of the parameters of the potential: Left plot: $A_1 = 0.000605$, $c_1 = 100$, $B = -0.03$. Right plot: $A_1 = -0.3$, $c_1 = 100$, $B = -0.03$. The two sets of parameters correspond to the first and third row of fig. 4.1.

freezing of the oscillatory behaviour is not instantaneous, while the crossing of the horizon is essentially a continuous process with a certain width. An exact analytical treatment is difficult, and the evolution of each mode can be computed only numerically. In fig. 4.4 we present the evolution of the curvature perturbation $\tilde{\mathcal{R}}_{\tilde{k}}(N)$ (blue line) for a given Fourier mode $\tilde{k} = 2.66 \times 10^5$ for an inflaton background arising from a potential with three steps. The red and green lines depict the functions $f(N)$ and $g(N)$ defined by eqs. (4.25) and (4.26) respectively. The enhancement of the curvature perturbation during the periods of inflation with negative $f(N)$ is apparent. Similarly, the freezing of the perturbation during the periods with positive $f(N)$ is also apparent, resulting in $\tilde{\mathcal{R}}_{\tilde{k}}(N)$ becoming asymptotically constant.

A striking feature is the series of oscillations for the amplitude of perturbations, which approaches zero at several values of $N$. At these points the function $g(N)$ becomes very negative, thus preventing the amplitude from crossing zero. The origin of the oscillations is explained in detail in the next chapter, where we make an analytical approximation of the power spectrum of curvature perturbations.

In fig. 4.5 we look in detail at the role of the slow-roll parameters in the enhancement of the spectrum. We contrast the case of an inflection point in the potential (left plot) with that of a step-like feature (right plot). In the first case, the solution remains inflationary during the whole evolution. The Hamilton-Jacobi parameter $\epsilon_H$ has a constant value, apart from the part of the evolution near the inflection point, during which it approaches

zero. The parameter $\eta_H$ starts from a value close to zero during the slow-roll regime, first turns positive and subsequently negative, eventually returning close to zero during the second slow-roll regime. The "effective-friction" term is strongly influenced by $\eta_H$ and becomes negative during the time that $\eta_H$ is significantly larger than zero. In the case of a step-like feature, the parameter $\epsilon_H$ grows large during the interval that this feature is traversed. For sharp steps or when the second plateau is sufficiently low, the solution ceases to be inflationary for a short time, as can be verified by computing the equation of state parameter $w = -1 + 2\epsilon_H/3$. The parameter $\eta_H$ first turns negative, but then positive as the inflaton "decelerates" while settling on a slow-roll regime on the second plateau. The "effective friction" is again mainly influenced by $\eta_H$ and becomes negative when $\eta_H$ takes large positive values. The effect is sufficiently strong for the friction term to be negative even when $\epsilon_H$ is of order 1.

### 4.2.2 A specific model

The analysis of the previous subsection relied on a simplified potential which did not allow us to make contact with the physical scales of the power spectrum. In order to obtain a more complete picture, we study in this subsection a potential inspired by the Starobinsky model [150], to which we introduce step-like features. The potential is given by the expression

$$V(\varphi) = V_0 \left(1 - e^{B\varphi}\right)^2 \left(1 + \frac{1}{2}\sum_i A_i \left(1 + \tanh(c_i(\varphi - \varphi_i))\right)\right). \qquad (4.28)$$

It is important to mention that we do not engage in model building at this point, as we do later in this thesis when we construct models in the framework of $\alpha$-attractors. Thus, the above potential has not been derived from a more fundamental framework, such as supergravity. It is a phenomenological construction that has enough flexibility to allow for a sufficient number of efoldings, as well as power-spectrum scale and spectral index compatible with the CMB observations.

In fig. 4.6 we present the various elements in the calculation of the power spectrum of curvature perturbations for this model. The first plot depicts the potential with the characteristic step-like feature. The values of the parameters are: $A_1 = A_2 = A_3 = 0.05$, $c_1 = c_2 = c_3 = 200$, $\varphi_1 = 5$, $\varphi_2 = 4.8$, $\varphi_3 = 4.6$, $B = -\sqrt{2/3}$. Dimensionful parameters are given in units of $M_{\rm Pl}$. The evolution of the inflaton $\varphi$ as a function of the number of efoldings $N$ is shown in the second plot. We count the number of efoldings from the

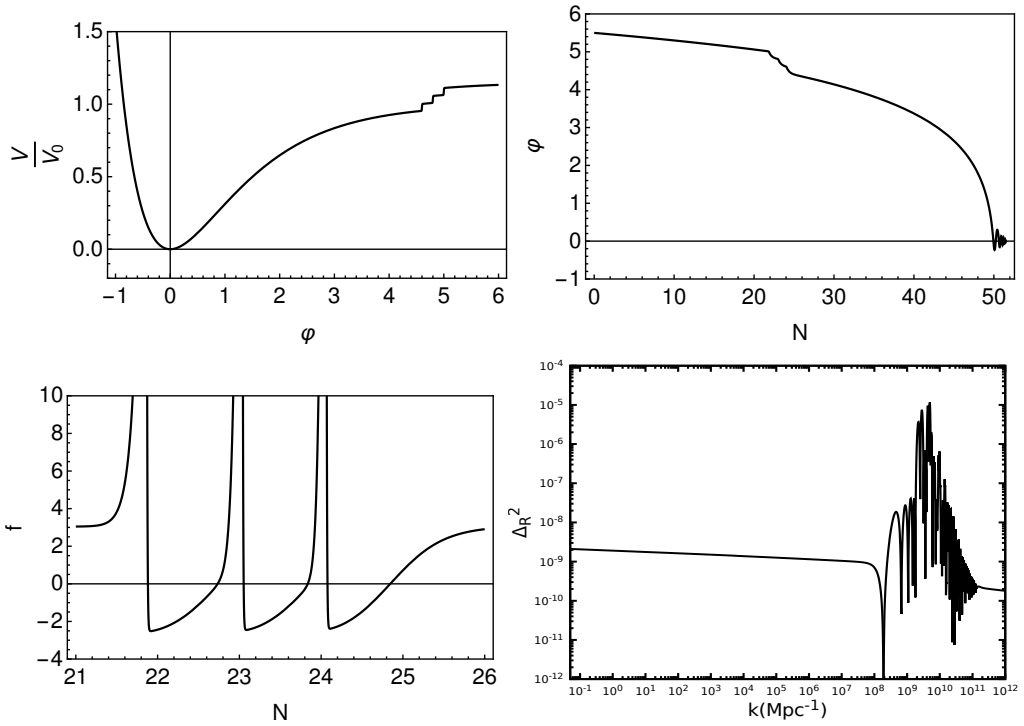


Figure 4.6: The inflaton potential $V(\varphi)$ defined in (4.28), the evolution of the inflaton $\varphi$ as a function of the number of efoldings $N$, the function $f(N)$ defined in eq. (4.25), and the power spectrum of curvature perturbations with wavenumber $k$, for $A_1 = A_2 = A_3 = 0.05$, $c_1 = c_2 = c_3 = 200$, $\varphi_1 = 5$, $\varphi_2 = 4.8$, $\varphi_3 = 4.6$, $B = -\sqrt{2/3}$. Dimensionful parameters in units of $M_{\rm Pl}$. The scale of the potential $V_0$ has been adjusted in order to reproduce the amplitude of curvature perturbations in the CMB range.

moment that the scale with wavenumber $k_* = 0.05\,\mathrm{Mpc}^{-1}$, which we use as a pivot scale, exits the horizon. The above parameters result in a power spectrum in the CMB range with a spectral index $n_s \simeq 0.969$ and a tensor to scalar ratio $r \simeq 0.0027$. The third plot depicts the "effective-friction" function $f(N)$ defined in eq. (4.25). It deviates from the standard value 3 during the period in which the inflaton field takes values in the vicinity of the step-like feature of the potential. When $f(N)$ is negative, it acts as negative friction, leading to the enhancement of the curvature modes that cross the horizon during this period. The enhancement for certain wavenumber bands can be significant. For this particular choice of parameters the spectrum is enhanced by roughly four orders of magnitude. The enhancement can be made larger with an appropriate choice of the potential, or with the inclusion

of additional step-like features. The curvature power spectrum is depicted in the last plot. It has been normalized to the standard value $\simeq 2.1 \times 10^{-9}$ for $k_* = 0.05\,\mathrm{Mpc}^{-1}$ through an appropriate choice of the scale $V_0$ of the potential.

The strong features in the spectrum appear deep in the nonlinear regime, where the phenomenological constraints are not strict because of the lack of analytical understanding of the evolution of the perturbations. The approximate wavenumber value $k_f$ for which these features appear can be estimated by noting that $k_f = \exp(N_f)H_f$ must hold at horizon crossing. For the pivot scale this relation is $k_* = \exp(N_*)H_*$, and we have set $N_* = 0$. If the Hubble parameter does not change substantially between $N_*$ and $N_f$, we have $k_f/k_* \sim \exp(N_f)$. From the second plot of fig. 4.6 we obtain $N_f \sim 23$, which gives $k_f \sim 10^9\,\mathrm{Mpc}^{-1}$, in agreement with the last plot.

# Chapter 5

# Analytical calculation of the spectrum

In this chapter we discuss an approximate analytical treatment of the spectrum of curvature perturbations in cases that the slow-roll approximation is strongly violated. We assume that the inflaton potential displays the standard plateau that can lead to an almost scale-invariant spectrum. In addition, it contains a strong feature within a finite range of field values, which can lead to the violation of the slow-roll conditions or even cause inflation to cease momentarily. In order to be as model independent as possible, we do not focus on specific potentials with these properties. The material of this chapter is mainly drawn from [151] and [152].

## 5.1 Approximation with "pulses"

### 5.1.1 General considerations

In the previous chapter we saw that the evolution equation for the comoving curvature perturbation takes the form

$$R_{k,NN} + f(N)\, R_{k,N} + \frac{k^2}{e^{2N} H^2} R_k = 0, \tag{5.1}$$

with the quantity

$$f(N) = 3 + \frac{2\varphi_{,NN}}{\varphi_{,N}} - \frac{\varphi_{,N}^2}{2} = 3 + \varepsilon_H - 2\eta_H \tag{5.2}$$

playing a crucial role in determining the qualitative behaviour of the solutions. In the slow-roll regime it acts as a generalized friction term. However,

if $\eta_H$ becomes positive and large it can lead to a dramatic enhancement of the perturbations.

In the approximation that the slow-roll parameters are neglected and $H$ remains constant, the solution of eq. (5.1) can be expressed in terms of the Bessel functions $J_{\pm 3/2}$ as

$$R_k(N; C_p, C_m, 3) = A\, e^{-\frac{3}{2}N} \left( C_p J_{3/2}\left(e^{-N}\frac{k}{H}\right) + C_m\, J_{-3/2}\left(e^{-N}\frac{k}{H}\right)\right), \tag{5.3}$$

where we take $A$ to be real without loss of generality. We also emphasize that, even though $C_p$, $C_m$ are constants with respect to $N$, they are generally $k$-dependent. For the values $C_p = 1$, $C_m = i$ the two Bessel functions combine into the Hankel function of the first kind $H^{(1)}_{3/2}$. The curvature pertubation is $R_k(N; 1, i, 3) \propto \left(e^{-ik\tau}/\sqrt{k}\right)(1 - i/(k\tau))/a(\tau)$, where the conformal time is $H\tau = -e^{-N} = -1/a$. For $\tau \to -\infty$ this is the standard expression for the Bunch-Davies vacuum in the slow-roll regime, which is taken as the initial condition for the evolution of the fluctuations. For $\tau \to 0^-$ or $N \to \infty$ the curvature perturbation approaches a constant value $\propto k^{-3/2}$ as the mode with wavenumber $k$ moves out of the horizon and freezes. The power spectrum of curvature perturbations $\Delta^2_R = (k^3/2\pi^2)|R_k|^2$ is scale invariant. It is important to notice that the value of the curvature perturbation at late times, or $N \to \infty$, comes from the second term in eq. (5.3), as the first one vanishes. This can be easily seen if one considers eq. (5.3) for large values of $N$. In this limit, it takes the form

$$\begin{aligned} R_k(N) = A\sqrt{\frac{2}{\pi}}\left(\frac{k}{H}\right)^{-3/2} e^{-N}\Bigg[ &- \left(C_m e^N + C_p \frac{k}{H}\right)\cos\left(e^{-N}\frac{k}{H}\right) \\ &+ \left(C_p e^N - C_p \frac{k}{H}\right)\sin\left(e^{-N}\frac{k}{H}\right)\Bigg], \end{aligned} \tag{5.4}$$

Therefore, it is the absolute value of $C_m$ that determines the power spectrum.

The above picture is modified when the function $f(N)$ of eq. (5.2) deviates from a constant value equal to 3. For small values of $\varepsilon_H$, $\eta_H$ the deviations from scale invariance can be computed analytically through the standard slow-roll analysis. However, our interest lies with strong modifications of $\varepsilon_H$, $\eta_H$ that result in the enhancement of the spectrum by several orders of magnitude.

The typical forms of the effective-friction function $f(N)$ that we would like to analyse are like those depicted in fig. 4.1 of the previous chapter, which result from the potential (4.27) for specific choices of its parameters. The

function $f(N)$ remains close to 3, apart from a range of efoldings in which it deviates strongly from this value. Similar features can be obtained with other types of potentials in single- or multi-field inflation, such as potentials with inflection points, or multiple inflationary stages. The pattern can be repeated several times. As we have already mentioned, when $f(N)$ becomes negative, it induces a strong enhancement of the spectrum. The modifications to the spectrum appear for wavenumbers of density perturbations deep in the nonlinear regime today.

In order to obtain an analytical solution, we model $f(N)$ through a sequence of square "pulses", each with constant $f(N) = \kappa_i \neq 3$. At early and late times we assume that the inflaton is in a slow-roll regime, with negligible slow-roll parameters, so that $f(N) = 3$ and the curvature perturbation is given by eq. (5.3). We approximate the Hubble parameter $H$ as constant. This is a good approximation, as our focus is on modifications of the spectrum by several orders of magnitude. In comparison, the change in the Hubble parameter for an inflection point in the potential is less than 1%, while for a step in the potential it is of order 10%. We use an arbitrary normalization for the number of efoldings by absorbing a factor of $\exp(N_0)$ in $k$, where $N_0$ corresponds to the actual number of efoldings since the beginning of inflation until the moment in time that we denote by $N = 0$. In practice this means that the physical value of the wavenumber is $\exp(N_0)\, k$.

Our starting point is the solution (5.3), which defines the initial condition for $N \to -\infty$. For $C_p = 1$, $C_m = i$, this expression corresponds to the Bunch-Davies vacuum. We neglect slow-roll corrections and approximate the evolution through eq. (5.3) until the value of $N$ at which the first nontrivial "pulse" appears in $f(N)$. In subsection 5.1.3 we analyse the modification of the curvature perturbation induced by this and the following "pulses", until the system returns to a slow-roll regime. For $N \to \infty$ the solution becomes constant. We are interested in the relative increase of the asymptotic value of $|C_m|$ in comparison to the value $|C_m| = 1$ corresponding to a scale-invariant spectrum. In this sense, the value of the $k$-independent parameter $A$ in eq. (5.3) is not of interest to us. This parameter would determine the amplitude of the spectrum in the CMB region, and needs to be adjusted to a phenomenologically correct value.

An important point concerns the form of $f(N)$. Negative values of this function result only from $\eta_H$ taking large positive values, as can be seen through eqs. (4.12), (4.13), (5.2). In general, large deviations from 3 can result from the term $2\varphi_{,NN}/\varphi_{,N}$ being the dominant one in eq. (5.2). The integral of $f(N) - 3$ over $N$, from an early to a late slow-roll regime separated

by nontrivial evolution, is

$$\begin{aligned}\int_{N_e}^{N_l} dN(f(N)-3) = \int_{N_e}^{N_l} dN(\varepsilon_H - 2\,\eta_H) &= 2\log\frac{(\varphi_{,N})_l}{(\varphi_{,N})_e} + \log\frac{H_l}{H_e} \\ &= \log\frac{(dH/dN)_l}{(dH/dN)_e},\end{aligned} \tag{5.5}$$

where we have used the definitions (4.12), (4.13). This quantity is approximately zero for inflaton potentials with a strong feature localized within a region supporting slow-roll inflation and with similar values of $dH/dN$ before and after the feature. Here we neglect the slow-roll corrections and analyse only the very large enhancement resulting from such a strong feature, by imposing the constraint that positive and negative "pulses" have integrated areas that cancel.

### 5.1.2 Toy-model analysis

Several features that appear in the spectra that we study in the following subsections can be understood in a much simpler context. We are interested in the effect of a "pulse" on the evolution of a mode with a free-wave initial condition. It is instructive to ignore the background expansion and consider the toy-model equation

$$R_{k,tt} + \kappa R_{k,t} + k^2 R_k = 0. \tag{5.6}$$

The solutions are oscillatory with an amplitude that gets suppressed or enhanced, depending on the sign of the friction parameter $\kappa$. It is straightforward to derive the solution for a friction term that vanishes at all times apart from the interval $0 < t < t_p$, by requiring the continuity of the solution and its first derivative at $t = 0$ and $t_p$.

For an early-time solution $R_k(t) = e^{-ikt}$, the evolution is depicted in fig. 5.1. We observe the suppression of the amplitude for positive $\kappa$ and the enhancement for negative $\kappa$. However, the most striking feature is the appearance of oscillations in the amplitude. Their origin lies in the modification by the "pulse" of the relative phase between the real and imaginary parts. For sufficiently large $|\kappa|$ the relative phase in the late stage of the evolution almost vanishes (as in the plot), so that the amplitude approaches zero at certain instances. In the cosmological context, the oscillatory form of the evolution as a function of time can be transferred to the spectrum of perturbations. At late times, each mode $k$ exits the horizon and eventually freezes. This can occur at any point of the oscillatory cycle, depending on the value

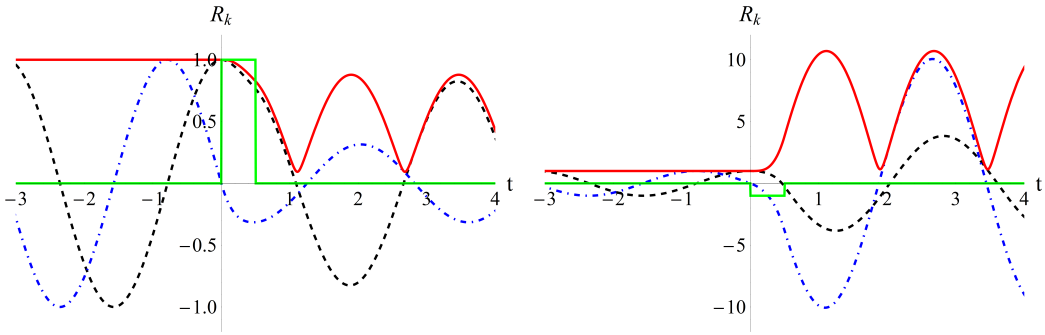


Figure 5.1: The real part (dashed curve), the imaginary part (dot-dashed curve) and the amplitude (solid curve) of the solution of eq. (5.6) with $k = 2$, for a "pulse" in the interval $0 \leq t \leq 0.5$. We also display the "pulse", with a rescaled maximum $\kappa/5$. Left plot: $\kappa = 5$. Right plot: $\kappa = -5$.

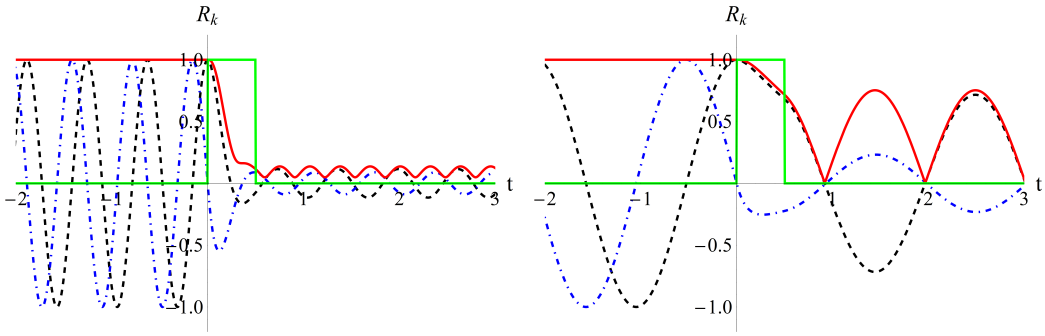


Figure 5.2: The real part (dashed curve), the imaginary part (dot-dashed curve) and the amplitude (solid curve) of the solution of eq. (5.6) for a "pulse" with $\kappa = 10$ in the interval $0 \leq t \leq 0.5$. We also display the "pulse", with a rescaled maximum $\kappa/10$. Left plot: $k = 10$; right plot: $k = 3$, in arbitrary units.

of $k$. As a result, the asymptotic values of the perturbations depend strongly on the freezing time, and the spectrum displays oscillations as a function of $k$.

As we mentioned in the previous chapter, it is known that it is possible to obtain an oscillatory pattern in the spectrum if inflation stops for a certain time interval, so that modes that had exited the horizon reenter and start oscillating again until their next exit. However, our toy example implies a more general pattern: Any feature during the evolution of the perturbations that detunes the relative phase between the real and imaginary parts of the solution results in an oscillatory spectrum, even if inflation is not halted.

Another interesting property of the late-time evolution is displayed in fig. 5.2: The relative suppression of the amplitude of a mode for a given positive friction parameter $\kappa$ is larger for higher wavenumber $k$. This is counter-intuitive at first sight, as one would expect the last term of eq. (5.6) to become more dominant for larger $k$ and limit the suppression induced by the second term. However, the opposite happens. For small $k$, the strong friction tends to freeze the evolution during the "pulse", so that the real and imaginary parts resume their oscillations after the "pulse" with amplitudes comparable to the initial ones. As a general rule of thumb, for a duration of the "pulse" of order 1, a strong suppression of the solution occurs for $k \gtrsim \kappa$.

### 5.1.3 Analytical expressions for "pulses"

We turn next to the analysis of eq. (5.1). For constant $f(N) = \kappa$ the solution involves a linear combination of the Bessel functions $J_{\pm\kappa/2}$ and has the form

$$R_k(N; C_p, C_m, \kappa) = A e^{-\frac{1}{2}\kappa N} \left( C_p J_{\kappa/2}\left(e^{-N}\frac{k}{H}\right) + C_m\, J_{-\kappa/2}\left(e^{-N}\frac{k}{H}\right)\right). \tag{5.7}$$

Let us suppose that the coefficients of the solution $C_{p_i}, C_{m_i}$ are known for a range of efoldings for which $\kappa$ takes a specific value $\kappa_i$. If this range is followed by a transition at $N = N_{fi}$ to a second range in which $\kappa$ takes a differrent value $\kappa_f$, we would like to compute the corresponding values of the coefficients $C_{p_f}, C_{m_f}$. This can be achieved by requiring the continuity of the solution and its first derivative at $N = N_{fi}$. A similar analysis has been performed in refs. [153, 154], using conformal time as the independent variable. We aim here at providing a more transparent picture of the oscillatory patterns in the spectrum, by identifying the characteristic frequencies.

We find that the new coefficients are given through the relation

$$\begin{pmatrix} C_{p_f} \\ C_{m_f} \end{pmatrix} = M(N_{fi}, \kappa_i, \kappa_f, k) \begin{pmatrix} C_{p_i} \\ C_{m_i} \end{pmatrix}, \tag{5.8}$$

where the matrix $M(N_{fi}, \kappa_i, \kappa_f, k)$ has components

$$\begin{aligned}
M_{11} &= C\left(J_{-\frac{\kappa_f}{2}}\left(e^{-N_{fi}}\frac{k}{H}\right) J_{-1+\frac{\kappa_i}{2}}\left(e^{-N_{fi}}\frac{k}{H}\right) + J_{1-\frac{\kappa_f}{2}}\left(e^{-N_{fi}}\frac{k}{H}\right) J_{\frac{\kappa_i}{2}}\left(e^{-N_{fi}}\frac{k}{H}\right)\right) \\
M_{12} &= C\left(-J_{-\frac{\kappa_f}{2}}\left(e^{-N_{fi}}\frac{k}{H}\right) J_{1-\frac{\kappa_i}{2}}\left(e^{-N_{fi}}\frac{k}{H}\right) + J_{1-\frac{\kappa_f}{2}}\left(e^{-N_{fi}}\frac{k}{H}\right) J_{-\frac{\kappa_i}{2}}\left(e^{-N_{fi}}\frac{k}{H}\right)\right) \\
M_{21} &= C\left(-J_{\frac{\kappa_f}{2}}\left(e^{-N_{fi}}\frac{k}{H}\right) J_{-1+\frac{\kappa_i}{2}}\left(e^{-N_{fi}}\frac{k}{H}\right) + J_{-1+\frac{\kappa_f}{2}}\left(e^{-N_{fi}}\frac{k}{H}\right) J_{\frac{\kappa_i}{2}}\left(e^{-N_{fi}}\frac{k}{H}\right)\right) \\
M_{22} &= C\left(J_{\frac{\kappa_f}{2}}\left(e^{-N_{fi}}\frac{k}{H}\right) J_{1-\frac{\kappa_i}{2}}\left(e^{-N_{fi}}\frac{k}{H}\right) + J_{-1+\frac{\kappa_f}{2}}\left(e^{-N_{fi}}\frac{k}{H}\right) J_{-\frac{\kappa_i}{2}}\left(e^{-N_{fi}}\frac{k}{H}\right)\right),
\end{aligned} \tag{5.9}$$

with

$$C = \frac{\pi}{2} e^{\frac{1}{2}N_{fi}(-2+\kappa_f-\kappa_i)} \frac{k}{H} \csc\left(\frac{\pi\kappa_f}{2}\right). \tag{5.10}$$

The above matrix has the property

$$M(N_{fi}, \kappa_m, \kappa_f, k) \cdot M(N_{fi}, \kappa_i, \kappa_m, k) = M(N_{fi}, \kappa_i, \kappa_f, k).$$

This implies that we can select the value $\kappa = 3$ as a reference point for all transitions between different values of $\kappa$.

The next step is to define a matrix corresponding to a "pulse" of height $\kappa$ different from the value corresponding to the scale-invariant case. The function $f(N)$ is

$$f(N) = \kappa \left(\Theta(N - N_1) - \Theta(N - N_2)\right) \tag{5.11}$$

and the corresponding matrix is given by the relation

$$M_{pulse}(N_1, N_2, \kappa, k) = M(N_2, \kappa, 3, k) \cdot M(N_1, 3, \kappa, k). \tag{5.12}$$

As we explained earlier, the increase of the power spectrum relative to the scale invariant one is given by the value of $|C_m|^2$ after a mode of given $k$ has evolved past the strong features in the background. A product of several $M_{pulse}$ matrices can reproduce the final values of the coefficients $(C_p, C_m)$ of the Bessel functions $J_{\pm 3/2}$ after the fluctuations have evolved from an initial configuration corresponding to $(C_p, C_m) = (1, i)$ through a period of strong features in the function $f(N)$. Clearly, it is possible to reconstruct any smooth function $f(N)$ in terms of short intervals of $N$ during which the function takes constant values. Multiplying the corresponding $M_{pulse}$ matrices would provide a solution to the problem of the evolution of perturbations. However, such an approach is not very efficient for a numerical solution. We are mainly interested in obtaining intuitive analytical expressions for forms of $f(N)$ such as those depicted in fig. 4.1, for which a product of a small number of $M_{pulse}$ matrices suffices.

Simple analytical expressions can be obtained in the limits of large and small $k$, using the corresponding expansions of the Bessel functions. For a large real argument we have

$$J_a(z) = \sqrt{\frac{2}{\pi z}} \left[\cos\left(z - \frac{a\pi}{2} - \frac{\pi}{4}\right) - \frac{4a^2 - 1}{8z} \sin\left(z - \frac{a\pi}{2} - \frac{\pi}{4}\right) + \mathcal{O}\left(z^{-2}\right)\right]. \tag{5.13}$$

Using this expression we find for large $k$

$$M^{(\infty)}_{pulse}(N_1, N_2, \kappa, k) = e^{-\frac{1}{2}(N_2 - N_1)(\kappa - 3)} \left\{ \begin{pmatrix} 1 & 0 \\ 0 & 1 \end{pmatrix} + \frac{1}{8}(\kappa - 3)\frac{H}{k} \begin{pmatrix} S_{11} & S_{12} \\ S_{21} & S_{22} \end{pmatrix} \right\} \tag{5.14}$$

where

$$\begin{aligned}
S_{11} &= 2e^{N_1}\sin\left(2e^{-N_1}\frac{k}{H}\right) - 2e^{N_2}\sin\left(2e^{-N_2}\frac{k}{H}\right), \\
S_{12} &= -e^{N_1}\left(1+\kappa+2\cos\left(2e^{-N_1}\frac{k}{H}\right)\right) + e^{N_2}\left(1+\kappa+2\cos\left(2e^{-N_2}\frac{k}{H}\right)\right), \\
S_{21} &= e^{N_1}\left(1+\kappa-2\cos\left(2e^{-N_1}\frac{k}{H}\right)\right) - e^{N_2}\left(1+\kappa-2\cos\left(2e^{-N_2}\frac{k}{H}\right)\right), \\
S_{22} &= -2e^{N_1}\sin\left(2e^{-N_1}\frac{k}{H}\right) + 2e^{N_2}\sin\left(2e^{-N_2}\frac{k}{H}\right). \qquad (5.15)
\end{aligned}$$

Keeping the leading contribution, we find that the power spectrum is scale invariant at late times (or $N \to \infty$) for $k \to \infty$, but has a value multiplied by the factor

$$\left[\delta\Delta_R^{(\infty)}\right]^2 = |C_m|^2 = e^{-(N_2-N_1)(\kappa-3)}, \qquad (5.16)$$

relative to its scale-invariant value for modes that have sufficiently small $k$, so that they exit the horizon and decouple very early with $C_m = i$, without being affected by the features in $f(N)$. The exponent in the above expression is simply the area of the "pulse" exceeding the value 3. For $\kappa > 3$ the spectrum is suppressed, while for $\kappa < 3$ it is enhanced. By breaking a general function $f(N)$ in infinitesimal "pulses", it is easy to see that the enhancement is given by the more general expression

$$\left[\delta\Delta_R^{(\infty)}\right]^2 = \exp\left(-\int_{-\infty}^{\infty}(f(N)-3)\,dN\right). \qquad (5.17)$$

The corrections subleading in $H/k$ introduce oscillatory patterns in the spectrum. The characteristic periods can be deduced from eqs. (5.15). The spectrum is expected to have a deep minimum once per period, i.e. at intervals $\delta k/H = e^{N_1}\pi$ and $\delta k/H = e^{N_2}\pi$. Moreover, when $N_1 \simeq N_2$ we expect interference patterns.

Analytical expressions for $k \to 0$ are more difficult to obtain because the (1,2)-component of the matrix $M_{pulse}$ scales as $1/k$ in this limit. As a result, the effect of several "pulses", which involves the product of several such matrices, is not described by a simple analytical expression. However, the components (2,1) and (2,2), which are relevant for the spectrum, are simpler. The $(2,1)$-component becomes nonzero only at order $(k/H)^3$, while the $(2,2)$-component is equal to $1+\mathcal{O}\left((k/H)^2\right)$. So, up to order $(k/H)^2$, the (2,2)-component is sufficient for the calculation of the spectrum. We give the

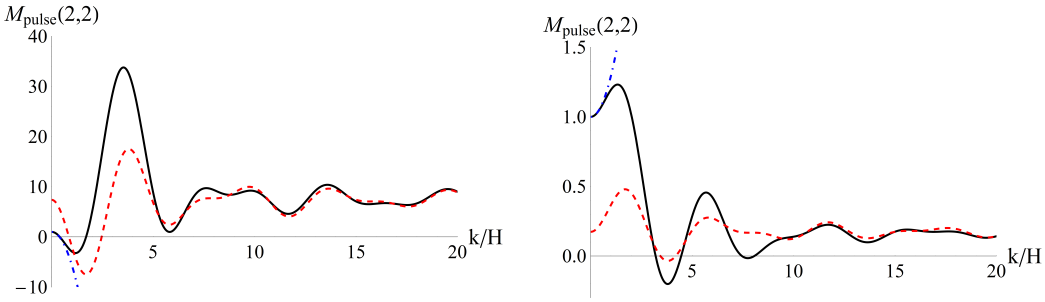


Figure 5.3: The (2,2)-component of the matrix $M_{pulse}$ defined in eq. (5.12) (solid curve), along with the approximations for large $k/H$ (dashed curve) and small $k/H$ (dot-dashed curve). Left plot: $N_1 = 0$, $N_2 = 0.5$, $\kappa = -5$. Right plot: $N_1 = 0$, $N_2 = 0.5$, $\kappa = 10$.

result for the sequence of two "pulses":

$$M^{(0)}_{pulse}(N_1, N_2, N_3, \kappa_1, \kappa_2, k)|_{2,2} \equiv [M(N_3, \kappa_2, 3, k) \cdot M(N_2, \kappa_1, \kappa_2, k) \cdot M(N_1, 3, \kappa_1, k)]_{2,2}$$
$$= 1 + \frac{1}{6}\left(\frac{k}{H}\right)^2 \times \left[\frac{\kappa_1 - 3}{\kappa_1(\kappa_1 - 2)}\left(-2(\kappa_1 - 3)e^{N_1(\kappa_1 - 2) - N_2\kappa_1} + 3(\kappa_1 - 2)e^{-2N_1} - \kappa_1 e^{-2N_2}\right)\right.$$
$$- \frac{2(\kappa_1 - 3)(\kappa_2 - 3)}{\kappa_2(\kappa_1 - 2)}\left(e^{N_3\kappa_2} - e^{N_2\kappa_2}\right)\left(e^{-2N_2 - N_3\kappa_2} - e^{N_1(\kappa_1 - 2) - N_2\kappa_1 - N_3\kappa_2}\right)$$
$$\left. + \frac{\kappa_2 - 3}{\kappa_2(\kappa_2 - 2)}\left(-2(\kappa_2 - 3)e^{N_2(\kappa_2 - 2) - N_3\kappa_2} + 3(\kappa_2 - 2)e^{-2N_2} - \kappa_2 e^{-2N_3}\right)\right]. \tag{5.18}$$

For $\kappa_2 = 3$ the second "pulse" is eliminated and only the first term in the bracket survives, while for $\kappa_1 = 3$ the first "pulse" is eliminated and the last term survives. For $\kappa_1, \kappa_2 \neq 3$ there is a mixing term, which indicates that the effects of the various "pulses" are not simply additive, even within this approximation.

The oscillatory behaviour of the solutions can be observed in the components of the matrix $M_{pulse}$ defined in eq. (5.12). In fig. 5.3 we depict the (2,2)-component of this matrix (solid lines) for $N_1 = 0$, $N_2 = 0.5$. This component gives the leading contribution to the power spectrum. The left plot corresponds to a negative-friction "pulse" with $\kappa = -5$ that causes the enhancement of the spectrum. The right plot is obtained for positive friction $\kappa = 10$ that leads to suppression. The asymptotic expansions of this component for large $k/H$ (dashed curve), given by eq. (5.14), and small $k/H$ (dot-dashed curve), given by eq. (5.18), are also plotted. Oscillatory behaviour is observed, associated with interference patterns from two almost equal frequencies corresponding to $\delta k/H = e^{N_1}\pi$ and $\delta k/H = e^{N_2}\pi$. It is

interesting that the oscillatory frequencies are correctly reproduced by the asymptotic expansion even for small $k/H$. Another feature that can be observed is the strong decrease of $M_{pulse}$ for $k/H \gtrsim \kappa/2$ for positive $\kappa$, in agreement with the discussion at the end of the previous subsection.

### 5.1.4 The integral of $f(N)$

The form of $f(N)$ that we assume in our discussion should result from the time evolution of the parameters $\varepsilon_H$ and $\eta_H$. We saw at the end of subsection 5.1.1 that the integral of this function over $N$ is constrained by eq. (5.5). In this subsection we discuss the type of field evolution, as given by the function $\varphi_{,N}$, that is consistent with our approximate treatment.

The Mukhanov-Sasaki equation (4.3) implies that the Wronskian of each Fourier mode of its solution

$$W[v_k] = -i(v_k\, v_k^{*\prime} - v_k^* v_k') \tag{5.19}$$

remains constant during the evolution. Here the prime denotes a derivative with respect to conformal time $\tau = -e^{-N}/H$. As we know, the solution of eq. (4.3) plays the role of the mode function in the canonical quantization of the field $v$. For the Bunch-Davies vacuum, the initial condition at early times, when $k^2 \gg z''/z$, is chosen so that the mode function has the standard form in Minkowski spacetime. Selecting positive-energy solutions fixes the sign of the Wronskian to be positive, while the appropriate normalization results in $W[v_k] = 1$. This choice is automatically preserved at later times if $v_k$ is a solution of eq. (4.4). This can be seen by multiplying eq. (4.4) by $v_k^*$ and subtracting the conjugate of the same equation multiplied by $v_k$.

We have based our analysis on the curvature perturbation $R_k$, related to $v_k$ through $R_k = -v_k/z$, with $z = e^N \varphi_{,N}$. The consistency of our approximation of describing $f(N)$ through a sequence of "pulses" implies a specific form of $\varphi_{,N}$ during the evolution through the strong features in the potential. We can deduce this form by considering the Wronskian of $R_k$

$$W[R_k] = -i(R_k\, R_k^{*\prime} - R_k^* R_k') = \frac{W[v_k]}{z^2} = \frac{1}{z^2}. \tag{5.20}$$

The solution (5.7) gives

$$W[R_k] \propto i\left(C_p C_m^* - C_m C_p^*\right) \exp((1-\kappa)N). \tag{5.21}$$

Consistency with eq. (5.20) requires that $\varphi_{,N} \propto \exp((\kappa-3)N/2)$. The inflaton "velocity" must grow fast with $N$ for $\kappa > 3$, and decay for $\kappa < 3$.

This is the behaviour observed in all cases of fig. 4.1. We have already mentioned that any function $f(N)$ can be reconstructed as a sequence of very short "pulses" of variable height $\kappa$. For small $N$ the change of $\varphi_{,N}$, starting from some initial value at $N = 0$, is linear in $N$ with a slope proportional to $\kappa$. Thus, by breaking $f(N)$ into many "pulses" one can obtain the required evolution of $\varphi_{,N}$ as a function of $N$. In this sense our analysis is very general. For consistency, of course, the deduced evolution must result from an appropriate inflaton potential.

Our main aim is to obtain an intuitive understanding of the form of the spectrum by focusing on the gross properties of $f(N)$. Let us consider a feature in the evolution resulting from two successive "pulses" with heights $\kappa_1$ and $\kappa_2$, between early and late slow-roll regimes with $\kappa = 3$. The solution after the feature is traversed is given by eq. (5.3) with

$$\begin{pmatrix} C_p \\ C_m \end{pmatrix} = M(N_3, \kappa_2, 3, k) \cdot M(N_2, \kappa_1, \kappa_2, k) \cdot M(N_1, 3, \kappa_1, k) \begin{pmatrix} 1 \\ i \end{pmatrix}, \quad (5.22)$$

where the matrix $M$ is given by eq. (5.9). Before the "pulse" we have $i(C_p C_m^* - C_m C_p^*)/2 = 1$, while after the "pulse" one finds

$$\frac{i}{2}(C_p C_m^* - C_m C_p^*) = e^{-(n_2-n_1)(\kappa_1-3)-(n_3-n_2)(\kappa_2-3)}. \quad (5.23)$$

The exponent is exactly (minus) the integral of $f(N) - 3$. By comparing the Wronskian $W[R_k]$ at late and early times (before and after the "pulses"), it becomes clear that the quantity (5.23) is equal to the ratio $\left(\varphi_{,N}^2\right)_e / \left(\varphi_{,N}^2\right)_l$, with both quantities being constant. In this way we reproduce the result of eq. (5.5), under our assumption that $H_l/H_e \simeq 1$.

Let us summarize the basic points: According to our assumptions, the system is in a slow-roll regime during an early and a late period, with values of the Hubble parameter that we have approximated as equal. We can assume that the values of $\varphi_{,N}$ are also approximately equal during these periods. These assumptions isolate the effect of the strong feature in the intermediate part of the evolution from the properties in the slow-roll regimes. During the intermediate part the inflaton "velocity" $\varphi_{,N}$ changes fast, by growing or decaying depending on the sign of $f(N) - 3$. The integral of $f(N) - 3$ over $N$ must vanish for $\varphi_{,N}$ to have equal values at early and late times. For realistic situations one must take into account the breaking of scale invariance in the slow-roll regimes as well. However, these are included in the standard slow-roll analysis and are not of interest to us here.

Finally, it can be checked through the asymptotic form of the Bessel functions that for both $k \to 0$ and $k \to \infty$, and for a vanishing integral of

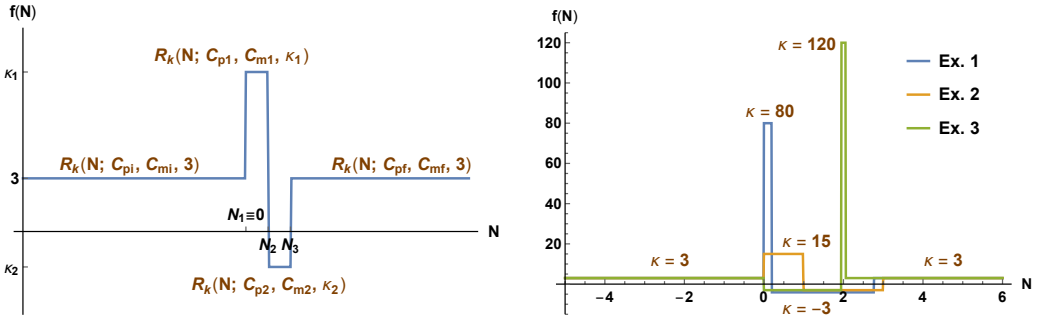


Figure 5.4: An illustration of the approximate form of the function $f(N)$ that we assume for the analytical study. Left panel: a double-"pulse" model, with a positive-friction "pulse" followed by a negative-friction one. Right panel: the double-"pulse" form assumed in the three examples resulting in the spectra of figs. 5.5, 5.6, 5.7.

$f(N) - 3$, we have $(C_p, C_m) = (1, i)$ at all times during the evolution. This indicates that the low- and high-$k$ modes are not affected by the presence of the feature. As a result the scale-invariant form of the spectrum is modified only for a finite range of wavenumbers $k$.

### 5.1.5 Examples of spectra

In this subsection we consider spectra that display the features we discussed in the previous subsections. The range of possible spectra is large, as we do not focus on a particular underlying model, but simply consider various forms of the function $f(N)$ defined in eq. (5.2). We assume that the integral of $f(N) - 3$ over $N$ vanishes, so that the spectrum is scale invariant with the same amplitude for very low and very high wavenumbers $k$. We focus only on the relative enhancement of the spectrum at intermediate scales as a result of the presence of strong features in the underlying inflaton evolution. As the absolute scale of the spectrum is not of interest for our discussion, we set $A = 1$ in eq. (5.3). We discuss next three particular examples of the form of the friction function $f(N)$.

In our first example (Ex. 1) the spectrum results from a function $f(N)$ which is displayed in fig. 5.4. The feature consists of a positive-friction "pulse" with $\kappa_1 = 80$ in the interval between $N_1 = 0$ and $N_2 = 0.2$, followed by a negative-friction "pulse" with $\kappa_2 = -3$ in the interval between $N_2 = 0.2$ and $N_3 = 2.77$. The value of the spectrum for a given value of $k/H$ is equal to $|C_m|^2$, where $(C_p, C_m)$ are given by eq. (5.22). The result is depicted by the middle curve of the top plot in fig. 5.5, in the $k$-range $k/H = 10^{-2} - 10^3$

that corresponds to $N \simeq -4.6$ up to 6.9. In the same figure we also display the spectra that would result from a single "pulse". These are computed from the expression

$$\begin{pmatrix} C_p \\ C_m \end{pmatrix} = M(N_2, \kappa_1, 3, k) \cdot M(N_1, 3, \kappa_1, k) \begin{pmatrix} 1 \\ i \end{pmatrix}, \tag{5.24}$$

for the positive-friction "pulse" (lower curve in fig. 5.5), and

$$\begin{pmatrix} C_p \\ C_m \end{pmatrix} = M(N_3, \kappa_2, 3, k) \cdot M(N_2, 3, \kappa_2, k) \begin{pmatrix} 1 \\ i \end{pmatrix}, \tag{5.25}$$

for the negative-friction "pulse" (upper curve in fig. 5.5). As we discussed in the previous subsection, the fact that the integral of the function $f(N) - 3$ over $N$ does not vanish for these cases means that the quantity $\varphi_{,N}^2$ changes across the "pulse" by a factor equal to the exponential of this integral. The two slow-roll regimes are quite distinct in this case and the effect of the "pulse" is not clear. We display the spectra because they provide intuition on the features appearing in the two-"pulse" spectrum, for which the integral of $f(N) - 3$ vanishes. Details for the latter are presented in the next two plots of fig. 5.5, for two successive $k/H$ ranges on a linear horizontal axis. Notice the huge difference in the scale of the vertical axis in the two plots.

Several features of the spectra are apparent in these plots:

1. The two-"pulse" spectrum has a first minimum at a value of $k/H$ well approximated by the positive root of the polynomial of eq. (5.18).

2. The subsequent strong increase of the spectrum results from the effect of the negative-friction "pulse". The spectrum reaches a maximal value comparable to that of the negative-friction single-"pulse" spectrum. A rough estimate can be obtained from the asymptotic value of the single-"pulse" spectrum, which is $\exp((N_3 - N_2)(3 - \kappa_2)) = \mathcal{O}(10^7)$.

3. The envelope of the positive-friction single-"pulse" spectrum (lower curve) displays a sharp drop to almost zero at a characteristic value of $k/H$. As we discussed earlier, we expect that the positive friction will affect most strongly the high-$k$ modes. A more quantitative estimate can be made by observing that the matrix $M$ of eqs. (5.9) involves the Bessel functions $J_{\pm\kappa_1/2}$ and $J_{\mp 1 \pm \kappa_1/2}$. For large $\kappa_1$ these functions have a zero at a value of their argument roughly equal to $\kappa_1/2$. The relevant argument in our case is $e^{-\bar{N}} k/H$, with $\bar{N} \simeq (N_1 + N_2)/2$. Thus, we expect the spectrum to approach zero at $k/H \simeq e^{\bar{N}} \kappa_1/2 \simeq 44$, consistently with what is observed.

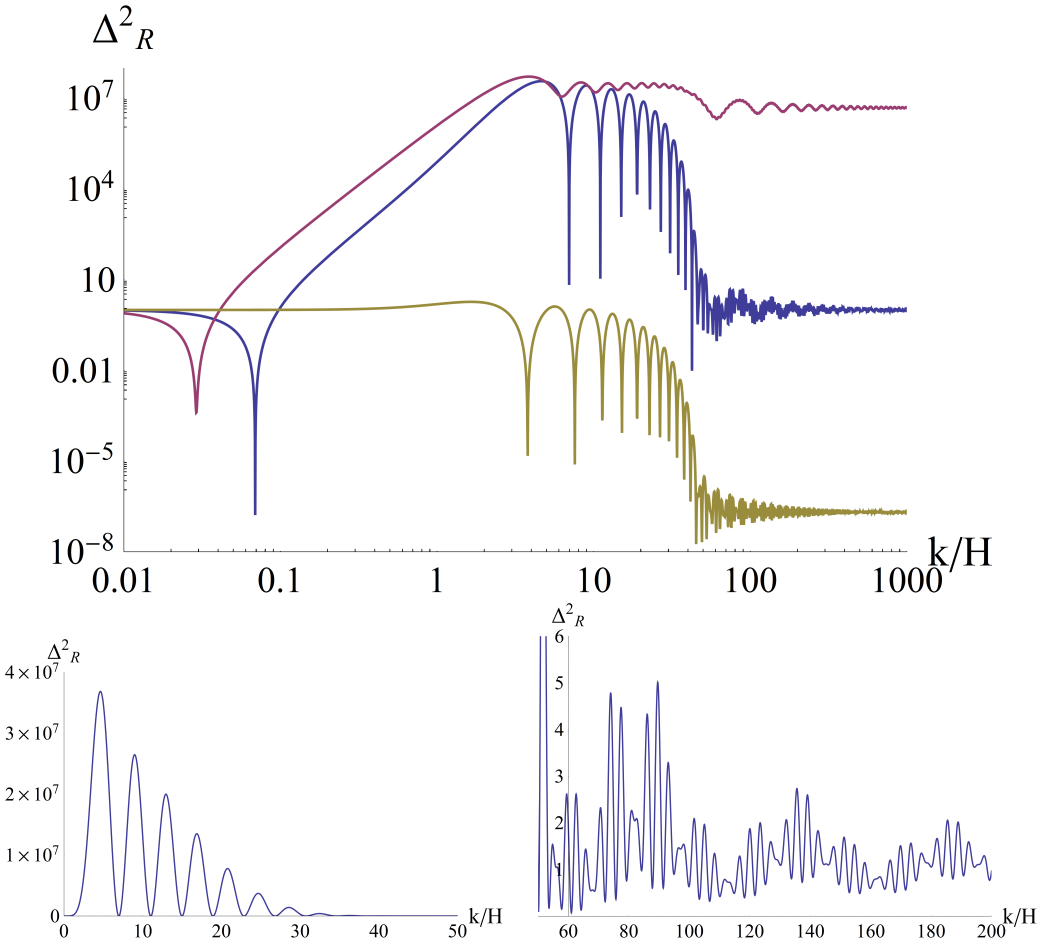


Figure 5.5: Middle curve: Spectrum resulting from a double "pulse" with $N_1 = 0$, $N_2 = 0.2$, $N_3 = 2.77$, $\kappa_1 = 80$, $\kappa_2 = -3$ (Ex. 1). Upper curve: Spectrum resulting from a negative-friction single "pulse" with $\kappa_2 = -3$ between $N_2 = 0.2$, $N_3 = 2.77$. Lower curve: Spectrum resulting from a positive-friction single "pulse" with $\kappa_1 = 80$ between $N_1 = 0$, $N_2 = 0.2$.

4. For $k/H \to \infty$, all three spectra become asymptotically constant, with values given by the exponential of the integral of $f(N) - 3$ over $N$. For the middle spectrum, we have fine-tuned this integral to zero, so that the spectrum returns to the value 1 to which we have normalized the spectrum for $k \to 0$.

5. Apart from the main features that we described above, which are consistent with the general expectations [149], the spectra display oscillations with characteristic scales. As we discussed in subsection 5.1.3, the asymptotic expansions of eqs. (5.15) indicate that the spectrum

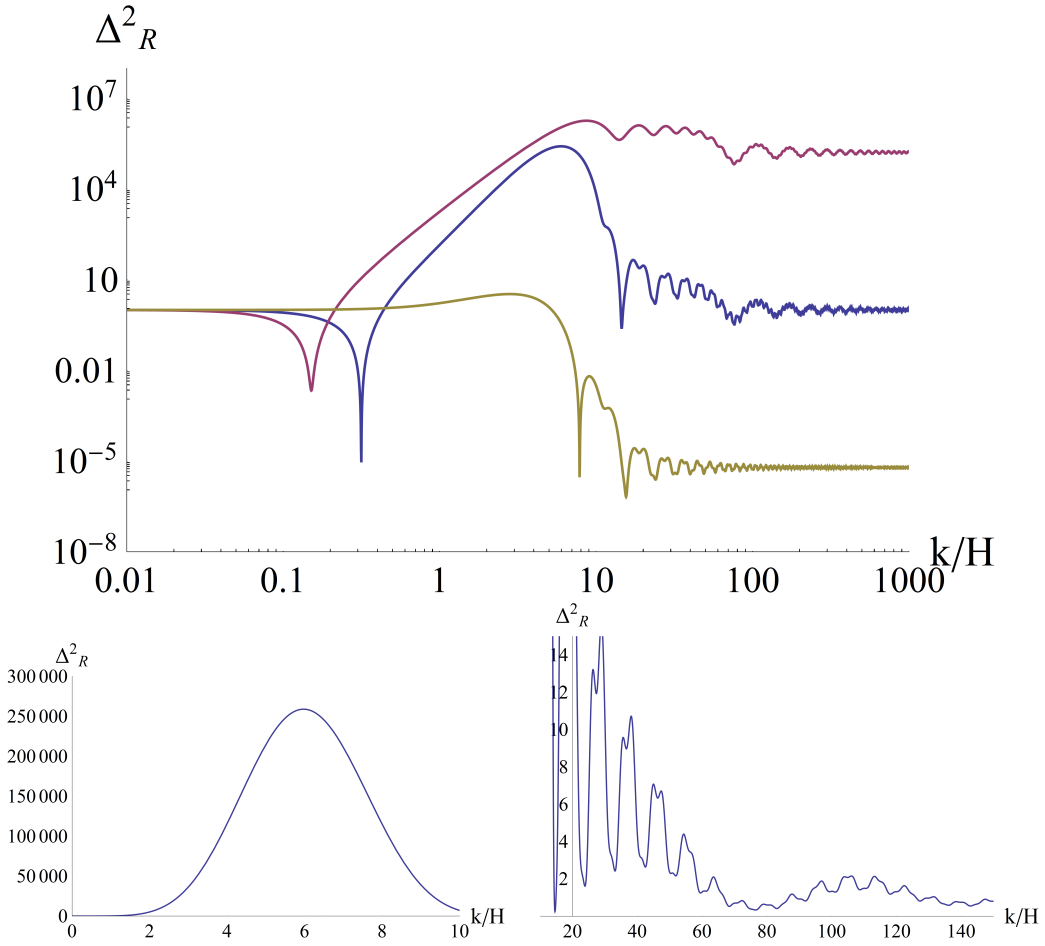


Figure 5.6: Middle curve: Spectrum resulting from a double "pulse" with $N_1 = 0$, $N_2 = 1$, $N_3 = 3$, $\kappa_1 = 15$, $\kappa_2 = -3$ (Ex. 2). Upper curve: Spectrum resulting from a negative-friction single "pulse" with $\kappa_2 = -3$ between $N_2 = 1$, $N_3 = 3$. Lower curve: Spectrum resulting from a positive-friction single "pulse" with $\kappa_1 = 15$ between $N_1 = 0$, $N_2 = 1$.

should oscillate with periods $\delta k/H \simeq e^{N_1}\pi = 3.1$, $\delta k/H \simeq e^{N_2}\pi = 3.8$ and $\delta k/H \simeq e^{N_3}\pi = 50$. These characteristic modes, as well as interference patterns between them, are visible in the bottom plots of fig. 5.5.

The most important conclusion that can be drawn from this example is that strong features in the background evolution can induce a spectrum of fluctuations which displays, apart from an enhancement by several orders of magnitude, strong oscillatory patterns. This is clearly visible in the bottom

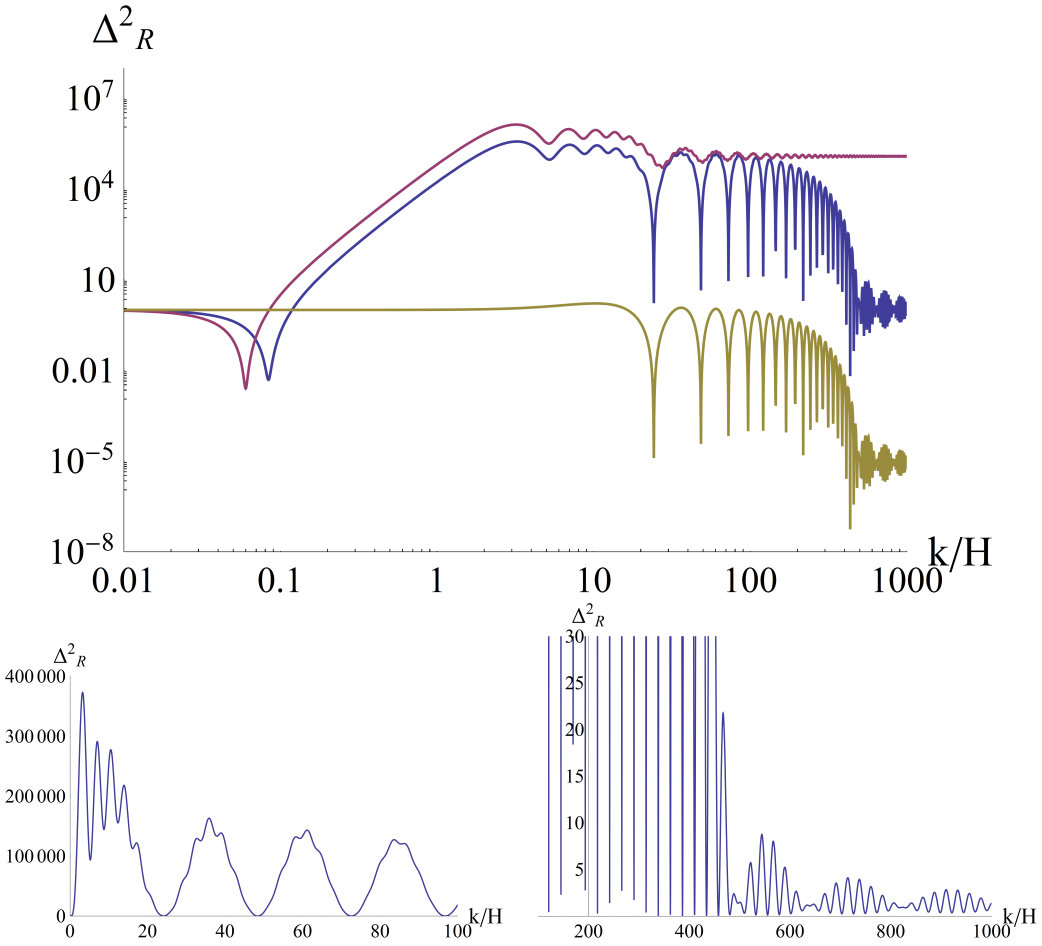


Figure 5.7: Middle curve: Spectrum resulting from a double "pulse" with $N_1 = 0$, $N_2 = 1.95$, $N_3 = 2.05$, $\kappa_1 = -3$, $\kappa_2 = 120$ (Ex. 3). Upper curve: Spectrum resulting from a negative-friction single "pulse" with $N_1 = 0$, $N_2 = 1.95$, $\kappa_1 = -3$. Lower curve: Spectrum resulting from a positive-friction single "pulse" with $\kappa_2 = 120$ between $N_2 = 1.95$, $N_3 = 2.05$.

left plot of fig. 5.5.

We turn next to our second example (Ex. 2). The oscillatory features in the spectrum are less pronounced for different forms of the "pulses". Reducing the height of the positive-friction "pulse" leads to a suppression of the spectrum at smaller values of $k/H$. As a result, the oscillatory patterns may be confined within the high-$k$ part of the spectrum, which does not get enhanced. This is visible in fig. 5.6, where we plot the spectrum in the $k$-range, $k/H = 10^{-2} - 10^3$ or from $N \simeq -4.6$ up to 6.9. The spectrum results from a positive-friction "pulse" with $\kappa_1 = 15$ in the interval between $N_1 = 0$ and

$N_2 = 1$, followed by a negative-friction "pulse" with $\kappa_2 = -3$ in the interval between $N_2 = 1$ and $N_3 = 3$. The drop of the spectrum arising from only the positive-friction "pulse" is expected to appear at $k/H \simeq e^{\bar{N}}\kappa_1/2 \simeq 12$, where $\bar{N} \simeq (N_1 + N_2)/2$. Indeed, the small-$k$ region displays a large enhancement, but the oscillations appear only at large values of $k/H$, at which the spectrum is suppressed. The bottom left plot of fig. 5.6 shows that the enhanced part of the spectrum is smooth in this case. The expected oscillatory modes with periods $\delta k/H \simeq e^{N_1}\pi = 3.1$, $\delta k/H \simeq e^{N_2}\pi = 8.5$ and $\delta k/H \simeq e^{N_3}\pi = 63$, as well as interference patterns between them, are visible in the bottom right plot of fig. 5.6.

Our third example (Ex. 3) demonstrates that spectra with a different structure can result from different forms of the function $f(N)$. More specifically, the positive- and negative-friction "pulses" may occur in the reverse order compared to the one we assumed up till now. In fig. 5.7 we plot the resulting spectra in the range $k/H = 10^{-2} - 10^3$ ($N \simeq -4.6$ up to 6.9) considering an effective friction function $f(N)$ composed of a negative-friction "pulse" with $\kappa_1 = -3$ in the interval between $N_1 = 0$ and $N_2 = 1.95$, followed by a strong positive-friction "pulse" with $\kappa_2 = 120$ in the interval between $N_2 = 1.95$ and $N_3 = 2.05$. The reduction of the spectrum is expected at a scale $k/H \simeq e^{\bar{N}}\kappa_2/2 \simeq 440$, where $\bar{N} \simeq (N_2 + N_3)/2$. The oscillatory patterns have characteristic periods $\delta k/H \simeq e^{N_1}\pi = 3.1$, $\delta k/H \simeq e^{N_2}\pi = 22.1$ and $\delta k/H \simeq e^{N_3}\pi = 24.4$. All these features, as well as strong interference patterns arising from the proximity of two characteristic periods, are visible in fig. 5.7.

### 5.1.6 Sharp feature approximation

Explicit expressions can be obtained for the case of a "pulse" of large positive amplitude and very short duration. For large positive values of $\kappa$ and a short interval $\delta N$, we can approximate the Bessel function as

$$J_a(z) = \frac{1}{\Gamma(a+1)}\left(\frac{z}{2}\right)^a \left(1 - \frac{z^2}{4(1+a)} + \mathcal{O}(z^4)\right). \tag{5.26}$$

We find that

$$M^{(\mathrm{sharp})}_{\mathrm{pulse}}(N_1, k) = e^{N_1}\frac{H}{k}\begin{pmatrix} T_{11} & T_{12} \\ T_{21} & T_{22}\end{pmatrix}\left(1 + \mathcal{O}\left(\frac{1}{2\kappa}\left(e^{-N_1}\frac{k}{H}\right)^2\right)\right), \tag{5.27}$$

where

$$\begin{aligned}
T_{11} &= \cos\left(e^{-N_1}\frac{k}{H}\right)\left(e^{-N_1}\frac{k}{H}\cos\left(e^{-N_1}\frac{k}{H}\right)-\sin\left(e^{-N_1}\frac{k}{H}\right)\right),\\
T_{12} &= \cos\left(e^{-N_1}\frac{k}{H}\right)\left(e^{-N_1}\frac{k}{H}\sin\left(e^{-N_1}\frac{k}{H}\right)+\cos\left(e^{-N_1}\frac{k}{H}\right)\right),\\
T_{21} &= \sin\left(e^{-N_1}\frac{k}{H}\right)\left(e^{-N_1}\frac{k}{H}\cos\left(e^{-N_1}\frac{k}{H}\right)-\sin\left(e^{-N_1}\frac{k}{H}\right)\right),\\
T_{22} &= \sin\left(e^{-N_1}\frac{k}{H}\right)\left(e^{-N_1}\frac{k}{H}\sin\left(e^{-N_1}\frac{k}{H}\right)+\cos\left(e^{-N_1}\frac{k}{H}\right)\right). \qquad (5.28)
\end{aligned}$$

For $k/H \lesssim e^{N_1}\sqrt{2\kappa}$ the presence of the "pulse" does not induce a suppression of the perturbation. The only effect is the introduction of oscillations in the spectrum. The spectrum is expected to have a deep minimum once per period, i.e. at intervals $\delta k/H = e^{N_1}\pi$. The suppression of the perturbation by $\exp(-\kappa\,\delta N)$ is expected to occur for $k/H \gtrsim e^{N_1}\sqrt{2\kappa}$.

After a step in the potential is crossed, the inflaton settles in a slow-roll regime on a flat part of the potential. During the approach to slow-roll, the evolution is dominated by the first two terms in the equation of motion of the background field: $\ddot{\phi} + 3H\dot{\phi} = 0$. This means that, during an interval $N_1 \leq N \leq N_2$, we have $\eta_H \simeq 3$ and $\kappa = -3$. We can define the matrix

$$M^{(\mathrm{negative})}_{\mathrm{pulse}}(N_1, N_2, k) = M(N_2, -3, 3, k)\cdot M(N_1, 3, -3, k) \qquad (5.29)$$

in order to account for the effect on the curvature perturbation, similarly to the treatment above. Then, the total effect on the coefficients of the Bessel functions, arising from crossing a step in the potential, is given by

$$\begin{pmatrix} C_{p_f} \\ C_{m_f} \end{pmatrix} = M^{(\mathrm{negative})}_{\mathrm{pulse}}(N_1, N_2, k)\cdot M^{(\mathrm{sharp})}_{\mathrm{pulse}}(N_1, k)\begin{pmatrix} 1 \\ i \end{pmatrix}. \qquad (5.30)$$

The value of the spectrum relative to the scale-invariant case is determined by $|C_{m_f}|^2$. We can obtain an explicit expression for the enhancement of the spectrum by evaluating $C_{m_f}$ through eq. (5.30), keeping the leading contribution for $M^{(\mathrm{sharp})}_{\mathrm{pulse}}(N_1, k)$. By defining $\tilde{k} = e^{-N_1}k/H$ and $\epsilon = \exp(-N_2+N_1)$, we find

$$|C_{m_f}|^2 = \frac{1+\tilde{k}^2}{4\epsilon^{12}\tilde{k}^{12}}\left(A_1\sin(\tilde{k}) + A_2\cos(\tilde{k}) + A_3\sin(\tilde{k}-2\epsilon\tilde{k}) + A_4\cos(\tilde{k}-2\epsilon\tilde{k})\right)^2, \qquad (5.31)$$

with

$$\begin{aligned} A_1 &= 9\tilde{k} + 9\epsilon^2\tilde{k}^3 - 6\epsilon^3\tilde{k}^3 + 2\epsilon^3\tilde{k}^5 \\ A_2 &= 9 - 3\tilde{k}^2 + 9\epsilon^2\tilde{k}^2 - 3\epsilon^2\tilde{k}^4 + 6\epsilon^3\tilde{k}^4 \\ A_3 &= -9\tilde{k} + 18\epsilon\tilde{k} - 6\epsilon\tilde{k}^3 + 9\epsilon^2\tilde{k}^3 \\ A_4 &= -9 + 3\tilde{k}^2 - 18\epsilon\tilde{k}^2 + 9\epsilon^2\tilde{k}^2 - 3\epsilon^2\tilde{k}^4. \end{aligned} \tag{5.32}$$

In order for a step to increase the spectrum by several orders of magnitude, one must have $N_2 - N_1 \gtrsim 1$. Modes with $e^{-N_1}k/H = \mathcal{O}(1)$ satisfy $e^{-N_2}k/H \ll 1$. In this momentum range we can expand eq. (5.31) in $\epsilon$ and keep the leading contribution

$$|C_{m_f}|^2 \simeq e^{6(N_2-N_1)}\frac{4(1+\tilde{k}^2)}{\tilde{k}^6}\left(3\tilde{k}\cos(\tilde{k}) + (-3+\tilde{k}^2)\sin(\tilde{k})\right)^2. \tag{5.33}$$

The maximal enhancement is given by eq. (5.17), taking into account only the contribution from the negative "pulse". There is also oscillatory behaviour induced by sines and cosines of $\exp(-N_1)k/H$. The combined effect indicates that the power spectrum near its maximum is enhanced through the negative "pulse", but also develops strong oscillations at intervals $\delta k/H = e^{N_1}\pi$. We emphasize that the expressions (5.31) and (5.33) are valid only near the maximum of the spectrum. They do not account for the expected drop of the spectrum for $e^{-N_1}k/H \gtrsim \sqrt{2\kappa}$, with $\kappa$ the height of the positive sharp "pulse".

In fig. 5.8 we test the accuracy of the various analytic results of this subsection in the case of square "pulses". The top row displays the spectra for two cases: a) a positive "pulse" of height $\kappa = 100$ between $N_1 = 0$ and $N_1' = 0.05$, followed by a negative "pulse" of height $-3$ between $N_1' = 0.05$ and $N_2 = 0.858$, and b) a positive "pulse" of height $\kappa = 50$ between $N_1 = 0$ and $N_1' = 0.1$, followed by a negative "pulse" of height $-3$ between $N_1' = 0.1$ and $N_2 = 0.883$. These are simplified versions of the typical evolution of $f(N)$ when the background inflaton crosses steps in the potential of variable steepness. The integrated area of the negative "pulse" is approximately the same in both cases, so that a comparable enhancement of the spectrum is expected. The spectra in the top row have been computed through the numerical solution of eq. (5.1) and the complete expression of eq. (5.30). These methods agree very well. The bottom row displays the approximation of eq. (5.31) (left plot) and the approximation of eq. (5.33) (right plot). Both these expressions assume $N_1' \simeq N_1$, while they do not depend on the height $\kappa$ of the positive "pulse", as long as this is very large. We have used

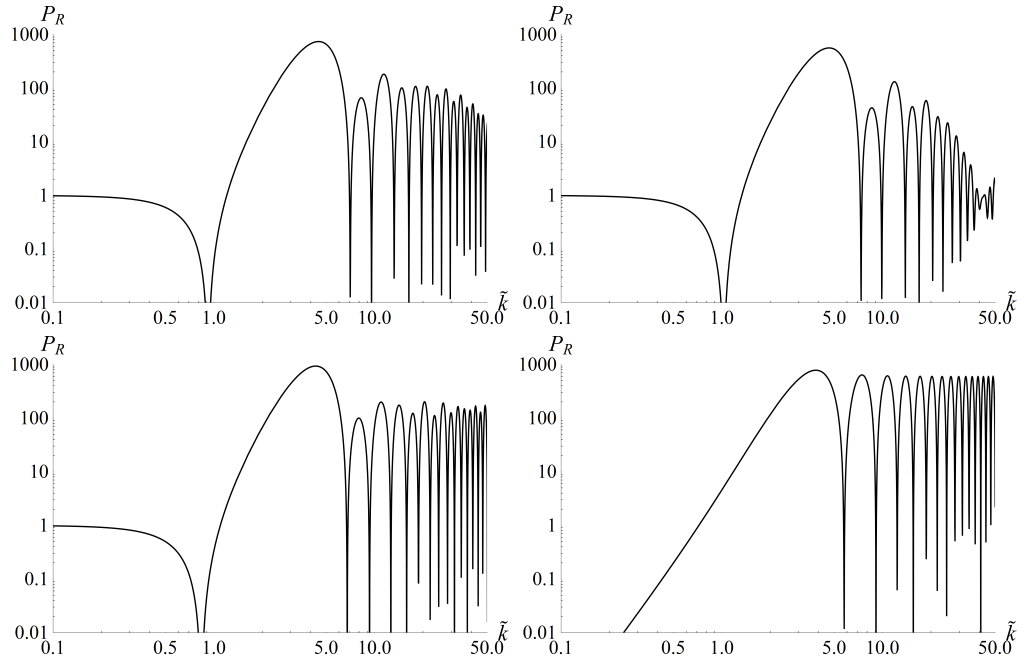


Figure 5.8: The power spectrum induced by a positive "pulse" of height $\kappa$ between $N_1$ and $N_1'$, followed by a negative "pulse" of height $-3$ between $N_1'$ and $N_2$, as a function of $\tilde{k} = e^{-N_1}k/H$. Top row, left plot: $\kappa = 100$, $N_1 = 0$, $N_1' = 0.05$, $N_2 = 0.858$. Top row, right plot: $\kappa = 50$, $N_1 = 0$, $N_1' = 0.1$, $N_2 = 0.883$. Bottom row, left plot: The approximation of eq. (5.31) for $N_1 = 0$, $N_2 = 0.833$. Bottom row, right plot: The approximation of eq. (5.33) for $N_1 = 0$, $N_2 = 0.833$. We have symbolised $P_R \equiv \Delta_R^2$.

$N_1 = 0$, $N_2 = 0.833$. It is apparent that eq. (5.31) reproduces very well the form of the spectrum for $e^{-N_1}k/H \lesssim \sqrt{2\kappa}$. For larger values of $k$, the expected drop of the spectrum is not captured by this approximation. The deviation is clearer in the right plot, for which $\kappa$ is smaller and the drop sets in earlier. On the other hand, eq. (5.33) is a cruder approximation. However, its simplicity makes it very useful for estimating the magnitude of the enhancement of the spectrum, as well as the fundamental frequency of oscillations.

### 5.1.7 Multiple "pulse" features

In this subsection we examine the effect on the power spectrum of several "pulses" in the evolution of $f(N)$. A similar effect has already been discussed in the previous chapter through a numerical solution of eq. (5.1).

We specialize in the case of "pulses" generated through steps in the in-

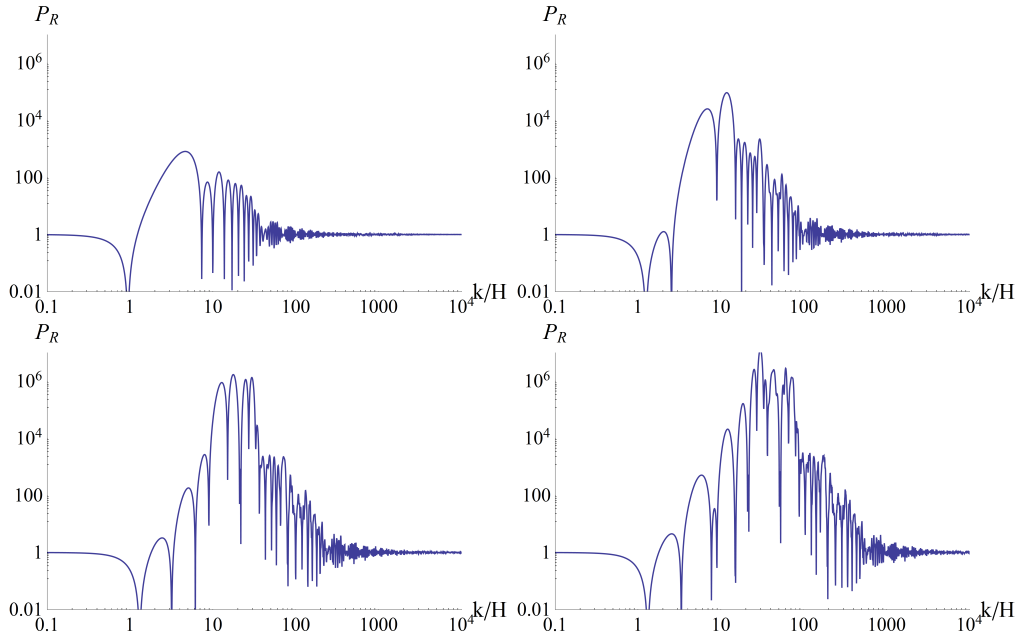


Figure 5.9: Power spectra induced by successive occurrences of a feature consisting of a positive "pulse" of height $\kappa = 50$ between $N_1 = 0$ and $N_1' = 0.1$, followed by a negative "pulse" of height $\kappa = -3$ between $N_1' = 0.1$ and $N_2 = 0.883$. Top row: one feature (left plot), two features (right plot). Bottom row: three features (left plot), four features (right plot).

flaton potential. The effect of one step is captured by the relation (5.30). In most cases one step is not sufficient to induce an enhancement of the spectrum by more than three or four orders of magnitude. It must be noted, however, that an enhancement by up to seven orders of magnitude is possible for an appropriately engineered potential and step profile [155]. The generalization to several steps is straightforward, through the inclusion of several $M_{\rm pulse}$ matrices, and can lead to further enhancement.

In fig. 5.9 we present spectra induced by one or more features in the evolution of $f(N)$, consisting of a positive "pulse" of height $\kappa = 50$ between $N_1 = 0$ and $N_1' = 0.1$, followed by a negative "pulse" of height $\kappa = -3$ between $N_1' = 0.1$ and $N_2 = 0.883$. We present four spectra, arising when one, two (top row), three or four (bottom row) such features occur, one immediately after the other. As has been discussed in the previous chapter, such features result from multiple steep steps in the inflaton potential. The spectra obtained for one feature are consistent with those derived through similar approaches [149,156]. Moreover, it is apparent that multiple features

act constructively, increasing the enhancement of the spectrum. A multitude of characteristic frequencies also appear through the dependence of the spectrum on combinations of the form $e^{-N_i}k/H$, with $N_i$ corresponding to the time that a sharp transition occurs in the evolution of $f(N)$.

It is important to note that the various sets of "pulses" should be placed close to each other for the enhancement of the power spectrum to be significant. Similarly, the corresponding steps in the inflaton potential must be close. If we increase the distance in efoldings between the sets of "pulses", the additive effect is not as strong. Beyond a certain distance, each set acts independently on the spectrum, giving a moderate enhancement within a different $k$-range.

## 5.2 Analytical treatment for general $f(N)$

### 5.2.1 Integral equations

In this subsection we derive analytical expressions for the curvature spectrum resulting from an arbitrary friction function $f(N)$. We start by rewriting eq. (5.1) as

$$R_{k,NN} + 3R_{k,N} + \frac{k^2}{e^{2N}H^2}R_k = (3 - f(N))R_{k,N}. \tag{5.34}$$

We would like to compute the Green's function $G_k(N, n)$ for the operator in the lhs. This function satisfies the equation

$$G_{k,NN}(N, n) + 3G_{k,N}(N, n) + \frac{k^2}{e^{2N}H^2}G_k(N, n) = \delta(N - n). \tag{5.35}$$

Then, the solution of eq. (5.34) is

$$R_k(N) = \bar{R}_k(N; 1, i, 3) + \int_{-\infty}^{\infty} G_k(N, n)\,(3 - f(n))\,R_{k,n}(n)\,dn, \tag{5.36}$$

with

$$\bar{R}_k(N; 1, i, 3) = -\sqrt{\frac{2}{\pi}}\left(\frac{H}{k}\right)^{3/2}\left(i + e^{-N}\frac{k}{H}\right)\exp\left(ie^{-N}\frac{k}{H}\right) \tag{5.37}$$

the solution of the homogeneous equation, corresponding to $f(N) = 3$.

The evolution is classical, so we must use the retarded Green's function, which satisfies $G_{k>}(N, n) = 0$ for $n > N$. For $n < N$ the Green's function is

$$G_{k<}(N, n) = e^{-\frac{3}{2}N}\left(A(n)J_{3/2}\left(e^{-N}\frac{k}{H}\right) + B(n)\,J_{-3/2}\left(e^{-N}\frac{k}{H}\right)\right). \tag{5.38}$$

The total Green's function is continuous at $N = n$. Its first derivative has a discontinuity, obtained by integrating eq. (5.35) around $N = n$. This gives $\partial G_{k<}(N,n)/\partial N|_{N=n} = 1$. Imposing these constraints results in

$$A(n) = -\sqrt{\frac{\pi}{2}} e^{3n} \left(\frac{k}{H}\right)^{-\frac{3}{2}} \left[\cos\left(e^{-n}\frac{k}{H}\right) + e^{-n}\frac{k}{H}\sin\left(e^{-n}\frac{k}{H}\right)\right] \quad (5.39)$$

$$B(n) = \sqrt{\frac{\pi}{2}} e^{3n} \left(\frac{k}{H}\right)^{-\frac{3}{2}} \left[e^{-n}\frac{k}{H}\cos\left(e^{-n}\frac{k}{H}\right) - \sin\left(e^{-n}\frac{k}{H}\right)\right]. \quad (5.40)$$

Despite its simple form, it is difficult to find solutions of eq. (5.36). However, the equation becomes simpler for $N \to \infty$, which is the limit of interest for the late-time spectrum. From eq. (5.38) we obtain

$$G_{k<}(N,n) \to -\sqrt{\frac{2}{\pi}} \left(\frac{H}{k}\right)^{3/2} B(n) \quad (5.41)$$

in this limit. Eq. (5.36) now becomes

$$R_k(\infty) = \bar{R}_k(\infty;1,i,3) - \sqrt{\frac{2}{\pi}} \left(\frac{H}{k}\right)^{3/2} \int_{-\infty}^{\infty} (3 - f(n))\, B(n)\, R_{k,n}(n)\, dn, \quad (5.42)$$

with

$$\bar{R}_k(\infty;1,i,3) = -i\sqrt{\frac{2}{\pi}} \left(\frac{H}{k}\right)^{3/2}. \quad (5.43)$$

Even though an analytical solution of this equation is not available, some conclusions about its form can be drawn when the function $f(N)$ displays strong features. The clearest example is a feature that can be approximated through a $\delta$-function centered at $N_1$. The integration over $n$ results in an expression that includes $\sin(e^{-N_1}k/H)$ and $\cos(e^{-N_1}k/H)$, producing oscillatory patterns. A similar conclusion can be reached if $f(N)$ involves sharp step-like features approximated through $\Theta$-functions, as we discussed in the previous section. These patterns are expected to become less prominent when the features in $f(N)$ become smoother.

An approximate expression, which can be considered as the first step in an iterative solution of the above equation, can be obtained if we replace the full solution $R_k(n)$ in the integral with the solution for $f(n) = 3$, given by $\bar{R}_k(n,1,i,3)$. We have

$$\bar{R}_{k,n}(n,1,i,3) = \sqrt{\frac{2}{\pi}} \left(\frac{k}{H}\right)^{1/2} e^{-2n} \left[i\cos\left(e^{-n}\frac{k}{H}\right) - \sin\left(e^{-n}\frac{k}{H}\right)\right]. \quad (5.44)$$

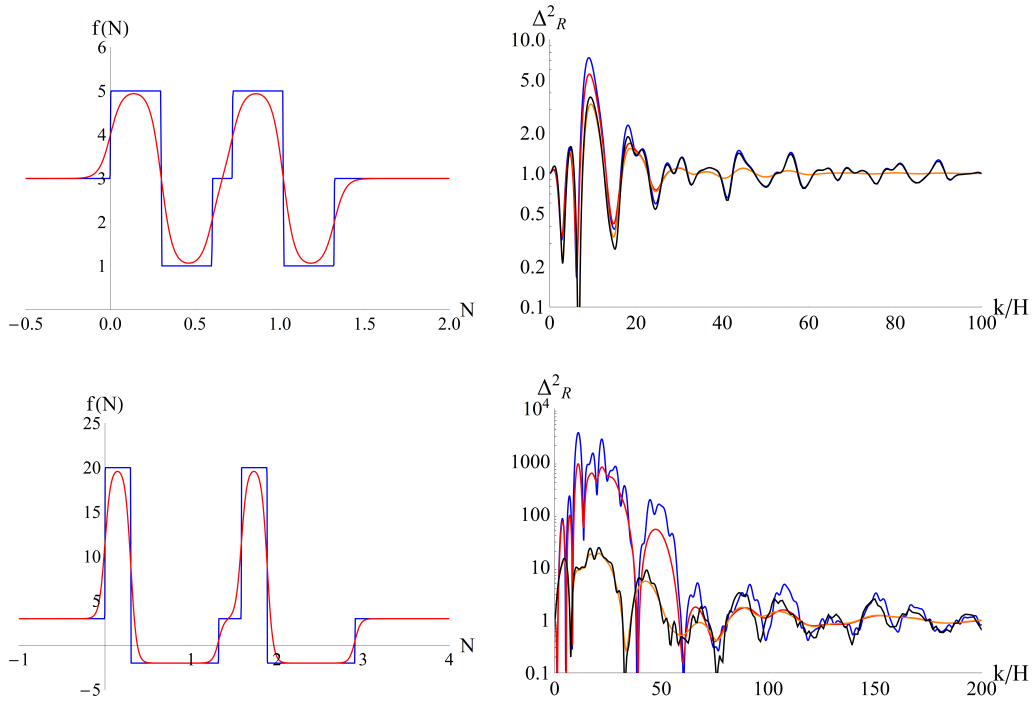


Figure 5.10: Curvature power spectra for various forms of the friction function $f(N)$ (blue and red curves), compared to predictions by eq. (5.45) (black and orange curves).

Combining the above expressions, we obtain

$$R_k(\infty) = \bar{R}_k(\infty;1,i,3)\Bigg\{1 - i\frac{H}{k}\int_{-\infty}^{\infty}(3-f(n))\,e^n\times$$
$$\left[e^{-n}\frac{k}{H}\cos\left(e^{-n}\frac{k}{H}\right) - \sin\left(e^{-n}\frac{k}{H}\right)\right]\left[i\cos\left(e^{-n}\frac{k}{H}\right) - \sin\left(e^{-n}\frac{k}{H}\right)\right]\,dn\Bigg\}, \tag{5.45}$$

This result is expected to be valid only for cases without a large enhancement of the spectum. However, it is a compact expression that can be used in order to deduce the expected oscillatory patterns for a general form of $f(N)$.

In fig. 5.10 we examine the validity of eq. (5.45) for $f(N)$ with sharp and smooth features. In the left plot of the first line we depict the sharp and smoothed version (blue and red lines, respectively) of a friction function with moderate deviations from 3. In the right plot we depict the corresponding exact spectra (blue and red lines, respectively), as well as the ones computed through the approximate expression of eq. (5.45) (black and orange lines,

respectively). It is apparent that this expression captures with very good accuracy the complicated oscillatory patterns: the blue and black lines, as well as the red and orange lines, are in very good agreement. Small deviations from the exact solutions are observed when the amplitude becomes large. In the second line we repeat the calculation for a function $f(N)$ with very strong features that result in a large enhancement of the spectrum. The limitations of eq. (5.45) in capturing the magnitude of the enhancement become apparent. The agreement between black-blue lines and red-orange lines is good only for large values of $k/H$, for which the deviations from the scale-invariant spectrum are small (but still of O(1)). Clearly, higher orders in the iterative solution of eq. (5.42) are needed in order to capture the strong enhancement of the spectrum at small values of $k/H$.

Despite the limited range of validity of eq. (5.45), it is interesting that the predicted oscillatory pattern appears in good agreement with the exact result in all cases. This indicates that the characteristic frequencies are determined by the convolution of the friction function $f(n)$ with the functions $\sin(e^{-n}k/H)$ and $\cos(e^{-n}k/H)$ in eq. (5.42), even if $R_k(n)$ deviates strongly from the unperturbed solution $\bar{R}_k(n;1,i,3)$ of eq. (5.37). In this respect, eq. (5.45) provides the means for estimating the frequencies that appear in the power spectra for a general form of the friction function $f(N)$.

### 5.2.2 System of differential equations

It is apparent that we can rewrite eq. (5.36) as

$$R_k(N) = \bar{R}_k(N;1,i,3) + \int_{-\infty}^{N} G_k(N,n)\,(3-f(n))\,R_{k,n}(n)\,dn, \qquad (5.46)$$

as the function $G_k(N,n)$ vanishes for $n > N$. Through a partial integration, we can recast this equation as

$$R_k(N) = \bar{R}_k(N;1,i,3) - \int_{-\infty}^{N} \frac{\partial}{\partial n}\left[G_k(N,n)\,(3-f(n))\right]\,R_k(n)\,dn, \qquad (5.47)$$

where we have used that $G_k(N,N) = 0$ and $f(n) \to 3$ for $n \to -\infty$. The form (5.38) of the Green's function suggests the ansatz

$$R_k(N) = e^{-\frac{3}{2}N}\left(D(N)J_{3/2}\left(e^{-N}\frac{k}{H}\right) + E(N)\,J_{-3/2}\left(e^{-N}\frac{k}{H}\right)\right). \qquad (5.48)$$

Substituting in eq. (5.47) and matching the coefficients of the Bessel functions, we obtain

$$D(N) = 1 - \int_{-\infty}^{N} \frac{\partial}{\partial n} \left[A(n)\,(3 - f(n))\right] e^{-\frac{3}{2}n} \Bigg[ J_{\frac{3}{2}}\left(e^{-n}\frac{k}{H}\right) D(n) + J_{-\frac{3}{2}}\left(e^{-n}\frac{k}{H}\right) E(n) \Bigg] dn \tag{5.49}$$

$$E(N) = i - \int_{-\infty}^{N} \frac{\partial}{\partial n} \left[B(n)\,(3 - f(n))\right] e^{-\frac{3}{2}n} \Bigg[ J_{\frac{3}{2}}\left(e^{-n}\frac{k}{H}\right) D(n) + J_{-\frac{3}{2}}\left(e^{-n}\frac{k}{H}\right) E(n) \Bigg] dn. \tag{5.50}$$

In the first step of an iterative solution of the above equations, one substitutes $D(n) = 1$ and $E(n) = i$ within the integrals in the rhs. For $N \to \infty$ the solution (5.48) is dominated by the term proportional to $J_{-3/2}$. Making use of a partial integration within the integral in eq. (5.50), we recover the approximate solution (5.45).

In order to improve on this result, we can differentiate the relations (5.49), (5.50) with respect to $N$, in order to obtain a system of two first-order differential equations:

$$\frac{\partial}{\partial N} \begin{pmatrix} D(N) \\ E(N) \end{pmatrix} = F(N) \begin{pmatrix} D(N) \\ E(N) \end{pmatrix}, \tag{5.51}$$

where

$$F(N) = e^{-\frac{3}{2}N} \begin{pmatrix} \frac{\partial}{\partial N}\left[A(N)\,(f(N)-3)\right] J_{\frac{3}{2}}\left(e^{-N}\frac{k}{H}\right) & \frac{\partial}{\partial N}\left[A(N)\,(f(N)-3)\right] J_{-\frac{3}{2}}\left(e^{-N}\frac{k}{H}\right) \\ \frac{\partial}{\partial N}\left[B(N)\,(f(N)-3)\right] J_{\frac{3}{2}}\left(e^{-N}\frac{k}{H}\right) & \frac{\partial}{\partial N}\left[B(N)\,(f(N)-3)\right] J_{-\frac{3}{2}}\left(e^{-N}\frac{k}{H}\right) \end{pmatrix}. \tag{5.52}$$

The matrix $F(N)$ has vanishing determinant. Its nonzero eigenvalue is $3 - f(N)$. The system of equations (5.51) can be solved numerically with the initial condition $(D(N), E(N)) = (1, i)$ that corresponds to the Bunch-Davies vacuum. This formulation provides an advantage over the numerical solution of eq. (5.1), for which the initial condition is strongly oscillatory. Moreover, it makes it straightforward to analyze alternative assumptions for the vacuum.

The solution of eq. (5.51) can be expressed as

$$\begin{pmatrix} D(N) \\ E(N) \end{pmatrix} = Q(N) \begin{pmatrix} 1 \\ i \end{pmatrix}, \tag{5.53}$$

where $Q(N)$ is the fundamental matrix. An exact determination of $Q(N)$ in closed form is not possible because of the $N$-dependence of $F(N)$. For a slowly varying $F(N)$ (adiabatic limit), an approximate solution is given by

$$Q(N) = \exp(C(N)), \qquad C(N) = \int_{-\infty}^{N} F(n)\, dn. \tag{5.54}$$

In appendix A we provide an assessment of the accuracy of the approximate expression (5.54) as well as (5.45) once again. Both approximations give a very accurate description of the spectrum when its value is of order 1. When the spectrum is significantly enhanced, both approximations lose accuracy. However, eq. (5.54) gives a reasonable approximation to the maximal value of the spectrum and its characteristic frequencies, even for an enhancement by three orders of magnitude.

# Chapter 6

# $\alpha$-attractor models and applications

In this chapter, we consider a specific theoretical framework in which we construct inflationary models with step-like features in the inflaton potential. As we shall see, the conclusions of the two previous chapters apply to these models. Moreover, the models can predict a significant abundance of primordial black holes (PBHs) and produce induced gravitational waves (GWs) that may be detected in the near future. For both PBHs and induced GWs, we do not present a detailed review of the production mechanisms, but we provide instead a short summary that is necessary for the clearness of our calculations. This chapter is based on [151].

## 6.1 The framework of $\alpha$-attractors

A specific framework, which we shall use as the basis for the potentials that we shall consider, is provided by the models of $\alpha$-attractors in supergravity [157,158]. A toy model that demonstrates the role of symmetries is described by the Lagrangian [159]

$$\mathcal{L} = \sqrt{-g}\Bigg[\frac{1}{2}\partial_\mu\chi\partial^\mu\chi + \frac{1}{12}\chi^2 R(g) - \frac{1}{2}\partial_\mu\phi\partial^\mu\phi - \frac{1}{12}\phi^2 R(g) \\ -\frac{1}{36}F^2(\phi/\chi)\left(\chi^2-\phi^2\right)^2\Bigg], \tag{6.1}$$

which is invariant under the conformal transformation

$$g_{\mu\nu} \to e^{-2\sigma(x)} g_{\mu\nu}, \qquad \phi \to e^{\sigma(x)}\phi, \qquad \chi \to e^{\sigma(x)}\chi. \tag{6.2}$$

For constant $F(\phi/\chi)$, there is a global $SO(1,1)$ symmetry that keeps $\chi^2-\phi^2$ constant. The field $\chi$ does not have any physical degrees of freedom and can be eliminated through the gauge-fixing condition $\chi^2-\phi^2=6$. (All dimensionful quantities are expressed in units of $M_{\rm Pl}$.) We parametrize the fields as $\chi=\sqrt{6}\cosh(\varphi/\sqrt{6})$, $\phi=\sqrt{6}\sinh(\varphi/\sqrt{6})$ [159]. The Lagrangian becomes

$$\mathcal{L}=\sqrt{-g}\left[\frac{1}{2}R(g)-\frac{1}{2}\partial_\mu\varphi\partial^\mu\varphi-F^2\left(\tanh\frac{\varphi}{\sqrt{6}}\right)\right]. \tag{6.3}$$

A constant function $F(x)$, which preserves the $SO(1,1)$ symmetry, results in a cosmological constant in this formulation. The value of the cosmological constant is not constrained by the symmetry and is arbitrary.

We can introduce a minimal deformation of the symmetry by assuming that $F(x)$ takes two different values over two continuous ranges of $x$, with a rapid transition in between. A stronger deformation that has been used extensively in the literature assumes that $F(x)$ has a polynomial form. We shall employ a combination of the above choices by assuming that $F(x)$ has the schematic form

$$F(x)=x^n+\sum_i A_i\,\Theta(x-x_i), \tag{6.4}$$

allowing for more than one transition points. In order to avoid unphysical features in the evolution of the inflaton, each step-function is replaced by a continuous function with a sharp transition at $x_i$. A more general framework is provided by the $\alpha$-attractors [157–159]. The Lagrangian includes an additional free parameter $\alpha$ and takes the form

$$\mathcal{L}=\sqrt{-g}\left[\frac{1}{2}R(g)-\frac{1}{2}\partial_\mu\varphi\partial^\mu\varphi-F^2\left(\tanh\frac{\varphi}{\sqrt{6\alpha}}\right)\right]. \tag{6.5}$$

The potentials that result from our assumption for the function $F(x)$ with positive $A_i$ are generalizations of the potential of the Starobinsky model [150], with the addition of one or more steep steps. Allowing for negative values of $A_i$ makes it possible to include inflection points in the potential as well. As our analysis focuses on the phenomenological consequences of general features in the potential, we consider parameters $A_i$ that can take values over the whole real axis. Another important feature of the potential in eq. (6.5) is the sharpness of the transition between ranges of constant vacuum energy. This transition is modelled by a $\Theta$-function in eq. (6.4), but it is smooth in practice. Its steepness affects the oscillatory patterns appearing in the spectra. Because of our lack of understanding of the essence of the cosmological constant, we refrain from explicit model-building, and treat the

steepness as a free parameter. We only point out that the framework of $\alpha$-attractors results in the dependence of the potential on $\tanh(\varphi/\sqrt{6\alpha})$, with $\alpha$ a free parameter. This allows, in principle, for potentials with transitions of arbitrary steepness.

### 6.1.1 Specific models

As we said before, we want to replace the step-functions in eq. (6.4) by continuous functions. In practice, we assume the following form for the function $F$:

$$F(x) = F_0 \left( x + \sum_{i=1}^{n} c_i \tanh\left(d(x - x_i)\right) \right) . \tag{6.6}$$

The corresponding inflationary potential for the field $\varphi$ in the Einstein frame (we regard $\alpha = 1$)

$$V(\varphi) = F^2 \left( \tanh \frac{\varphi}{\sqrt{6}} \right) \tag{6.7}$$

features $n$ step-like transitions. (All dimensionful quantities are given in units of $M_{\rm Pl}$.) Such a potential can lead to an enhancement of the power spectrum of scalar perturbations at particular scales, which can be sufficiently large to trigger PBH formation and induce detectable GWs. In addition, the shape of the scalar power spectrum around its peak is characterized by an oscillatory pattern that can be inherited by the tensor power spectrum. We will discuss these notable phenomenological implications of potentials with steps in the next sections.

The enhancement induced by a step has an upper bound corresponding roughly to a multiplicative factor $\exp(-\Delta N(\kappa - 3))$, see eq.(5.16). Here $\Delta N$ is the interval during which the value $\kappa$ of the effective-friction term (5.2) is smaller than the value $\kappa = 3$ that results in a scale-invariant spectrum. Negative values of $\kappa$ are realized when the background inflaton "decelerates" on the lower plateau, after a sharp transition through a step in the potential. During this stage, which lasts a few efoldings, we have $\varphi_{,NN} \simeq -3\varphi_{,N}$ and $\kappa \simeq -3$. As a result, a single step generally enhances the scalar power spectrum by roughly two or three orders of magnitude. However, it is possible that the potential includes several step-like features. In fig. 6.1 we plot a set of specific examples of inflationary potentials with steps, described by eq. (6.7). These potentials yield 50 to 60 efoldings after the crossing of the CMB scale ($k = 0.05\,\mathrm{Mpc}^{-1}$) and a spectral index value $n_s = 0.969$, within the 68% CL range of Planck [160]. The parameters of these models are $c_i = 7 \times 10^{-3}$. We consider from one ($n = 1$) up to five steps ($n = 5$) in eq. (6.7), placed at $\varphi_1 = 5.7$, $\varphi_2 = 5.55$, $\varphi_3 = 5.4$, $\varphi_4 = 5.25$, $\varphi_5 = 5.1$, respectively. The

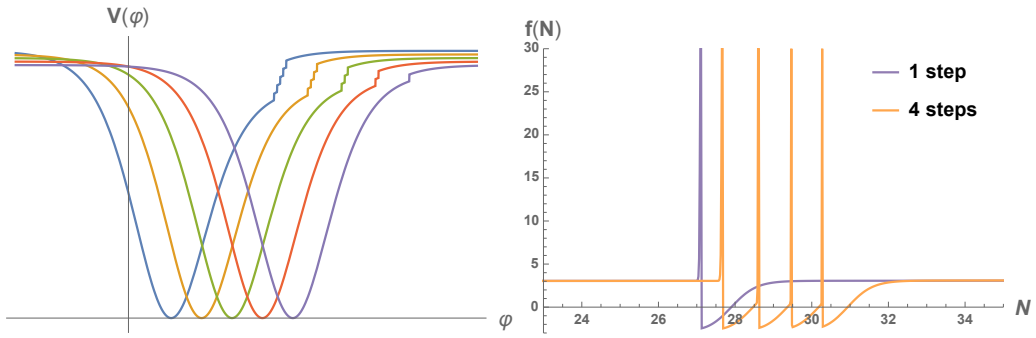


Figure 6.1: Left panel: The inflationary potentials described by eq. (6.7), arbitrary placed on the $\varphi$ axis in order to make the step-like structure visible. Right panel: The function $f(N)$ of eq. (5.2) in terms of the number of efoldings for inflationary potentials with one and four steps.

value of $F_0$ is adjusted each time in order to be consistent with the measured amplitude of the spectrum at the CMB scale. For the initial value of the inflaton field we choose $\varphi_{\rm CMB} = 6.33$, so as to obtain appropriate values for the spectral index $n_s$ and the number of efoldings $N$. The choice of the value of the parameter $d$ is not crucial, as long as it is taken sufficiently large for the transition through the steps to occur quickly, but continuously. Typical values are of order $10^3 - 10^5$.

We also examine the inflationary dynamics of models that feature both a step and a near-inflection point. The production of PBHs and induced GWs due to the presence of a near-inflection point in the framework of $\alpha$-attractors has been studied in [53,56,161]. Such models result in a significant enhancement of the scalar power spectrum, while the presence of a step-like feature adds a prominent oscillatory pattern around the peak value. In fig. 6.2 we plot an example of such a potential, within the $\alpha$-attractor framework, with parameters $c_1 = 8.70 \times 10^{-2}$, $c_2 = -2.77 \times 10^{-4}$. The step is placed at $\varphi_1 = 5.4$ and a shallow nearly-inflection point exists at $\varphi_2 = 4.8$. The spectral index value for this model is $n_s = 0.968$, within the 68% CL region of Planck [160]. The number of efoldings after the crossing of the CMB scale is $N = 51$ for an initial field value $\varphi_{\rm CMB} = 6.17$. In figs. 6.1 and 6.2 we also plot the function $f(N)$ that determines key characteristics of the scalar power spectrum, such as the amplitude and the oscillatory pattern, as discussed in the previous chapters.

In the following sections we examine the cosmological implications for PBH formation and GW production arising from the amplification of the

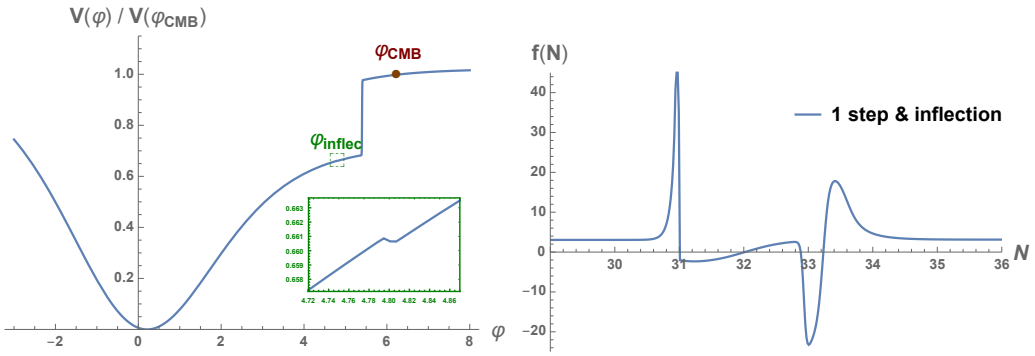


Figure 6.2: Left panel: The inflationary potential with one step and an inflection point as a function of $\varphi$ in Planck units. The model gives $n_s = 0.968$ for an initial field value $\phi_{\rm CMB} = 6.17\, M_{\rm Pl}$. The inflection point at $\phi_{\rm inflec} = 4.8\, M_{\rm Pl}$ is clearly visible through the magnification of the potential in the box. Right panel: The effective-friction function $f(N)$ during the part of the evolution in which it deviates from the standard value $f(N) \simeq 3$.

scalar spectrum by the step-like features in the potential (6.7). Remarkably, models of this type yield striking predictions for the induced GWs that render them testable by the forthcoming GW detection experiments.

## 6.2 Primordial black holes

Inflationary potentials with steps enhance the amplitude of the primordial density perturbations at particular scales and might lead to gravitational collapse and PBH production. We review briefly the observational bounds on the PBH abundance, relevant for our analysis.

In the largest part of the mass spectrum there are stringent upper bounds on $\Omega_{\rm PBH}/\Omega_{\rm DM}$ arising from observational constraints, see fig. 6.3 for monochromatic PBH spectra. Light PBHs are constrained by the extra-galactic gamma ray background (EGB); black holes of mass above $10^{17}$g are subject to constraints from gravitational lensing of stars by Subaru (HSC), Ogle (O), EROS (E) and MACHO (M), microlensing of supernova (SN) and other experiments. The CMB anisotropies measured by Planck (PA) constrain the PBHs with masses above $10^{33}$g. In the large-mass region there are also constraints from accretion limits in X-ray and radio observations and X-ray binaries (XB), and dynamical limits from disruption of wide binaries (WB) and survival of star clusters in Eridanus II (Er). Advanced LIGO/Virgo searches for compact binary systems with component masses in the range $0.2 - 1 M_\odot$ find no GW events. For a detailed discussion and references on the PBH

constraints we refer the reader to [162].

The maximal value of the PBH abundance can be achieved in the mass range $M_{\rm PBH} \sim 10^{-15} - 10^{-10} M_\odot$. Here we focus on this mass window that can be tested by near-future GW experiments, such as LISA. Nonetheless, the parameters of the same inflationary model with step-like features can be adjusted in order to generate PBHs in other mass windows, such as the $\mathcal{O}(10)$ solar mass window that is relevant for the LIGO/Virgo observed events.

The theoretical framework for the PBH formation that we shall follow next is based on the traditional Press-Schechter formalism [163]. Large density perturbations can create overdense regions that may collapse to form black holes after the horizon reentry. We examine separately the two most interesting cosmological scenarios for the very early Universe: the radiation (RD) and matter domination (MD) scenarios.

### 6.2.1 Radiation-dominated era

For a Gaussian distribution function of the primordial density perturbations and for spherically symmetric regions, the mass fraction of PBHs at formation is

$$\beta(M) = \int_{\delta_c} d\delta \frac{1}{\sqrt{2\pi\sigma^2(k)}} e^{-\frac{\delta^2}{2\sigma^2(k)}} \simeq \frac{1}{2}\mathrm{erfc}\left(\frac{\delta_c}{\sqrt{2}\sigma(k)}\right) \simeq \frac{1}{\sqrt{2\pi}}\frac{\sigma(k)}{\delta_c} e^{-\frac{\delta_c^2}{2\sigma^2(k)}}. \tag{6.8}$$

The parameter $\delta_c$ is the threshold density perturbation and $\mathrm{erfc}(x)$ is the complementary error function. For $\delta > \delta_c$ density perturbations overcome the internal pressure and collapse. The $\beta$ parameter can be regarded as the probability that the density contrast is larger than $\delta_c$. The PBH abundance is exponentially sensitive to the threshold $\delta_c$. Different values for $\delta_c$ are quoted in the literature, see e.g. [9, 164–170], so that its precise value seems to be rather uncertain. In the comoving gauge, ref. [168] finds $\delta_c = 0.41$ for $w = 1/3$. Numerical simulations demonstrate that there is no unique value for the threshold, because it depends on the density profile.

In the comoving gauge, assuming a nearly scale-invariant curvature power spectrum for a few efoldings around horizon crossing, the curvature perturbation $R$ can be related to the density perturbation $\delta$ as $\delta(k,t) = 2(1+w)/(5+3w)\,(k/aH)^2\, R(k,t)$. The variance of the density perturbations $\sigma(k)$, smoothed on a scale $k$ in the radiation-dominated era, is given by [171]

$$\sigma^2(k) = \left(\frac{4}{9}\right)^2 \int \frac{dq}{q} W^2(qk^{-1})(qk^{-1})^4 \Delta_R^2(q)\,, \tag{6.9}$$

where $\Delta_R^2(q)$ is the power spectrum of the curvature perturbations, usually calculated numerically. Here $W(z)$ represents the Fourier transform of the

Gaussian window function. In order to estimate the mass spectrum of the PBHs, the horizon scale at the time of reentry of the perturbation mode $k$ has to be related to the mass of formed PBHs. During the radiation era, the wavenumber scales as $k \propto g_*^{1/2} g_s^{-2/3} S^{2/3} a^{-1}$ and the Hubble horizon as $H \propto g_*^{1/2} g_s^{-2/3} S^{2/3} a^{-2}$, where $S$ denotes the entropy, and $g_*$, $g_s$ count the total number of the effectively massless degrees of freedom for the energy and entropy densities respectively. Assuming conservation of the entropy between the reentry moment and the epoch of radiation-matter equality, the relation between the PBH mass $M$ and the comoving wavenumber $k$ is given by

$$M(k) = \gamma \rho \frac{4\pi H^{-3}}{3}\Big|_{k=aH} \simeq 2.4 \times 10^{-16} M_\odot \left(\frac{\gamma}{0.2}\right) \left(\frac{g_*(T)}{106.75}\right)^{-\frac{1}{6}} \left(\frac{k}{10^{14}\,\mathrm{Mpc}^{-1}}\right)^{-2}, \tag{6.10}$$

where we took the effective degrees of freedom $g_*$ and $g_s$ approximately equal. The factor $\gamma$ gives the fraction of the horizon mass $M_H$ that collapses to form PBHs. Its value depends on the details of the gravitational collapse and an analytical estimation [9] gives $\gamma = 0.2$. The present ratio of the abundance of PBHs with mass $M$ over the total dark matter (DM) abundance, $f_{\mathrm{PBH}}(M) \equiv \Omega_{\mathrm{PBH}}(M)/\Omega_{\mathrm{DM}}$, can be expressed as

$$f_{\mathrm{PBH}}(M) = \left(\frac{\beta(M)}{3.3 \times 10^{-14}}\right) \left(\frac{\Omega_{\mathrm{DM}} h^2}{0.12}\right)^{-1} \left(\frac{\gamma}{0.2}\right)^{\frac{3}{2}} \left(\frac{g_*}{106.75}\right)^{-\frac{1}{4}} \left(\frac{M}{10^{-12} M_\odot}\right)^{-\frac{1}{2}}. \tag{6.11}$$

The abundance of PBHs produced during RD can be significant if the scalar spectrum is amplified by roughly 7 orders of magnitude. In our single field models, described by the $\alpha$-attractors potential (6.7), such an enhancement is achieved if the potential involves several steps or a step and an inflection point. In fig. 6.3 we plot the PBH fractional abundance for a potential with a step and an inflection point, for the parameter values listed in section 6.1.1. The scalar power spectrum of this model is depicted in fig. 6.5. For the estimation of the PBH abundance we assumed a threshold value $\delta_c = 0.45$ [167]. We see that, although the scalar power spectrum is characterized by an oscillatory pattern around the peak, the PBH abundance is predominantly monochromatic. However, the induced GW spectrum is much more informative, as we will discuss in the following.

### 6.2.2 Matter-dominated era

PBHs might also form in the matter-dominated era (MD). In the absence of pressure, even minute perturbations will evolve and deviations from spherical

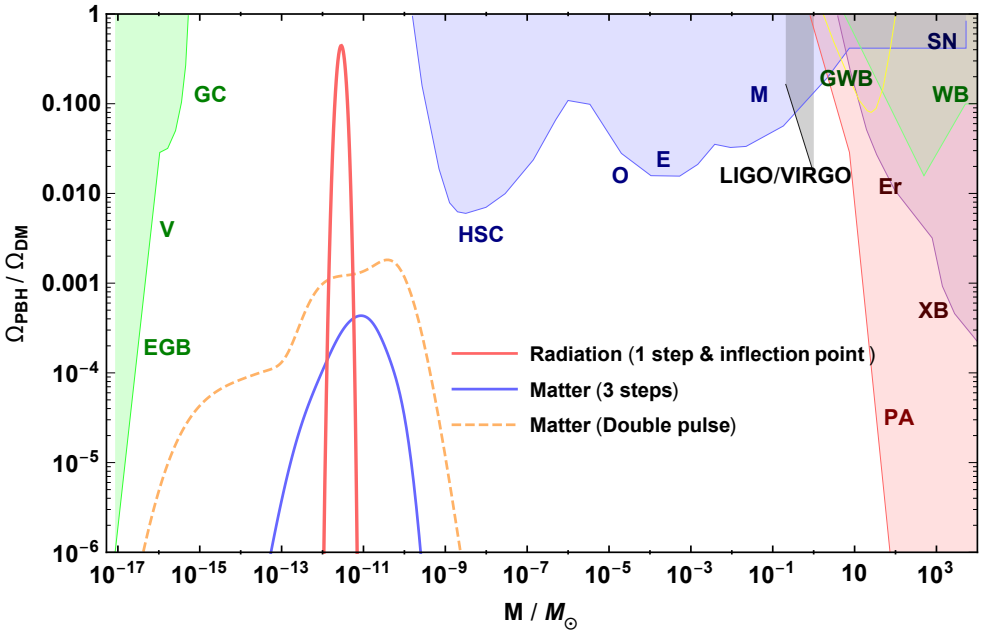


Figure 6.3: The red curve depicts the abundance of PBHs produced by an inflationary model with a step and an inflection point during the RD era. The blue curve depicts the abundance of PBHs produced by an inflationary model with three steps during the MD era. The dashed curve is the PBH abundance produced during the MD era for the double-"pulse" model (termed Ex. 3) of fig. 5.7, in which a negative-friction "pulse" is followed by a positive-friction "pulse".

configurations play an essential role. Refs. [172–174] examined the PBH production in a matter-dominated Universe and considered the non-spherical effects during gravitational collapse. The PBH production rate $\beta$ tends to be proportional to the fifth power of the variance $\sigma$ [174]:

$$\beta(\sigma) \;=\; 0.056\,\sigma^5\,. \tag{6.12}$$

This expression has been derived with semi-analytical calculations and applies to $0.005 \lesssim \sigma \lesssim 0.2$, whereas for $\sigma \lesssim 0.005$ the PBH production rate is modified if there is significant angular momentum in the collapsing region [175]. The PBH fractional abundance is

$$f_{\rm PBH} \simeq 1.3\times 10^9\,\gamma\,\beta\,\frac{T_{\rm rh}}{\rm GeV}\,, \tag{6.13}$$

where $T_{\rm rh}$ is the reheating temperature.

There are two very interesting implications of PBH production during the MD era. Firstly, the PBH abundance is found to be larger compared

to RD for a given amplitude of the curvature power spectrum. Inflationary potentials with steps, which enhance the curvature power spectrum by 4 or 5 orders of magnitude, can have an observational effect by generating a significant cosmological PBH abundance. Secondly, the PBH production during the MD era yields a PBH mass spectrum that is not predominantly monochromatic. It has a distribution over a few orders of the PBH mass values, which might reveal a non-trivial shape for the underlying power spectrum of the primordial density perturbations. Although the specific inflationary models that we examine here do not have a very strong effect on the PBH mass spectrum, inflationary models with steps can in principle produce mild modulations in the distribution of PBHs. The blue curve in fig. 6.3 depicts the PBH abundance produced by an inflationary potential given by eq. (6.7) for three steps, with amplitude $\Delta_R^2 \sim 10^{-4}$ and $T_{\rm rh} \sim 10^3$ GeV. In the same figure, the dashed curve depicts the PBH abundance produced by the double-"pulse" model of fig. 5.7 with $\Delta_R^2 \sim 10^{-3}$ and $T_{\rm rh} \sim 1$ GeV. The spectrum is sufficiently wide and oscillating in order to have an observational impact on the PBH mass distribution.

## 6.3 Induced gravitational waves

Primordial density perturbations that seed PBHs also produce stochastic GWs through the mode-mode coupling of the density perturbations beyond the linear order in the perturbative expansion. The GW production takes place mainly at the time when the perturbations reenter the Hubble horizon. If density perturbations enter during the RD era, the stochastic spectrum of second order GWs can be computed following cosmological perturbation theory [176–185]. The same density perturbations will also produce PBHs with abundance proportional to $\beta$ given by eq. (6.8). On the other hand, if perturbations enter deep in an early MD era, a different analysis has to be followed in order to find the GW energy density spectrum [186, 187]. The corresponding PBH abundance will now be proportional to $\beta$ given by eq. (6.12). In the following we will consider GW production only during the RD era, leaving the study of the early MD era scenario for future work. We will also assume that curvature perturbations are described by Gaussian statistics[1].

The spectrum of the induced GWs is sourced and shaped by the curvature perturbations. We have seen that inflationary potentials with steps generate a distinct oscillatory profile for the curvature power spectrum. We expect

[1]Non-Gaussian statistics may also generate modulations in the GW energy density spectrum [188].

that this profile is transmitted to GWs. In the following we will further elaborate on the modulations of the amplitude in the GW energy density spectrum, which will be found to display a multiple peak structure. We will show in particular that the amplitude and the frequency of the peaks in the GW spectrum are determined by the position and the number of the steps in the inflaton potential. The GW spectrum inherits the pattern characteristics of the curvature power spectrum and, hence, serves as a portal to the inflationary dynamics.

Different GW experiments are sensitive to different frequency bands. Curvature power spectra with a prominent peak at the PBH mass range $10^{-15} - 10^{-10} M_\odot$ generate induced GWs at the frequency band $1 - 10^{-4}$ Hz, and can be tested by space-based interferometers like LISA [189], scheduled to operate in the following decade.

### 6.3.1 The formalism of induced GWs

GWs are described by the tensor perturbation $h_{ij}$ in the FRW spacetime

$$ds^2 = a^2(\tau)\left[-(1+2\phi)d\tau^2 + \left((1-2\psi)\delta_{ij} + \frac{1}{2}h_{ij}\right)dx^i dx^j\right], \tag{6.14}$$

where $\phi$ and $\psi$ are scalar perturbations and vector perturbations are neglected. In the absence of anisotropic stress, which is a good approximation for our purposes, we have $\phi = \psi$. The Fourier components of the tensor modes are defined via the relation

$$h_{ij}(\tau, \mathbf{x}) = \sum_\lambda \int \frac{d^3k}{(2\pi)^{3/2}} h_\lambda(\tau, \mathbf{k}) e_{ij}^{(\lambda)}(\mathbf{k}) e^{i\mathbf{kx}} \tag{6.15}$$

where $e_{ij}^{(\lambda)}$, with $\lambda = +, \times$, are polarization tensors. Through the definition of the dimensionless power spectrum

$$\langle h_\lambda(\tau, \mathbf{k}) h_{\lambda'}(\tau, \mathbf{k}')\rangle = \delta_{\lambda\lambda'}\delta^3(\mathbf{k}+\mathbf{k}')\frac{2\pi^2}{k^3}\mathcal{P}_h(\tau, k) \tag{6.16}$$

we have

$$\rho_{\rm GW}(\tau, k) = \frac{M_{\rm Pl}^2}{8}\frac{k^2}{a^2}\overline{\mathcal{P}_h(\tau, k)}\,. \tag{6.17}$$

The evolution of $h_{ij}$ is obtained by expanding the Einstein equations. At second order in scalar perturbations, the equation of motion for the Fourier components of the tensor perturbations is

$$h_\lambda'' + 2\mathcal{H}h_\lambda' + k^2 h_\lambda = 4S_\lambda(\tau, \mathbf{k})\,, \tag{6.18}$$

where $S_\lambda(\tau, \mathbf{k})$ is a source that consists of products of scalar perturbations:

$$S_\lambda(\tau,\mathbf{k}) = \int \frac{d^3q}{(2\pi)^{3/2}} e^{ij}(\mathbf{k}) q_i\, q_j \Bigg( 2\phi_{\mathbf{q}}\phi_{\mathbf{k}-\mathbf{q}} + \frac{4}{3(1+w)} (\mathcal{H}^{-1}\phi_{\mathbf{q}} + \phi_{\mathbf{q}})(\mathcal{H}^{-1}\phi_{\mathbf{k}-\mathbf{q}} + \phi_{\mathbf{k}-\mathbf{q}}) \Bigg). \tag{6.19}$$

The evolution of $\phi_{\mathbf{k}}$ is given in terms of the scalar transfer function. For radiation domination, we have $\phi_{\mathbf{k}}(\tau) = \phi(x)\ \Phi_{\mathbf{k}}$, with

$$\phi(x) = \frac{9}{x^2} \left( \frac{\sin(x/\sqrt{3})}{x/\sqrt{3}} - \cos(x/\sqrt{3}) \right), \tag{6.20}$$

where $x = k\tau$, and $\Phi_{\mathbf{k}}$ is the primordial value, related to the curvature perturbation as

$$\langle \Phi_{\mathbf{k}} \Phi_{\mathbf{k}'} \rangle = \delta^3(\mathbf{k}+\mathbf{k}') \frac{2\pi^2}{k^3} \left( \frac{3+3w}{5+3w} \right)^2 \Delta_R^2(\tau, k). \tag{6.21}$$

The solution of eq. (6.18) reads

$$h_\lambda(\tau,\mathbf{k}) = \frac{1}{a(\tau)} \int_0^\tau G_k(\tau,\bar{\tau}) a(\bar{\tau}) S_\lambda(\bar{\tau},\mathbf{k}) d\bar{\tau}. \tag{6.22}$$

where $G_k(\tau,\bar{\tau})$ is the Green's function for eq. (6.18). The power spectrum of induced GWs is expressed in a compact form as a double integral involving the power spectrum of the curvature perturbations [190]

$$\overline{\mathcal{P}_h(\tau,k)} = \int_0^\infty dt \int_{-1}^1 ds\ \mathcal{T}(s,t,\tau,k)\ \Delta_R^2\left(\frac{t+s+1}{2}k\right)\ \Delta_R^2\left(\frac{t-s+1}{2}k\right). \tag{6.23}$$

The overline denotes the oscillation average. The $t$ and $s$ variables are defined as $t = u + v - 1$, $s = u - v$, where $v = q/k$, $u = |\mathbf{k}-\mathbf{q}|/k$. The integral kernel $\mathcal{T}$ is given by the expression

$$\begin{aligned} \lim_{x\to\infty} x^2\ \mathcal{T}(s,t,x) = &\ 2\left(\frac{t(2+t)(s^2-1)}{(1-s+t)(1+s+t)}\right)^2 \frac{288(-5+s^2+t(2+t))^2}{(1-s+t)^6(1+s+t)^6} \times \\ &\left\{ \frac{\pi^2}{4} \left(-5+s^2+t(2+t)\right)^2 \Theta\left(t-(\sqrt{3}-1\right) + \right. \\ &\left. \left( -(t-s+1)(t+s+1) + \frac{1}{2}(-5+s^2+t(2+t)) \log\left| \frac{-2+t(2+t)}{3-s^2} \right| \right)^2 \right\}, \end{aligned} \tag{6.24}$$

where $\Theta$ is the Heaviside step function. The fraction of the GW energy density per logarithmic wavenumber interval is

$$\Omega_{\rm GW}(\tau,k)=\frac{1}{\rho_{\rm tot}(\tau)}\frac{d\rho_{\rm GW}(\tau,k)}{d\ln k}=\frac{1}{24}\left(\frac{k}{a(\tau)H(\tau)}\right)^2\overline{\mathcal{P}_h(\tau,k)}\,. \tag{6.25}$$

At a certain time $t_{\rm c}$ the production of induced GWs ceases, while their propagation becomes free. In a RD background the energy density parameter $\Omega_{\rm GW}$ remains constant. Its value at the current time $t_0$ is given by eq. (6.25) times the current radiation density parameter, $\Omega_{\gamma,0}h^2=4.2\times10^{-5}$, modulo changes in the number of the relativistic degrees of freedom $g_*$ in the radiation fluid:

$$\Omega_{\rm GW}(t_0,f)h^2=0.39\times\left(\frac{g_*}{106.75}\right)^{-1/3}\ \Omega_{\gamma,0}h^2\times\Omega_{\rm GW}(t_{\rm c},f). \tag{6.26}$$

The total energy density parameter of induced GWs is obtained by integrating the GW energy density spectrum over the entire frequency interval.

### 6.3.2 Oscillations in the induced GW power spectrum from potentials with steps

We start the discussion of the pattern of induced GWs produced in inflationary models with sharp features by looking at the spectrum characteristics of analytically calculable models, such as those depicted in figs. 5.5-5.7. In the previous chapter we performed a semi-analytic calculation of the curvature power spectrum by modeling the function $f(N)$ of eq. (5.2), which captures the dynamics of the inflaton field beyond the slow-roll regime, through a sequence of square "pulses". The amplitude of the produced curvature power spectrum is enhanced by the factor $|C_m|^2$ of eq. (5.16), while it also displays oscillatory patterns with characteristic periods $\delta k/H\sim e^N\pi$ in $k$-space, where $N$ is the number of efoldings at which the function $f(N)$ varies strongly. (See the discussion below eq. (5.16).) Roughly the same characteristic frequency is observed in the GW spectra. In fig. 6.4 the GW spectra for the three examples studied in section 5.1.5 are plotted. We also plot a function $\Omega_{\rm GWmax}(2+\sin(\alpha_{\rm GW}\,k-\theta))/3$ that highlights the periodic change of the GW amplitude around the peak through a fit of the $k$-space period $\delta k_{\rm GW}\sim 2\pi/\alpha_{\rm GW}$. We find $\alpha_{\rm GW}=\mathcal{O}(1)/H$, corresponding to the smallest period of the oscillations in the curvature spectrum $\delta k/H\sim\mathcal{O}(1)\pi$. It must be noted that larger periods of size $\delta k/H=\mathcal{O}(10)\,\pi$ appearing in $\Delta^2_R$ can also be discerned in the modulations of the amplitude of the GW spectrum at the corresponding scales. However, they are less visible, as they extend to regions in $k$-space far from the peak.

The short-period modulations of order $\pi$ imply that the peaks in the curvature spectrum are narrow. In fig. 6.4 a lognormal distribution with a certain width $\sigma_{\rm N} < 1$ is plotted together with $\Delta^2_R$. It elucidates the prominent two-peak structure induced in the GW spectrum [184, 191, 192], which appears when the main peak of the curvature spectrum is sufficiently narrow. In our first example, for a square pulse starting at $N = 0$, corresponding to the smallest period of oscillations $\delta k/H \simeq \pi$, the peak of $\Delta^2_R$ is found at a wavenumber $k_{\rm p}/H \simeq 4.5$, comparable to $\pi$. The $k$-range of the fitting lognormal distribution is determined by requiring that $\delta k \sim k_{\rm p}(e^{\sigma_{\rm N}} - 1)$, which implies that $\sigma_{\rm N} < 1$. As a result, and in agreement with the analysis of ref. [192], the GW spectrum is found to feature a major, relatively sharp peak at $(2/\sqrt{3})k_{\rm p}/H$. Additionally, in the low-$k$ side there is a relatively flat local maximum, at a wavenumber near $k_{\rm p}/e$. This characteristic two-peak structure is evident in all three examples we studied. In the second example in particular, in which $\Delta^2_R$ is dominated by a single peak because the smallness of the positive "pulse" confines the oscillatory patterns within the high-$k$ part of the spectrum, the two-peak structure is practically the only observable feature.

Let us now turn to the inflationary models with step-like features described by eq. (6.7). In these models, the effective-friction function $f(N)$ of eq. (5.2), depicted in fig. 6.1, can be approximated by a $2n$-"pulse" structure for $n$ steps, with each positive "pulse" followed by a negative one. In the semi-analytically calculable models that we studied before, the power spectrum was normalized such that the step features started at $N = 0$. We observed an enhancement by a factor $|C_m|^2$, together with oscillations of period $\delta k/H \sim e^N \pi$. In the inflationary models of eq. (6.7) we find numerically similar patterns. The curvature spectrum $\Delta^2_R$ is to a good approximation enhanced by $|C_m|^2$, with a main peak at a wavenumber $k_{\rm p}$ characteristic of the position of the step in terms of the number of efoldings $N$, which are now counted from the exit of the CMB scale. Oscillations are also produced with an approximate period $\delta k \sim k_p$.

In fig. 6.5 we plot four curvature power spectra together with the GW density spectra that they induce. For the three-step model, the curvature spectrum displays strong modulations and one can read off an oscillatory pattern with period $\delta k \simeq 2.5 \times 10^{11}\,{\rm Mpc}^{-1}$. The spectrum $\Delta^2_R$ has three prominent peaks at comparable wavenumbers $k_{\rm p1}$, $k_{\rm p2}$, $k_{\rm p3}$. Each peak is well described by a narrow lognormal distribution in the $k$-range with width $\sigma_{\rm N} < 1$. The combination of these three peaks induces a characteristic five-peak structure in the GW spectrum [193], along with the rather flat local

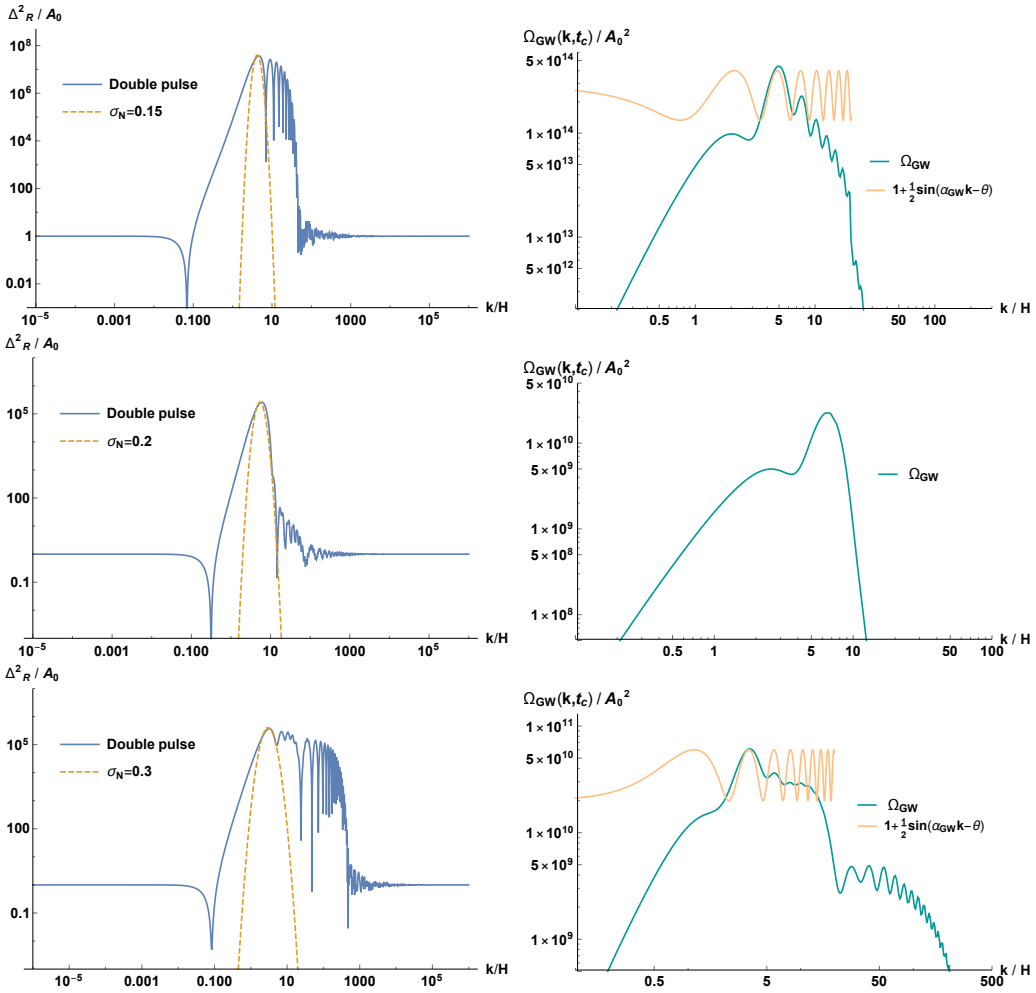


Figure 6.4: Left: The scalar power spectrum produced by a double square "pulse", normalized to the CMB measured amplitude. The dashed line is a lognormal power spectrum with width $\sigma_{\rm N}$. Right: The induced GW spectrum, along with a fitting periodic function. Each row, from top to bottom, corresponds to the "pulse" producing the spectrum of each of figs. 5.5, 5.6, 5.7, respectively.

maximum at lower $k$, as can be seen in the first row of panels in fig. 6.5. The first sharp peak in the GW spectrum is located at the value $k_{\rm GW,1} = 2k_{\rm p1}/\sqrt{3}$, the second at $k_{\rm GW,2} = (k_{\rm p1} + k_{\rm p2})/\sqrt{3}$, the third at $k_{\rm GW,3} = 2k_{\rm p2}/\sqrt{3}$, the fourth at $k_{\rm GW,4} = (k_{\rm p2} + k_{\rm p3})/\sqrt{3}$ and the fifth at $k_{\rm GW,5} = 2k_{\rm p3}/\sqrt{3}$. The rather flat local maximum at lower $k$ is located near $k_{\rm p2}/e$, where $k_{\rm p2}$ is the wavenumber of the highest peak. These values can be seen in fig. 6.5 in the frequency spectrum and in Hz units through the conversion $f = k/(2\pi)$,

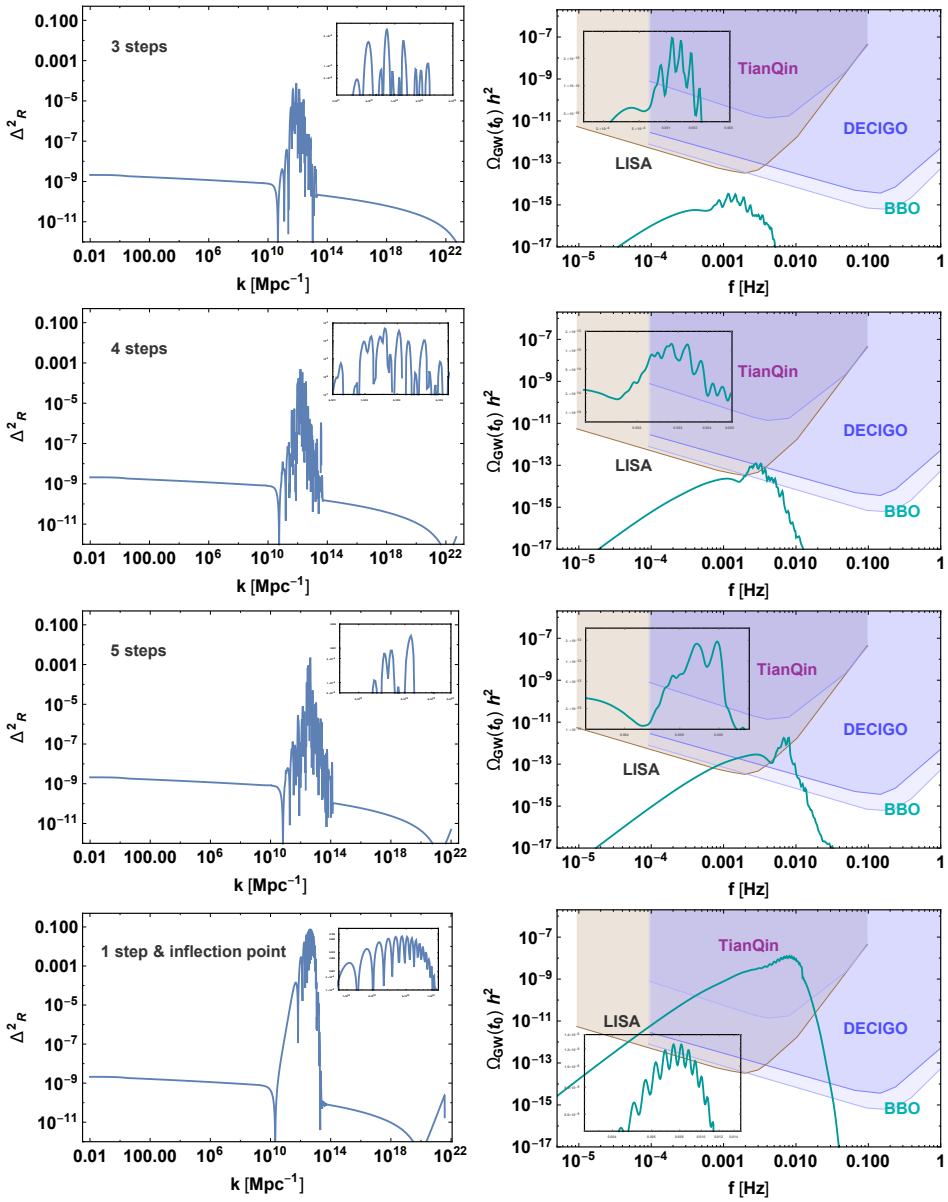


Figure 6.5: Left panels: The curvature power spectra produced by inflationary models with potentials given by eq. (6.7) and depicted in fig. 6.1, for parameter values given in the text. Right panels: The generated GW density parameter produced by each inflationary model. A zoom-in plot of the peak region has been included in each panel. Note that the last row of panels corresponds to an inflationary model that features both a step and an inflection point, depicted in fig. 6.2.

where $\mathrm{Mpc}^{-1} \simeq 0.97 \times 10^{-14}$ Hz. Similar conclusions can be drawn for the next two inflationary models that feature four and five steps, respectively.

For the inflationary model that features both an inflection point and a step, the resulting spectra are quite different compared to the previously discussed models that involve only steps. The inflection point is responsible for the strong enhancement of the curvature power spectrum and its relatively wide peak. Indeed, the envelope function that outlines the peak can be fitted by a lognormal distribution with width $\sigma_{\mathrm{N}} \simeq 0.4$. Hence the characteristic two-peak structure in the GW spectrum [192] is not very prominent here. The step-like feature has a minor contribution to the enhancement of the curvature spectrum, but it is the source of the oscillatory pattern around the peak with the characteristic period $\delta k \simeq 7 \times 10^{-11}\mathrm{Mpc}^{-1}$. These oscillations are also transferred to the GW spectrum. As before, the GW oscillatory pattern is well described by a periodic function and reflects the pattern in the curvature spectrum.

It is important to emphasize that, even though it is not clearly visible in the log-plot, the oscillations near the peak are substantial: The $\Omega_{\mathrm{GW}}$ spectrum displays variations in its amplitude that are 25% of its maximal value or larger. Such modulations in the amplitude are likely to be detectable by the near-future space interferometers.

# Chapter 7

# Two-field inflation and turns in field space

In the previous chapters we examined the features of the potential in single-field inflation that can result in an amplification of the curvature power spectrum by several orders of magnitude. Here, we are interested in similar phenomena in two-field inflation. This chapter is based mainly on [152].

## 7.1 Two-field inflation

In this section we summarise the basic formulae related to two-field inflation which are necessary for our analysis.

### 7.1.1 Background evolution

The action is of the form

$$S = \int d^4x \sqrt{-g} \left[ \frac{1}{2}R - \frac{1}{2} g^{\mu\nu} \gamma_{ab} \partial_\mu \phi^a \partial_\nu \phi^b - V(\phi) \right], \tag{7.1}$$

where $\gamma_{ab}$ with $a, b = 1, 2$ is the metric in field space. On an expanding, spatially flat background, with scale factor $a(t)$, the equations of motion of the background fields take the form [116, 134]

$$\frac{D}{dt}\dot{\phi}^a + 3H\dot{\phi}^a + V^a = 0 \tag{7.2}$$

$$3H^2 = \frac{1}{2}\dot{\phi}^2 + V, \tag{7.3}$$

where $V^a = \gamma^{ab} \partial V / \partial \phi^b$ and

$$\frac{D}{dt} X^a = \dot{X}^a + \Gamma^a_{bc} \dot{\phi}^b X^c. \tag{7.4}$$

By defining $\dot{\phi}^2 \equiv \gamma_{ab}\dot{\phi}^a\dot{\phi}^b$, we obtain

$$\dot{H} = -\frac{\dot{\phi}^2}{2}. \tag{7.5}$$

We next define vectors $T^a$ and $N^a$ tangent and normal to the path

$$T^a = \frac{\dot{\phi}^a}{\dot{\phi}} \tag{7.6}$$

$$N_a = (\det\gamma)^{1/2}\epsilon_{ab}T^b, \tag{7.7}$$

such that $T^aT_a = N^aN_a = 1$, $T^aN_a = 0$. Projecting eq. (7.2) along $T^a$, one finds

$$\ddot{\phi} + 3H\dot{\phi} + V_T = 0, \tag{7.8}$$

where $V_T = T^a\partial V/\partial\phi^a$. One also finds

$$\frac{DT^a}{dt} = -\frac{V_N}{\dot{\phi}}N^a, \tag{7.9}$$

with $V_N = N^a\partial V/\partial\phi^a$. The slow-roll parameters are defined as

$$\epsilon \equiv -\frac{\dot{H}}{H^2} = \frac{\dot{\phi}^2}{2H^2} \tag{7.10}$$

$$\eta^a \equiv -\frac{1}{H\dot{\phi}}\frac{D\dot{\phi}^a}{dt}. \tag{7.11}$$

Then $\eta^a$ can be decomposed as

$$\eta^a = \eta_\parallel T^a + \eta_\perp N^a, \tag{7.12}$$

with

$$\eta_\parallel = -\frac{\ddot{\phi}}{H\dot{\phi}} = -\frac{\dot{\epsilon}}{2H\epsilon} + \epsilon \tag{7.13}$$

$$\eta_\perp = \frac{V_N}{H\dot{\phi}}. \tag{7.14}$$

We also have

$$\frac{DT^a}{dt} = -H\eta_\perp N^a \tag{7.15}$$

$$\frac{DN^a}{dt} = +H\eta_\perp T^a. \tag{7.16}$$

### 7.1.2 Perturbations and relevant assumptions

The evolution equations for the curvature and isocurvature perturbations in two-field inflation can be cast in the form [1] [116, 134]

$$\mathcal{R}_{k,NN}+\left(3+\epsilon-2\eta_{\parallel}\right)\mathcal{R}_{k,N}+\frac{k^2}{H^2}e^{-2N}\mathcal{R}_k=-2\frac{\eta_{\perp}}{\sqrt{2\epsilon}}\left[\mathcal{F}_{k,N}+(3-\eta_{\parallel}-\xi_{\perp})\mathcal{F}_k\right] \tag{7.17}$$

$$\mathcal{F}_{k,NN}+(3-\epsilon)\mathcal{F}_{k,N}+\frac{k^2}{H^2}e^{-2N}\mathcal{F}_k+\left(\frac{M^2}{H^2}+\epsilon\,\mathbb{R}-\eta_{\perp}^2\right)\mathcal{F}_k=2\sqrt{2\epsilon}\,\eta_{\perp}\mathcal{R}_{k,N}, \tag{7.18}$$

with

$$\eta_{\parallel} = \epsilon-\frac{\epsilon_{,N}}{2\epsilon} \tag{7.19}$$

$$\xi_{\perp} = -\frac{\eta_{\perp,N}}{\eta_{\perp}}. \tag{7.20}$$

We have written the equations in Fourier space, using the number of efoldings $N$ as independent variable. The subscripts denote derivatives with respect to $N$. Here $\mathcal{R}_k$ is the curvature perturbation, while $\mathcal{F}_k$ is related to the isocurvature perturbation $\mathcal{S}$ through $\mathcal{F}_k=\sqrt{2\epsilon}\,\mathcal{S}_k$. The mass $M$ of the isocurvature perturbation is given by the curvature of the potential in the direction perpendicular to the trajectory of the background inflaton. The variable $\mathbb{R}$ is the Ricci scalar of the internal manifold spanned by the scalar fields [100]. It vanishes for a model with standard kinetic terms for the two fields.

In order to focus on the main features associated with the enhancement of the curvature spectrum, we make some simplifying assumptions:

- We approximate the Hubble parameter as constant. This is a good approximation, as its variation during the period of interest is $\mathcal{O}(10\%)$, while the spectrum may increase by several orders of magnitude.

- In a similar vein, we take the mass $M$ of the isocurvature modes to be constant. We also assume that $M \gtrsim H$, so that the isocurvature perturbations are suppressed apart from short periods during which the parameter $\eta_{\perp}$ becomes large.

- We do not consider the possibility of a curved field manifold, but assume that the fields have standard kinetic terms. This means that we can set $\mathbb{R}=0$.

[1] In this chapter we return to the symbol $\mathcal{R}$ in order to denote the comoving curvature perturbation.

- We assume that the parameter $\epsilon$ takes a small constant value while the system is in the slow-roll regime, consistently with the constraints from the cosmic microwave background (CMB). We neglect here corrections arising from the slow-roll regime that lead to small deviations from scale invariance. We focus instead on short periods of the inflaton evolution during which $\eta_\parallel$ or $\eta_\perp$ can grow large. These periods are reflected in strong deviations of the spectrum from scale invariance over a range of momentum scales.

We are interested in strong deviations from the slow-roll regime during short intervals in $N$, which can result in the strong enhancement of the curvature perturbations. There are two typical scenaria that we have in mind:

- For $\eta_\perp^2 \ll M^2/H^2$, the isocurvature mode is strongly suppressed and the rhs of eq. (7.17) vanishes. The curvature mode can be enhanced if the coefficient of the term $\sim \mathcal{R}_{k,N}$ in the lhs becomes negative. This requires large positive values of the parameter $\eta_\parallel$, from which the dominant effect comes, while $\epsilon$ takes values at most around 1 and can be neglected. The equation for the curvature perturbation can be approximated as

$$\mathcal{R}_{k,NN} + (3 - 2\,\eta_\parallel)\,\mathcal{R}_{k,N} + \frac{k^2}{H^2} e^{-2N} \mathcal{R}_k = 0, \tag{7.21}$$

  which is the same as (5.1) with $f(N) = 3 - 2\,\eta_\parallel$. This scenario corresponds to the case that the inflaton potential displays an inflection point or a sharp step, which we have analysed in detail in the previous chapters, when we studied single-field inflation.

- If $\eta_\perp^2 \gg M^2/H^2$ for a short period, the isocurvature modes can be temporarily excited very strongly. The rhs of eq. (7.17) then becomes large and acts as a source for the curvature perturbations, leading to their strong enhancement. At a later time, $\eta_\perp$ becomes small and the isocurvature perturbations become suppressed again. This process can take place while the slow-roll parameters $\epsilon$ and $\eta_\parallel$ remain small. In order to capture the essence of this mechanism, we assume that $\epsilon$ is small and roughly constant, and switch to the field $\mathcal{S}_k = \mathcal{F}_k/\sqrt{2\epsilon}$. The system of eqs. (7.17), (7.18) becomes

$$\mathcal{R}_{k,NN} + 3\mathcal{R}_{k,N} + \frac{k^2}{H^2} e^{-2N} \mathcal{R}_k = -2\,(\eta_\perp \mathcal{S}_{k,N} + \eta_{\perp,N} \mathcal{S}_k + 3\eta_\perp \mathcal{S}_k) \tag{7.22}$$

$$\mathcal{S}_{k,NN} + 3\mathcal{S}_{k,N} + \frac{k^2}{H^2} e^{-2N} \mathcal{S}_k + \left(\frac{M^2}{H^2} - \eta_\perp^2\right) \mathcal{S}_k = 2\,\eta_\perp \mathcal{R}_{k,N}. \tag{7.23}$$

Notice that $\mathcal{S}_k$ is the appropriate field on which the initial condition of a Bunch-Davies vacuum can be imposed, similarly to $\mathcal{R}_k$.

In both the above scenaria, it is the acceleration in the evolution of the background inflaton, either in the direction of the flow through $\eta_\parallel(N)$, or perpendicularly to it through $\eta_\perp(N)$, that causes the amplification of the spectrum of curvature perturbations. Another common characteristic is that the spectrum displays strong oscillatory patterns.

A weak point of the above scenaria is that the enhancement of the curvature spectrum by several orders of magnitude can be achieved only under special conditions. The inflaton potential around an inflection point must be fine-tuned with high accuracy [32, 34, 35, 53]. A step in the potential gives a limited enhancement, unless the potential is engineered in a very specific way [155]. Finally, a sharp turn in the inflaton trajectory must reach a value of $4\pi$ for the enhanced spectrum to have observable consequences [45]. This is possible only if the field manifold is curved.

However, a strong enhancement of the curvature spectrum is possible if several strong features in the inflaton potential combine constructively. We have already seen it in the case of steps and we are also going to come to analogous conclusions for turns in field space.

## 7.2 Turns in field space

Since the case of steps and inflection points has been analysed in the previous chapters, we now turn to the case of turns in field space. As we saw in section 7.1, such features occur when the parameter $\eta_\perp$ satisfies $\eta_\perp^2 \gg M^2/H^2$, with $M$ the typical mass of the mode perpendicular to the inflaton trajectory. The relevant equations are eqs. (7.22), (7.23). The evolution of the background can be rather complicated, depending on the characteristics of the two-field potential [116, 134]. We concentrate here on a simplified scenario, which preserves the relevant features without requiring a numerical calculation of the background evolution.

### 7.2.1 Maximal turn and multiple features

We consider models of a two-component field $\phi^a = (\chi, \psi)$ with a standard kinetic term, for which the curvature of the field manifold vanishes. We assume that the potential has an almost flat direction along a curve $\psi = f(\chi)$. A small constant slope along this direction results in a small value of the slow-roll parameter $\epsilon$, which we assume to be constant. Along the perpendicular direction the potential has a large curvature, so that the flat direction forms

a valley. We consider the simplest scenario, in which the fields evolve very close to the bottom of the valley, without perpendicular oscillations. We approximate the Hubble parameter as constant, with a value set by the average value of the potential along the flat direction. A particular realization of this setup, with $f(\chi) = a^2/\chi$, is given in ref. [116].

The unit vectors, tangential and normal to the valley at $\phi^a = (\chi, f(\chi))$, are

$$T^a = \frac{1}{\sqrt{1+f'^2(\chi)}}\,(1, f'(\chi)) \tag{7.24}$$

$$N^a = \frac{1}{\sqrt{1+f'^2(\chi)}}\,(f'(\chi), -1)\,. \tag{7.25}$$

If we assume that the norm of $\dot{\phi}^a$ stays constant and equal to $\sqrt{2\epsilon}\,H$, we find that

$$\chi_{,N} = \pm\frac{\sqrt{2\epsilon}}{\sqrt{1+f'^2(\chi)}}. \tag{7.26}$$

We now have

$$T^a_{,N} = \frac{\partial T^a}{\partial\chi}\chi_{,N} = \frac{f''(\chi)}{(1+f'^2(\chi))^{3/2}}\,\chi_{,N}\,(-f'(\chi), 1) = -\frac{f''(\chi)}{1+f'^2(\chi)}\,\chi_{,N}\,N^a. \tag{7.27}$$

From eq. (7.15) we deduce that

$$\eta_\perp = \frac{f''(\chi)}{1+f'^2(\chi)}\chi_{,N} = \pm\sqrt{2\epsilon}\frac{f''(\chi)}{(1+f'^2(\chi))^{3/2}}. \tag{7.28}$$

It is apparent that $\eta_\perp$ is nonzero only in regions in which $f''(\chi) \neq 0$, so that the valley of the potential is not linear.

We are interested in a scenario in which a linear part of the valley is succeeded by a sharp turn, leading to a second linear part. Without loss of generality we can assume that the turn is located near $\chi = \psi = 0$. The background evolution will be characterized by a short interval in which $\eta_\perp$ will rise and fall sharply from zero. The angle of rotation in field space obeys $\theta_{,N} = \eta_\perp$, from which we obtain

$$\Delta\theta = \int_{N_i}^{N_f}\eta_\perp(\chi)dN = \int_{\chi_i}^{\chi_f}\frac{f''(\chi)}{1+f'^2(\chi)}d\chi = \arctan\left(f'(\chi)\right)\Big|_{\chi_i}^{\chi_f}. \tag{7.29}$$

The maximal angle can be obtained if $f'(\chi_i) \to -\infty$ before the turn and $f'(\chi_f) \to \infty$ after, so that $\Delta\theta = \pi$.

In the model of ref. [116], in which $f(\chi) = a^2/\chi$, one can have $f'(\chi_i) \to -\infty$ before the turn and $f'(\chi_f) \to 0$ after, so that $\Delta\theta = \pi/2$. The maximal

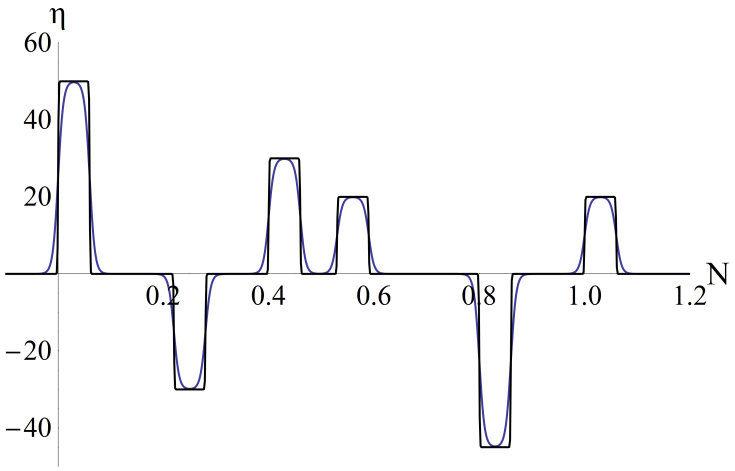


Figure 7.1: Typical evolution of the function $\eta_\perp(N)$ induced by turns in the inflaton potential. The approximation through "pulses" is also depicted.

value of $\eta_\perp$ is obtained for $\chi = \psi = a$. It is $\eta_{\perp\max} = \sqrt{\epsilon}/a$, and can be arbitrarily large for $a \to 0$. The duration of the turn is roughly $\Delta N \sim \Delta\theta/\eta_{\perp\max} = \pi a/(2\sqrt{\epsilon})$ and can be very short for $a \to 0$.

As the value of the integral in eq. (7.29) is bounded by $\pi$, the effect of sharp turns on the amplification of the isocurvature and curvature perturbations is limited. However, multiple turns can also occur. The sign of the rotation angle is arbitrary, so a sequence of turns with alternating signs is possible. The enhancement of the curvature perturbation depends only on $|\eta_\perp|$, as can be easily seen through inspection of eqs. (7.22), (7.23). In fig. 7.1 we depict the typical evolution of $\eta_\perp$ when the potential has several turns along its flat direction. We also present the approximation of the various features through "pulses", which we shall employ in the following. The integral over each feature must be smaller than $\pi$, so that the valley of the potential does not close on itself. This limits the possible enhancement arising from each turn. However, the combined effect of several turns can be substantial, as we show in this section.

### 7.2.2 The qualitative features of the evolution

As we discussed in section 7.1, the perturbations in the two-field system are governed by eqs. (7.22). (7.23). In order to simplify the picture, we assume that $M$ is constant and $M/H \gtrsim 1$, so that the isocurvature modes get suppressed during the parts of the evolution in which $\eta_\perp$ is small. However,

when $\eta_\perp \gg M/H$ the evolution becomes non-trivial, as both the curvature and isocurvature modes get excited. The term $\sim \eta_\perp^2$ in the lhs of eq. (7.23) acts as a negative mass term, triggering the rapid growth of the field $\mathcal{S}_k$. As a result, the rhs of eq. (7.22) becomes a strong source term for the field $\mathcal{R}_k$. The resulting growth of $\mathcal{R}_k$ generates a source term in the rhs of eq. (7.23) that moderates the maximal value of the field $\mathcal{S}_k$. The combined effect results in the enhancement of both modes. However, the late evolution of $\mathcal{S}_k$, when $\eta_\perp$ becomes negligible, is dominated by its nonzero mass, so that this field eventually vanishes. The curvature mode $\mathcal{R}_k$ freezes, similarly to the standard inflationary scenario, preserving its enhancement within a certain momentum range. Another characteristic consequence of the presence of strong features in the potential during inflation is the appearance of distinctive oscillations in the curvature spectrum.

In order to obtain an analytic understanding of the evolution of the perturbations, we consider the "pulse" approximation that we have already seen. For one "pulse" $\eta_\perp$ has the form

$$\eta_\perp(N) = \eta_{\perp 0}\left(\Theta(N-N_1) - \Theta(N-N_2)\right). \tag{7.30}$$

The parameter $\eta_\perp$ takes a constant value for $N_1 < N < N_2$, and approaches zero very quickly outside this range. For $N < N_1$ and $N > N_2$ the two equations of motion decouple

$$\mathcal{R}_{k,NN} + 3\mathcal{R}_{k,N} + \frac{k^2}{H^2}e^{-2N}\mathcal{R}_k = 0 \tag{7.31}$$

$$\mathcal{S}_{k,NN} + 3\mathcal{S}_{k,N} + \frac{k^2}{H^2}e^{-2N}\mathcal{S}_k + \frac{M^2}{H^2}\mathcal{S}_k = 0, \tag{7.32}$$

resulting in simple solutions of the following form

$$\mathcal{R}_k(N) = e^{-\frac{3}{2}N}\left[C_p J_{\frac{3}{2}}\left(e^{-N}\frac{k}{H}\right) + C_m J_{-\frac{3}{2}}\left(e^{-N}\frac{k}{H}\right)\right] \tag{7.33}$$

$$\mathcal{S}_k(N) = e^{-\frac{3}{2}N}\left[D_p J_{\frac{1}{2}\sqrt{9-4\frac{M^2}{H^2}}}\left(e^{-N}\frac{k}{H}\right) + D_m J_{-\frac{1}{2}\sqrt{9-4\frac{M^2}{H^2}}}\left(e^{-N}\frac{k}{H}\right)\right]. \tag{7.34}$$

Initial conditions corresponding to the Bunch-Davies vacuum are obtained for $C_{p_i} = 1$, $C_{m_i} = i$. For the massive mode, the coefficients must be chosen more carefully, so that they reproduce the free-wave solution for $N \to -\infty$ when $M$ becomes negligible. They read

$$D_{p_i} = -\sqrt{2}(1+i)\frac{e^{\frac{i\pi}{4}\sqrt{9-4M^2/H^2}}}{1-e^{i\pi\sqrt{9-4M^2/H^2}}}e^{i\phi} \tag{7.35}$$

$$D_{m_i} = \sqrt{2}(1+i)\frac{e^{\frac{3i\pi}{4}\sqrt{9-4M^2/H^2}}}{1-e^{i\pi\sqrt{9-4M^2/H^2}}}e^{i\phi}. \tag{7.36}$$

We have also included an arbitrary phase difference $\phi$ between the curvature and isocurvature modes at early times. This phase may affect the profile of the spectra by modifying the interference patterns when the two modes interact. However, we have found that the quantitative conclusions about the spectrum enhancement and the characteristic oscillations it may display are largely unaffected. For this reason, we use $\phi = 0$ in our analysis.

The evolution in the interval $N_1 < N < N_2$ is complicated because of the coupling between the two modes. The main features are more clearly visible if we neglect the expansion of space, which is a good approximation for $\Delta N = N_2 - N_1 \lesssim 1$. The evolution equations now become

$$\mathcal{R}_{k,NN} + \frac{k^2}{H^2}\mathcal{R}_k + 2\eta_{\perp 0}\mathcal{S}_{k,N} = 0 \tag{7.37}$$

$$\mathcal{S}_{k,NN} + \left(\frac{k^2}{H^2} + \frac{M^2}{H^2} - \eta_{\perp 0}^2\right)\mathcal{S}_k - 2\eta_{\perp 0}\mathcal{R}_{k,N} = 0. \tag{7.38}$$

Following refs. [45, 110], we look for solutions of the form

$$\mathcal{R}_k = Ae^{\omega N}, \quad \mathcal{S}_k = Be^{\omega N}. \tag{7.39}$$

There are four independent solutions

$$\omega_i = \pm\frac{1}{\sqrt{2}}\sqrt{-\left(\frac{M^2}{H^2} + 3\eta_{\perp 0}^2 + 2\frac{k^2}{H^2}\right) \pm \sqrt{\left(\frac{M^2}{H^2} + 3\eta_{\perp 0}^2\right)^2 + 16\frac{k^2}{H^2}\eta_{\perp 0}^2}}, \tag{7.40}$$

with $i = 1, 2, 3, 4$ corresponding to the combinations of signs $++$, $-+$, $+-$, $--$, respectively. The corresponding values of $B_i$ are

$$B_{1,2} = f_+\,\omega_{1,2}\,A_{1,2} \tag{7.41}$$

$$B_{3,4} = f_-\,\omega_{3,4}\,A_{3,4}, \tag{7.42}$$

with

$$f_\pm = \frac{4\,\eta_{\perp 0}}{\frac{M^2}{H^2} - 5\eta_{\perp 0}^2 \pm \sqrt{\left(\frac{M^2}{H^2} + 3\eta_{\perp 0}^2\right)^2 + 16\frac{k^2}{H^2}\eta_{\perp 0}^2}}. \tag{7.43}$$

The solutions on either side of $N_1$ and $N_2$ can be matched, assuming the continuity of $\mathcal{R}_k(N)$, $\mathcal{S}_k(N)$ and $\mathcal{S}_{k,N}(N)$. The first derivative of $\mathcal{R}_k(N)$ must account for the $\delta$-function arising from the derivative of $\eta_\perp(N)$ at these points. This leads to the conditions

$$\mathcal{R}_{k,N}(N_{1-}) = \mathcal{R}_{k,N}(N_{1+}) + 2\eta_{\perp 0}\mathcal{S}_k(N_1) \tag{7.44}$$

$$\mathcal{R}_{k,N}(N_{2-}) = \mathcal{R}_{k,N}(N_{2+}) - 2\eta_{\perp 0}\mathcal{S}_k(N_2). \tag{7.45}$$

For given initial conditions $C_{p_i}, C_{m_i}, D_{p_i}, D_{m_i}$ before the "pulse", one can calculate, through the use of these boundary conditions, the constants $A_i$ within the "pulse", and eventually the final coefficients of the free solutions $C_{p_f}, C_{m_f}, D_{p_f}, D_{m_f}$ after the "pulse". Similarly to what was done in chapter 5, one can thus determine the matrix $M_{\text{pulse}}$ that links the solutions before and after the "pulse":

$$\begin{bmatrix} C_{p_f} \\ C_{m_f} \\ D_{p_f} \\ D_{m_f} \end{bmatrix} = M_{\text{pulse}}(N_1, N_2, k, M, \eta_\perp) \begin{bmatrix} C_{p_i} \\ C_{m_i} \\ D_{p_i} \\ D_{m_i} \end{bmatrix}. \tag{7.46}$$

This matrix facilitates calculations for more complex problems with multiple "pulses", occurring when the linear valley of the potential is interrupted by multiple, successive turns. Unfortunately, the expressions for the matrix elements are extensive and not very illuminating. For this reason we do not present them explicitly.

The influence of the "pulse" on the evolution of the perturbations can be inferred through inspection of eq. (7.40). Two of the solutions ($\omega_3$ and $\omega_4$) are purely imaginary, resulting in oscillatory behaviour. The other two ($\omega_1$ and $\omega_2$) have a more complicated dependence on the parameters of the problem. For $\frac{k}{H} \geq \sqrt{\eta_{\perp 0}^2 - \frac{M^2}{H^2}}$ they are imaginary as well, but for $\frac{k}{H} \leq \sqrt{\eta_{\perp 0}^2 - \frac{M^2}{H^2}}$ they become real, thus inducing exponential growth or suppression. In the limit $\Delta N \to 0$, $\eta_{\perp 0} \to \infty$, with the total area of the "pulse" (or total angle of the turn) $\Delta\theta = \eta_{\perp 0}\Delta N$ kept constant, we have

$$\omega_{1,2} = \pm\frac{k}{H\sqrt{3}} + \mathcal{O}(\Delta N). \tag{7.47}$$

We expect then that the spectrum will be enhanced by a factor

$$P_{\mathcal{R}} \sim \exp\left[\frac{2k}{H\sqrt{3}}\Delta N\right] = \exp\left[\frac{2\Delta\theta}{\sqrt{3}}\frac{k/H}{\eta_{\perp 0}}\right]. \tag{7.48}$$

The fact that the maximal turn $\Delta\theta$ cannot exceed $\pi$ for canonical kinetic terms implies that the enhancement of the spectrum appears for scales $k/H$ comparable to $\eta_{\perp 0}$. As the general solution is a superposition of all independent solutions (7.39), (7.40), the exponential growth is accompanied by oscillatory behaviour with a characteristic frequency set by $\eta_{\perp 0}$. For large $k$ the spectrum returns to its scale-invariant form, as the effect of the "pulse" diminishes.

The constraint on $\Delta\theta$ implies that a single turn results only in a limited growth of the spectrum [45]. However, multiple turns can have an additive,

and often resonant, effect. In this respect it is important to point out another feature of the solutions. We are interested in the regime $\eta_{\perp 0} \gg M/H$, so that we can neglect the effect of the mass inside the "pulse". For $k/H \ll \eta_{\perp 0}$, strong oscillations, with a frequency set by $\eta_{\perp 0}$, occur within the "pulse". On the other hand, outside the "pulse" the characteristic frequency of oscillations, modulated by the expansion, is set by $k$ or $M$. The continuity of $\mathcal{S}_k(N)$ and its derivative implies that the amplitude of oscillations increases significantly when the perturbation exits the "pulse". The effect is visible if one matches at $N = 0$ the toy functions $f_i(N)$ and $f_f(N)$ given by

$$f_{i,f}(N) = A_{i,f} e^{-ik_{i,f}N} + B_{i,f} e^{ik_{i,f}N}. \tag{7.49}$$

This results in

$$\begin{aligned} A_f &= \frac{1}{2}\left(1 + \frac{k_i}{k_f}\right) A_i + \frac{1}{2}\left(1 - \frac{k_i}{k_f}\right) B_i \\ B_f &= \frac{1}{2}\left(1 - \frac{k_i}{k_f}\right) A_i + \frac{1}{2}\left(1 + \frac{k_i}{k_f}\right) B_i. \end{aligned} \tag{7.50}$$

For $k_i \ll k_f$, as when entering a "pulse", the constants $A_f$, $B_f$ are comparable to $A_i$, $B_i$, while for $k_i \gg k_f$, as when exiting a "pulse", they are greatly enhanced. We shall see realizations of this effect in the two-field context through the numerical solution of eqs. (7.22), (7.23) in the following.

Before completing the subsection, we point out that the alternative formulation of the calculation of the spectrum that was introduced in section 5.2 for the single field case can be generalized for two fields. We present the relevant expressions in appendix B.

### 7.2.3 Numerical evaluation of the spectra

The precise form of the power spectrum in the two-field case is not captured easily through an analytic approach, especially when multiple features appear in the inflaton potential. For this reason, we resort to the numerical integration of eqs. (7.22), (7.23). In fig. 7.2[2] we present the evolution of the amplitude of perturbations $\mathcal{R}_k(N)$ and $\mathcal{S}_k(N)$ in two distinct cases. The perturbations are normalized so that the curvature spectrum is equal to 1 for $\eta_\perp = 0$.

In the top row of fig. 7.2 we present $\mathcal{R}_k(N)$ (left plot) and $\mathcal{S}_k(N)$ (right plot) for a wide "pulse", also depicted in the plots. This example does not

[2]It is $P_\mathcal{R} \equiv \Delta^2_\mathcal{R}$ in this and the following figures.

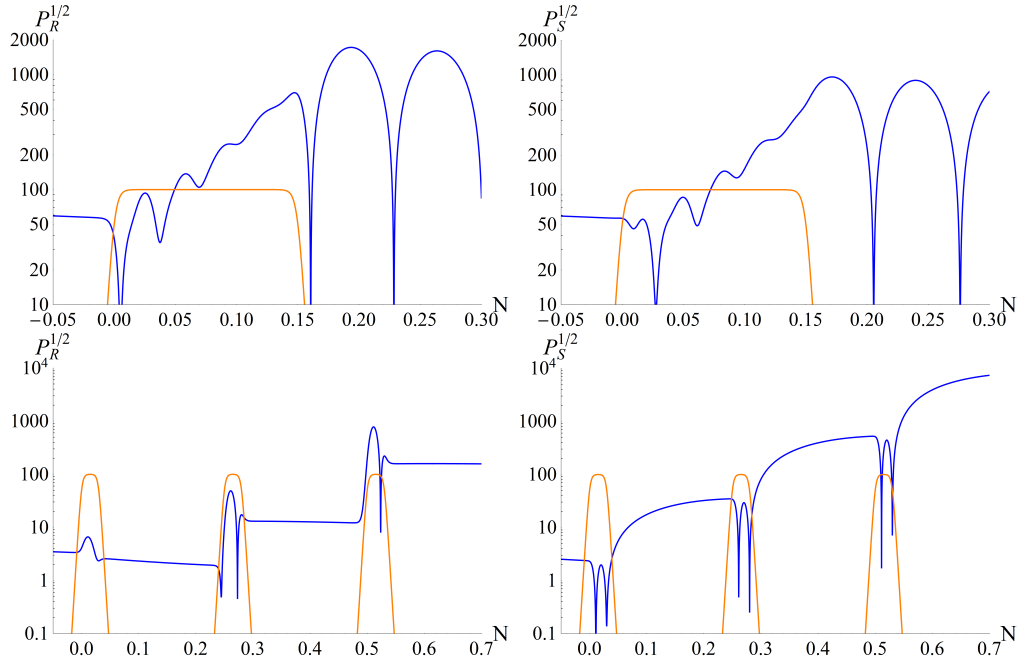


Figure 7.2: The evolution of the curvature mode (left plots) and isocurvature mode (right plots) for two types of time dependence for the parameter $\eta_\perp$: Top row: Thick "pulse". Bottom row: A sequence of three narrow "pulses" of alternating sign. The function $|\eta_\perp(N)|$ is also depicted. The mass of the isocurvature mode is $M/H = 5$. The momentum of both modes is $k/H \simeq 56$ in the top row and $k/H \simeq 3.2$ in the bottom row.

represent a physical situation for vanishing curvature $\mathbb{R}$ of the internal field manifold, because the total turn $\Delta\theta$ is approximately 15. It is presented in order to demonstrate the qualitative features discussed in the previous subsection, which become relevant for $\mathbb{R} \neq 0$. The mode momentum is $k/H \simeq 56$, of the same order as the height $\eta_{\perp 0} \simeq 100$ of the "pulse". The mass of the isocurvature mode is $M/H \simeq 5$. One sees clearly the rapid growth of the perturbations inside the "pulse" and the appearance of oscillations with frequency set by $\eta_{\perp 0}$. After exiting the "pulse", the perturbations oscillate with frequency set by $k$. For $N \to \infty$ (a region not depicted in the plots) the isocurvature mode asymptotically vanishes because of its nonzero mass. The curvature mode freezes when the horizon is crossed at a value larger than the one corresponding to the scale-invariant case ($\eta_\perp = 0$).

In the bottom row of fig. 7.2 we present the evolution in the case of multiple "pulses". The width of each "pulse" is much smaller than in the previous example, so that each turn —$\Delta\theta$— in field space is smaller than

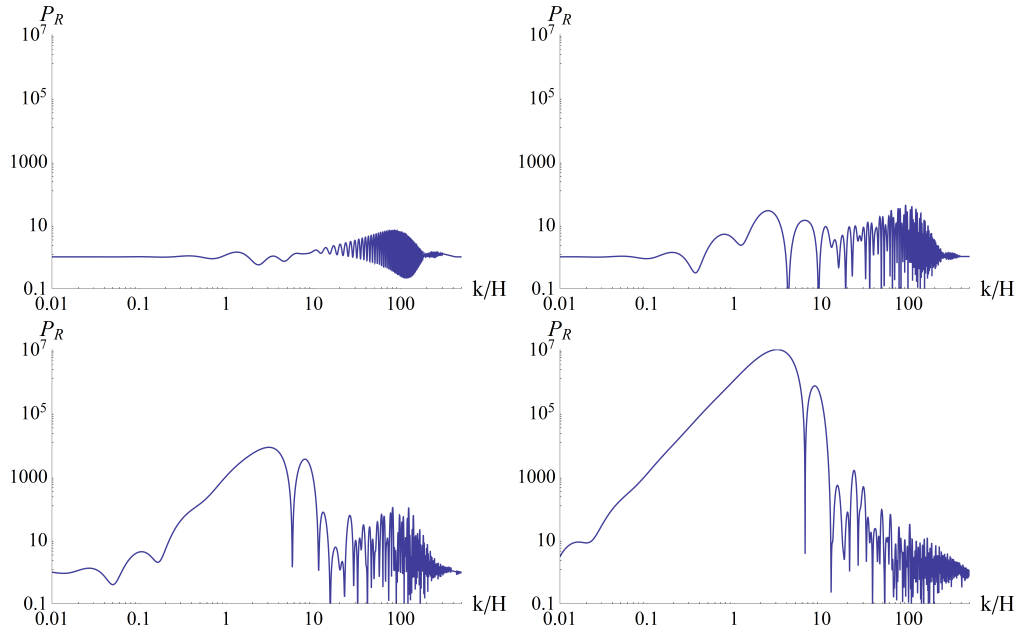


Figure 7.3: Curvature spectrum induced by a sequence of "pulses" of alternating signs in the function $\eta_\perp(N)$. Top row: one "pulse" (left), two "pulses" (right). Bottom row: three "pulses" (left), four "pulses" (right). We have kept the same scales for the axes in all plots for direct comparison.

$\pi$. The turns have alternating signs and in the plot we depict $|\eta_\perp(N)|$. The mode momentum is $k/H \simeq 3.2$, much smaller than $\eta_{\perp 0}$. The mass of the isocurvature mode is again $M/H \simeq 5$. It is apparent that the growth of both modes within the "pulses" is not substantial, even though strong oscillations occur with frequency set by $\eta_{\perp 0}$. The distinctive feature is the strong increase of the amplitude of the isocurvature mode when the perturbation exits the "pulse". This is expected, according to our discussion at the end of the previous subsection. The oscillation frequency for this mode outside the "pulses" is set by the mass and is rather low. The location of the "pulses" is such that a resonance effect occurs, with the amplitude of $\mathcal{S}_k$ being amplified each time a "pulse" is traversed. This effect also triggers the growth of the curvature mode. The late time behaviour of both modes (not depicted in the plot) is similar to the previous case.

In fig. 7.3 we depict the form of the curvature spectrum induced by a function $\eta_\perp(N)$ displaying a sequence of "pulses" such as those in the bottom row of fig. 7.2. The "pulses" have alternating signs and are located at a distance of 0.25 efoldings from each other. Each "pulse" has a width

of approximately 0.03 efoldings, a height $\eta_{\perp 0} \simeq 100$ and a total area smaller than $\pi$. We have used the same scales in all plots in order to be able to make direct visual comparisons. The top row includes the spectra generated by one (left plot) or two (right plot) "pulses". The bottom row includes the spectra generated by three (left plot) or four (right plot) "pulses". The spectra are normalized to the scale-invariant one. The location of the point $k/H = 1$ is arbitrary. It corresponds to the mode that crosses the horizon at the time at which we have set $N = 0$ for the number of efoldings, with $N$ also taking negative values. In order to make contact with observations, the normalization of $k$ must be set relative to the CMB scale.

In all plots we observe the enhancement of the spectrum in the region $k/H \sim \eta_{\perp 0}$. This enhancement increases with the number of "pulses", but not to a significant degree. On the other hand, a strong enhancement appears for multiple "pulses" at low values of $k/H$, which increases dramatically with each addition of a "pulse". This is the realization of the mechanism that we discussed above in relation to the bottom row of fig. 7.2. The resonance effect appears for $1/k$ comparable to the distance between the "pulses". For our plots we kept this distance fixed. However, similar patterns in the spectrum are obtained for variable locations of the "pulses", as long as their separations are comparable. The exact height of each "pulse" may also vary. It must be noted that the effect is strongly amplified by very sharp "pulses". We have chosen profiles that match the form of $\eta_\perp(N)$ expected by models such as the one we discussed in subsection 7.2.1.

## 7.3 GWs and the PBH counterpart

As we know, primordial inhomogeneities imprinted on the CMB are limited to scales of order larger than a Mpc. Large enhancements of the power spectrum of perturbations on small scales, such as those produced through the mechanisms discussed in this thesis, are not directly visible on the CMB sky due to photon diffusion damping. A method to probe small-scale perturbations is the search for a stochastic GW background. The formalism of stochastic or induced GWs was described in the previous chapter (see also ref. [194] for a recent review).

The enhancement of the curvature power spectrum due to several "pulses" in the evolution of $\eta_\parallel$ generates a GW spectrum with a characteristic peak structure, discussed in chapter 6. The main peak of the curvature spectrum is found to be narrow, $\sigma < 1$, and induces a GW spectrum with a major peak after a flat plateau. Additional oscillatory patterns are superimposed

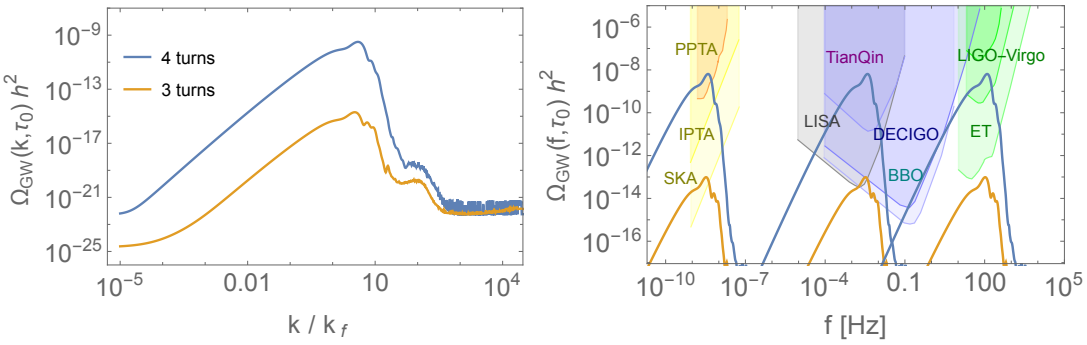


Figure 7.4: *Left plot*: The GW spectral density produced by inflationary trajectories with 3 and 4 successive turns occurring at the wavenumber $k_f$. The scale $k_f$ is the scale that crosses the horizon at the time when the first feature occurs. In the right plot, we select three different values for this scale. *Right plot*: The GW spectra placed at three benchmark frequencies that lie within the range of sensitivity of current and near future GW experiments.

on this main peak, reflecting the strong oscillations in the curvature spectrum depicted in fig. 5.9. A similar general peak structure is found for a "pulse" in the evolution of $\eta_\perp$, see Fig. 7.4. However, in this case the subleading oscillatory patterns are located after the main peak, which remains fairly smooth. This is a consequence of the smooth form of the main peak of the curvature spectrum depicted in fig. 7.3.

In order to make contact with physical scales we must eliminate the ambiguity in the definition of $N$. For this we can use the scale $k_f$ that crosses the horizon at the time $N_f$ when the first feature occurs. In the approximation of constant $H$ that we are using, we have $k_f = e^{N_f} H$. This allows us to eliminate $H$ in favour of $k_f$, and express every other scale as $k/k_f = e^{\delta N}$, with $\delta N = N - N_f$. In the previous section we were setting $N_f = 0$. Notice that varying $N_f$ is equivalent to varying $k_f$ and allows us to place the peak of the spectrum at a desired value. As a result, the GW spectrum can be shifted along the frequency axis, in order to check its detectability depending on the time of occurrence of the feature that causes the enhancement, as is done in the right plot of fig. 7.4.

The amplification of the spectrum with respect to the CMB scale depends on the number of turns, their size and sharpness. We considered turns smaller than $\pi$ and "pulses" of amplitude $|\eta_\perp| \lesssim 100$. Different configurations can produce an enhancement of the curvature spectrum $\mathcal{P}_\mathcal{R}$ of similar size. For example, a configuration of four turns of angular size $\lesssim \pi$ described by four pulses of size $|\eta_\perp| \sim 100$ that last $\Delta N \sim 0.1$ can enhance the power spectrum

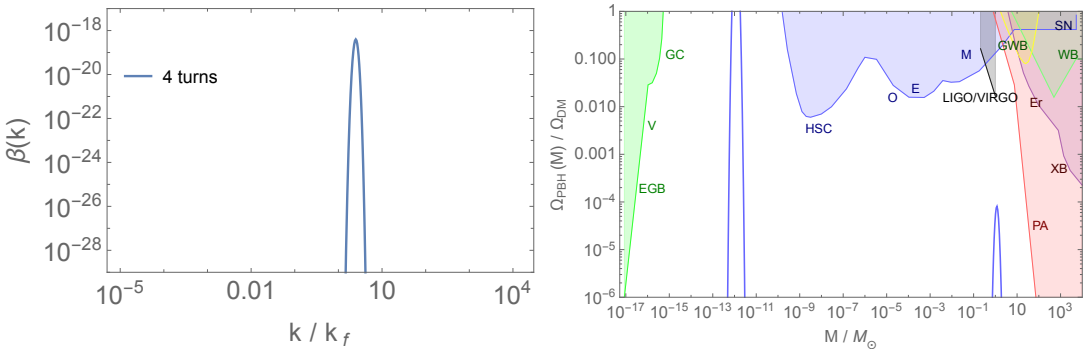


Figure 7.5: *Left plot*: The $\beta$ mass fraction produced by an inflationary trajectory with four successive turns occurring at the wavenumber $k_f$. *Right plot*: The corresponding fractional PBH abundance against the observational constraints [162], with masses placed at benchmark scales that can be probed by current and near future GW experiments. These are the same scales used for the right plot of fig. 7.4. The right curve corresponds to the left spectrum in fig. 7.4, the left curve to the middle spectrum, while the right spectrum in fig. 7.4 corresponds to very small black holes that have evaporated by today.

by a factor of $10^7$. A similar enhancement is produced by a configuration of eight turns of size $\lesssim \pi/2$ described by eight pulses of size $|\eta_\perp| \sim 10$. Although each configuration produces a different spectral shape, the relative differences are not that evident. The curvature spectrum generally exhibits a major narrow peak, as can be seen in fig. 7.3, which creates a characteristic GW spectral peak, common for different configurations. The differences appear at $k > k_{\rm peak}$ and correspond to complicated oscillatory patterns. These are reflected in the GW spectra of fig. 7.4 in frequency regions of lower amplitude.

We also point out that primordial curvature perturbations with large amplitudes at certain scales induce, apart from tensor modes, a gravitational collapse of sufficiently dense regions that enter the Hubble horizon. The mass fraction of PBHs at the formation time, $\beta(M)$, has an acute sensitivity to the amplitude of the power spectrum $\mathcal{P}_\mathcal{R}$. For the spherically symmetric gravitational collapse of a fluid with pressure, this sensitivity is exponential, $\beta \propto \sqrt{\mathcal{P}_\mathcal{R}} e^{-\delta_c^2/\mathcal{P}_\mathcal{R}}$, where $\delta_c$ is the density threshold for PBH formation. A sizable PBH abundance is obtained for $\mathcal{P}_\mathcal{R} \sim 10^{-2}$. The parameter $\beta$ can increase if the background pressure is decreased, as for example during the QCD phase transition [170, 195]. A further decrease of the pressure to vanishing values can affect the PBH formation rate significantly [168, 174] and induce GW signals with a different spectral density [186, 187].

In our set-up, large amplitudes of $\mathcal{P}_\mathcal{R}$ can be produced if several strong

features, turns or steps, occur during the inflationary trajectory. These features can give an observable result in the GW channel for three or more successive turns. In Fig. 7.4 we plot the spectral density of the induced GWs for curvature power spectra that have the form depicted in Fig. 7.3. In figure 7.5 we plot the corresponding PBH abundance for a threshold value $\delta_{\rm c} = 0.41$, together with the PBH experimental upper bounds [162]. For four turns the PBHs produced can constitute a significant fraction of the dark matter in the Universe. We recall that during radiation domination the PBH mass spectrum is related to the $\mathcal{P}_{\mathcal{R}}$ peak position $k_{\rm peak}$ as $M_{\rm PBH} \propto k_{\rm peak}^{-2}$, and the PBHs have abundance $\Omega_{\rm PBH} \propto \beta M_{\rm PBH}^{-1/2}$, see Ref. [11] for details. PBHs in the mass range $M \sim 10^{-12} M_{\odot}$ can constitute the entire dark matter in the Universe, while the associated GWs will be probed by LISA [20] and other future space GW antennas. PBHs with mass $M_{\rm PBH} \gtrsim M_{\odot}$ can form binaries and are directly detectable by LIGO-Virgo-KAGRA experiments, while the associated induced GWs can be probed by PTA experiments [16–19]. The LIGO-Virgo-KAGRA collaboration already constrains the stochastic GW background [27] in the frequency band $\mathcal{O}(1-10^2)$ Hz, even though PBHs associated with these frequencies are too light to survive in the late Universe.

# Chapter 8

# Conclusions

In this thesis we explored the possible enhancement of the power spectrum of curvature perturbations when particular features appear in the inflaton potential. In single-field inflation one characteristic feature that is known to induce the enhancement of the spectrum is an inflection point in the potential at some value of the inflaton field. However, we mainly focused here on the opposite case, i.e. a sharp decrease of the potential, which may result even in the interruption of inflation in certain cases, in contrast to what happens around an inflection point. We explored the conditions under which the enhancement can be larger by several orders of magnitude relative to its magnitude within the almost scale-invariant range. It must be noted that it is always possible to enhance the spectrum by engineering the transition to a second very flat plateau of the potential. The time derivative of the inflaton under slow-roll conditions on the plateau would be very small, resulting in an enhanced power spectrum. In our analysis we excluded this rather trivial possibility by keeping the slope roughly constant, apart from the transition point or points, and focused on the effect of the transition itself.

We found that sharp steps lead to the strong growth of the curvature perturbation. The reason can be traced to the "effective-friction" term of eq. (5.1), which is given by the function $f(N)$ defined in eq. (5.2). Even though this function is positive during the first part of the transition, thus suppressing the perturbation, it can become negative during the second part, when the inflaton approaches slow roll on the second plateau, and can lead to a dramatic enhancement. The effect is increased by the steepness of the potential, but is also limited by the size of the potential drop that bounds the maximal inflaton "velocity". However, successive nearby steps give an additive effect, leading to a spectrum enhancement by several orders of magnitude.

Another prominent feature of the spectrum is its strong oscillatory form as a function of wavenumber. Our analysis has revealed that these oscillations

are generated through the detuning of the phase difference between the real and imaginary parts of the curvature perturbation, which evolves according to eq. (5.1). More specifically, when the inflaton moves through a step in the potential, the background evolution deviates strongly from the standard slow-roll for a small number of efoldings, in a way that the real and imaginary parts of the solution are detuned. The detuning results in time-dependent oscillations of the amplitude. When the perturbations asymptotically freeze at superhorizon scales, an oscillatory pattern is induced on the wavenumber dependence of the power spectrum. It must be emphasized that oscillations in the spectrum are not a generic consequence of any feature in the potential that violates slow roll. In contrast to a steep step, an inflection point in general induces an enhanced, but smooth, power spectrum.

From the model-building perspective, a steep step can appear if the inflationary potential includes plateaus with different energy densities. A nearly constant potential energy density can be associated with underlying symmetries that are preserved in the plateau [159]. A deformation of the symmetry results in energy splitting, so that a transition between different energy levels can be induced. Such a behaviour can be captured by inflationary models constructed within the framework of $\alpha$-attractors [157, 158].

A strong motivation for analysing such models is that the induced tensor power spectrum inherits the oscillating profile of the primordial curvature spectrum. The combined pattern of an enhanced spectrum together with strong oscillations is potentially detectable by near future space interferometers. Through the detection of the GW spectrum, one can aim at inferring at least some basic features of the inflationary potential, such as whether step-like transitions are present. Motivated by this possibility, we examined in detail, numerically and analytically, the scalar and the induced tensor spectra and we identified correlations between them. The main characteristic property of both spectra, related to the transition through a step, is a series of peaks. Through a more refined analysis of the spectrum, one can look for more detailed information, such as the number of the steps, their position and exact shape, and whether there is, in addition to a step, an inflection point. We explored this possibility by studying several analytical examples, as well as inflationary models in the $\alpha$-attractor framework, always imposing consistency with the constraints for the spectral index $n_s$ and the amplitude of the scalar spectrum arising from the CMB measurements.

The detection of GWs from inflationary models with sharp features may be accompanied by the presence of PBHs as a significant fraction of dark matter. The enhancement of the power specrtum due to the presence of step-like features, though considerable, may be inefficient to trigger the production of a sizeable number of PBHs if radiation dominates the energy density of

the early Universe. However, it can be sufficient to induce gravitational collapse processes and PBH production if the Universe energy density is dominated by non-relativistic matter. We examined the profile of the PBH mass spectrum produced either in a radiation or an early matter-dominated Universe, looking for deviations from the common monochromatic profile. For the latter scenario we found that this is possible because of the multiple-peak structure of the curvature power spectrum.

Moreover, we extended our analysis on the enhancement of the curvature spectrum during inflation to the two-field case. In this case, we did not study a particular model, but looked instead for generic properties of the equations of motion for the perturbations which would lead to their enhancement. We identified the slow-roll parameter $\eta$ as the quantity that can trigger the rapid growth of perturbations. As we saw, this parameter can be projected onto the directions parallel and perpendicular to the trajectory of the background fields. The corresponding two components, $\eta_{\parallel}$ and $\eta_{\perp}$, remain small during most of the evolution, apart from short intervals during which they can take large, positive or negative, values.

The typical underlying reason for the appearance of strong features in the evolution of $\eta_{\parallel}$ is the presence of points in the inflaton potential that cannot support slow-roll, such as sharp steps or inflection points. However, the analysis of this case in the context of single-field inflation is sufficient, since there is nothing different when we extend to the two-field case. On the other hand, $\eta_{\perp}$ grows large during sharp turns in field space, which is a clearly multi-field phenomenon. The typical situation involves an inflaton potential that contains an almost flat valley, with straight parts interrupted by sharp turns. The evolution along the valley satisfies the slow-roll conditions, apart from the short intervals during which the fields go through the turns and $\eta_{\perp}$ takes large values, positive or negative, depending on the direction of the turn. The effect of $\eta_{\perp}$ is sign-independent and twofold: a) it triggers the strong growth of the perturbation perpendicular to the trajectory (the isocurvature mode), and b) couples the isocurvature mode to the curvature mode along the trajectory, thus inducing its growth as well.

The focal point of our analysis in the two-field context was the additive effect of several turns leading to the resonant growth of the curvature spectrum. We found that three or four features in the evolution of $\eta_{\perp}$ are sufficient in order to induce an enhancement of the power spectrum by six or seven orders of magnitude. The spectrum now displays a smooth main peak, followed by a region of strong oscillatory behaviour. It must be pointed out that the constructive interference of several features is affected by their separation. The resonance effect appears for $1/k$ comparable to the distance between the turns.

Scenarios with turns, similarly to those with steps, generate non-flat shapes with prominent peaks, which can also lead to PBH and GW production. In order that a detectable GW background is produced, e.g. within the sensitivity range of LISA, three or more successive turns have to occur, while a significant PBH abundance requires at least four sharp turns. A comparison of the GW spectra corresponding to steps and turns demonstrates that they both display a prominent maximum that may be localized within the range of sensitivity of designed GW detectors [196], such as LISA [21,22] and DECIGO [23]. The difference between GW spectra produced through the presence of several features in $\eta_{\parallel}$ and those produced through similar features in $\eta_{\perp}$ lies in the secondary maxima that are present around the main peak in the first case, while they are absent in the second case. Their identification depends crucially on the data resolution of the various experiments. However, in principle they provide a means for probing the mechanism that generates the enhancement of the spectrum.

A big part of our study in both single- and two-field inflation focused on the attempt to understand the evolution of the perturbations and the resulting spectra through analytic means. We employed two different approaches. In the first approach, we approximated the features in the evolution of $f(N)$ or $\eta_{\perp}$ as square "pulses" and used appropriate matching conditions at the beginning and end of each "pulse" in order to obtain a complete solution. In the second approach we reformulated the problem using Green's functions and deriving integral equations. Exploiting this approach even further, we reformulated the evolution equations as a system of differential equations for the coefficients of an expansion of the general solution in terms of Bessel functions. This formulation permits the analysis of non-minimal initial conditions in a straightforward manner and can reduce computational time.

The broader picture that emerges from our analysis is that the observable consequences of inflation can be much more complex than what is suggested by the standard analysis that assumes small deviations from scale invariance for the whole range of scales of the primordial spectrum. The possibility that multiple features may be present in the background evolution points to a paradigm with richer physical behaviour. It is exciting that the critical examination of such speculations is within the reach of experiment.

# Appendix A

# Accuracy of analytical estimates

In this appendix we provide an assessment of the accuracy of the approximate expressions (5.45) and (5.54). For the matrix $C(N)$, defined in eq. (5.54), we obtain

$$C_{11}(\infty) = \int_{-\infty}^{\infty} (3 - f(n)) \sin\left(e^{-n}\frac{k}{H}\right) \left[e^{n}\frac{H}{k}\cos\left(e^{-n}\frac{k}{H}\right) + \sin\left(e^{-n}\frac{k}{H}\right)\right] dn \quad \text{(A.1)}$$

$$C_{12}(\infty) = \int_{-\infty}^{\infty} (f(n) - 3) \cos\left(e^{-n}\frac{k}{H}\right) \left[e^{n}\frac{H}{k}\cos\left(e^{-n}\frac{k}{H}\right) + \sin\left(e^{-n}\frac{k}{H}\right)\right] dn \quad \text{(A.2)}$$

$$C_{21}(\infty) = \int_{-\infty}^{\infty} (3 - f(n)) \sin\left(e^{-n}\frac{k}{H}\right) \left[e^{n}\frac{H}{k}\sin\left(e^{-n}\frac{k}{H}\right) - \cos\left(e^{-n}\frac{k}{H}\right)\right] dn \quad \text{(A.3)}$$

$$C_{22}(\infty) = \int_{-\infty}^{\infty} (f(n) - 3) \cos\left(e^{-n}\frac{k}{H}\right) \left[e^{n}\frac{H}{k}\sin\left(e^{-n}\frac{k}{H}\right) - \cos\left(e^{-n}\frac{k}{H}\right)\right] dn, \quad \text{(A.4)}$$

where we have used appropriate partial integrations. The first two terms in a Taylor expansion of the exponential give an estimate for $E(\infty)$ that reproduces the approximate result of eq. (5.45). Additional terms account for higher-order corrections. These improve the convergence for slowly varying functions $f(N)$. However, for functions $f(N)$ that induce an enhancement of the spectrum by several orders of magnitude, the quantitative accuracy of this approach is limited.

In order to check the validity of the approximate expressions (5.45) and (5.54), we consider a sequence of typical patterns of the function $f(N)$, similar to those induced by steep steps in the inflaton potential. The forms of $f(N)$ are depicted in fig. A.1.

In fig. A.2 we depict the power spectra for the three different smooth curves of fig. A.1. The solid curves correspond to the exact numerical solution of eq. (5.1) or the system (5.51). The short-dashed curves correspond to

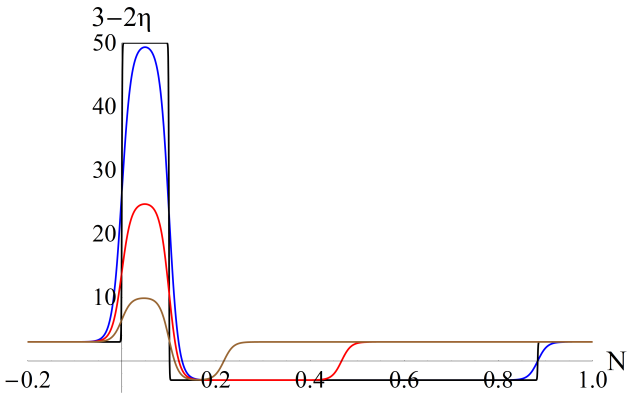


Figure A.1: Typical evolution of the function $f(N) \approx 3 - 2\eta(N)$ induced by steps in the inflaton potential.

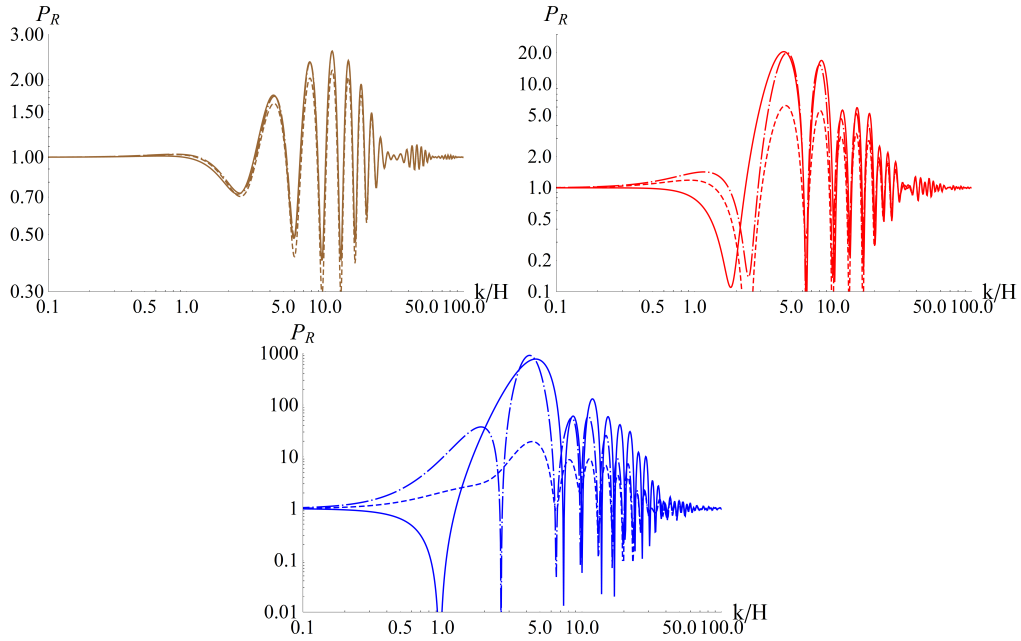


Figure A.2: Power spectra for the three different smooth curves of fig. A.1. The solid curves correspond to the exact numerical solution of eq. (5.1) or the system (5.51). The short-dashed curves correspond to the approximation of eq. (5.45), and the long-dashed curves to the approximation of eq. (5.54). Notice the large difference in the vertical scales of the three plots.

the approximation of eq. (5.45), and the long-dashed curves to the approximation of eq. (5.54). We are interested only in relatively strong deviations from scale invariance, and not in the absolute normalization of the spectrum.

For this reason we have assumed that the spectrum is scale invariant at early and late times and normalized with respect to its value in these regions. It is apparent from fig. A.2 that both approximations give a very accurate description of the spectrum when its value is of order 1. When the spectrum is significantly enhanced both approximations lose accuracy. However, eq. (5.54) gives a reasonable approximation to the maximal value of the spectrum and its characteristic frequencies, even for an enhancement by three orders of magnitude.

# Appendix B

# An alternative formulation in the two-field case

The differential equations (7.22), (7.23) can be turned into integral equations through the use of the appropriate Green's functions. For the curvature mode, the Green's function is given by eq. (5.38). For the massive isocurvature mode, the generalization is straightforward and the retarded Green's function $\bar{G}_k(N,n)$ for $n < N$ is

$$\bar{G}_{k<}(N,n) = e^{-\frac{3}{2}N}\left(P(n)J_{\frac{1}{2}\sqrt{9-4\frac{M^2}{H^2}}}\left(e^{-N}\frac{k}{H}\right) + Q(n)J_{-\frac{1}{2}\sqrt{9-4\frac{M^2}{H^2}}}\left(e^{-N}\frac{k}{H}\right)\right), \tag{B.1}$$

with

$$P(n) = -\frac{\pi}{2}e^{3n/2}\csc\left(\frac{\pi}{2}\sqrt{9-4\frac{M^2}{H^2}}\right)J_{-\frac{1}{2}\sqrt{9-4M^2/H^2}}\left(e^{-N}\frac{k}{H}\right) \tag{B.2}$$

$$Q(n) = \frac{\pi}{2}e^{3n/2}\csc\left(\frac{\pi}{2}\sqrt{9-4\frac{M^2}{H^2}}\right)J_{\frac{1}{2}\sqrt{9-4M^2/h^2}}\left(e^{-N}\frac{k}{H}\right). \tag{B.3}$$

Hence, the general solution can be expressed as:

$$\mathcal{R}_k(N) = \bar{\mathcal{R}}_k(N) - 2\int_{-\infty}^{N} G_{k<}(N,n)\left[\frac{\partial}{\partial n}(\eta_\perp(n)\mathcal{S}_k(n)) + 3\eta_\perp(n)\mathcal{S}_k(n)\right]dn \tag{B.4}$$

$$\mathcal{S}_k(N) = \bar{\mathcal{S}}_k(N) + \int_{-\infty}^{N}\bar{G}_{k<}(N,n)\left[\eta_\perp^2(n)\mathcal{S}_k(n) + 2\eta_\perp(n)\mathcal{R}_{k,n}(n)\right]dn, \tag{B.5}$$

where $\bar{\mathcal{S}}_k(N)$, $\bar{\mathcal{R}}_k(N)$ are the homogeneous solutions.

The form of the above equations suggests the ansatz

$$\mathcal{R}_k(N) = e^{-\frac{3}{2}N}\left[D(N)J_{3/2}\left(e^{-N}\frac{k}{H}\right) + E(N)J_{-3/2}\left(e^{-N}\frac{k}{H}\right)\right] \tag{B.6}$$

$$\mathcal{S}_k(N) = e^{-\frac{3}{2}N}\left[K(N)J_{\frac{1}{2}\sqrt{9-4\frac{M^2}{H^2}}}\left(e^{-N}\frac{k}{H}\right) + L(N)J_{-\frac{1}{2}\sqrt{9-4\frac{M^2}{H^2}}}\left(e^{-N}\frac{k}{H}\right)\right]. \tag{B.7}$$

By substituting in the derivative of eqs. (B.4), (B.5), and matching the coefficients of the Bessel functions, we obtain a system of four first-order differential equations:

$$\frac{\partial}{\partial N}\begin{bmatrix} D(N) \\ E(N) \\ K(N) \\ L(N) \end{bmatrix} = F(N)\begin{bmatrix} D(N) \\ E(N) \\ K(N) \\ L(N) \end{bmatrix} \tag{B.8}$$

where $F(N)$ is a $4\times 4$ matrix with elements $F_{ij}(N)$ given by

$$\begin{aligned}
F_{11}(N) &= F_{12}(N) = F_{21}(N) = F_{22}(N) = 0 \\
F_{13}(N) &= 2e^{-3N/2}\eta_\perp(N)\left(A'(N) - 3A(N)\right)J_{\frac{1}{2}\sqrt{9-4M^2/H^2}}\left(e^{-N}\frac{k}{H}\right) \\
F_{14}(N) &= 2e^{-3N/2}\eta_\perp(N)\left(A'(N) - 3A(N)\right)J_{-\frac{1}{2}\sqrt{9-4M^2/H^2}}\left(e^{-N}\frac{k}{H}\right) \\
F_{23}(N) &= 2e^{-3N/2}\eta_\perp(N)\left(B'(N) - 3B(N)\right)J_{\frac{1}{2}\sqrt{9-4M^2/H^2}}\left(e^{-N}\frac{k}{H}\right) \\
F_{24}(N) &= 2e^{-3N/2}\eta_\perp(N)\left(B'(N) - 3B(N)\right)J_{-\frac{1}{2}\sqrt{9-4M^2/H^2}}\left(e^{-N}\frac{k}{H}\right) \\
F_{31}(N) &= -2e^{-3N/2}\frac{d}{dN}\left(\eta_\perp(N)P(N)\right)J_{\frac{3}{2}}\left(e^{-N}\frac{k}{H}\right) \\
F_{32}(N) &= -2e^{-3N/2}\frac{d}{dN}\left(\eta_\perp(N)P(N)\right)J_{-\frac{3}{2}}\left(e^{-N}\frac{k}{H}\right) \\
F_{33}(N) &= e^{-3N/2}\eta_\perp^2(N)P(N)J_{\frac{1}{2}\sqrt{9-4M^2/H^2}}\left(e^{-N}\frac{k}{H}\right) \\
F_{34}(N) &= e^{-3N/2}\eta_\perp^2(N)P(N)J_{-\frac{1}{2}\sqrt{9-4M^2/H^2}}\left(e^{-N}\frac{k}{H}\right) \\
F_{41}(N) &= -2e^{-3N/2}\frac{d}{dN}\left(\eta_\perp(N)Q(N)\right)J_{\frac{3}{2}}\left(e^{-N}\frac{k}{H}\right) \\
F_{42}(N) &= -2e^{-3N/2}\frac{d}{dN}\left(\eta_\perp(N)Q(N)\right)J_{-\frac{3}{2}}\left(e^{-N}\frac{k}{H}\right) \\
F_{43}(N) &= e^{-3N/2}\eta_\perp^2(N)Q(N)J_{\frac{1}{2}\sqrt{9-4M^2/H^2}}\left(e^{-N}\frac{k}{H}\right) \\
F_{44}(N) &= e^{-3N/2}\eta_\perp^2(N)Q(N)J_{-\frac{1}{2}\sqrt{9-4M^2/H^2}}\left(e^{-N}\frac{k}{H}\right).
\end{aligned} \tag{B.9}$$

This system of equations must be solved with initial conditions at $N\to-\infty$. For the Bunch-Davies vacuum $(D,E) = (1,i)$, while $(K,L)$ are given by eqs. (7.35), (7.36).

# Bibliography


[1] V. F. Mukhanov and G. V. Chibisov, "Quantum Fluctuations and a Nonsingular Universe," JETP Lett. **33** (1981), 532-535;

[2] S. W. Hawking, "The Development of Irregularities in a Single Bubble Inflationary Universe," Phys. Lett. B **115** (1982), 295;

[3] A. A. Starobinsky, "Dynamics of Phase Transition in the New Inflationary Universe Scenario and Generation of Perturbations," Phys. Lett. B **117** (1982), 175-178;

[4] A. H. Guth and S. Y. Pi, "Fluctuations in the New Inflationary Universe," Phys. Rev. Lett. **49** (1982), 1110-1113

[5] Y. Akrami *et al.* [Planck], "Planck 2018 results. X. Constraints on inflation," Astron. Astrophys. **641** (2020), A10 [arXiv:1807.06211 [astro-ph.CO]].

[6] Ya. B. Zeldovich and I. D. Novikov, "The Hypothesis of Cores Retarded during Expansion and the Hot Cosmological Model," Sov. Astron. **10** (1967) 602.

[7] S. Hawking, "Gravitationally collapsed objects of very low mass," Mon. Not. Roy. Astron. Soc. **152** (1971), 75

[8] B. J. Carr and S. W. Hawking, "Black holes in the early Universe," Mon. Not. Roy. Astron. Soc. **168** (1974), 399-415

[9] B. J. Carr, "The Primordial black hole mass spectrum," Astrophys. J. **201** (1975), 1-19.

[10] B. Carr, F. Kuhnel and M. Sandstad, "Primordial Black Holes as Dark Matter," Phys. Rev. D **94**, no.8, 083504 (2016) [arXiv:1607.06077 [astro-ph.CO]].

[11] M. Sasaki, T. Suyama, T. Tanaka and S. Yokoyama, "Primordial black holes—perspectives in gravitational wave astronomy," Class. Quant. Grav. **35** (2018) no.6, 063001 [arXiv:1801.05235 [astro-ph.CO]].

[12] B. Carr and F. Kuhnel, "Primordial Black Holes as Dark Matter: Recent Developments," Ann. Rev. Nucl. Part. Sci. **70** (2020), 355-394 [arXiv:2006.02838 [astro-ph.CO]].

[13] A. M. Green and B. J. Kavanagh, "Primordial Black Holes as a dark matter candidate," J. Phys. G **48** (2021) no.4, 4 [arXiv:2007.10722 [astro-ph.CO]].

[14] https://www.skatelescope.org

[15] http://ipta4gw.org

[16] G. Hobbs, A. Archibald, Z. Arzoumanian, D. Backer, M. Bailes, N. D. R. Bhat, M. Burgay, S. Burke-Spolaor, D. Champion and I. Cognard, *et al.* "The international pulsar timing array project: using pulsars as a gravitational wave detector," Class. Quant. Grav. **27** (2010), 084013 [arXiv:0911.5206 [astro-ph.SR]].

[17] G. Janssen, G. Hobbs, M. McLaughlin, C. Bassa, A. T. Deller, M. Kramer, K. Lee, C. Mingarelli, P. Rosado and S. Sanidas, *et al.* "Gravitational wave astronomy with the SKA," PoS **AASKA14** (2015), 037 [arXiv:1501.00127 [astro-ph.IM]].

[18] L. Lentati, S. R. Taylor, C. M. F. Mingarelli, A. Sesana, S. A. Sanidas, A. Vecchio, R. N. Caballero, K. J. Lee, R. van Haasteren and S. Babak, *et al.* "European Pulsar Timing Array Limits On An Isotropic Stochastic Gravitational-Wave Background," Mon. Not. Roy. Astron. Soc. **453** (2015) no.3, 2576-2598 [arXiv:1504.03692 [astro-ph.CO]].

[19] Z. Arzoumanian *et al.* [NANOGrav], "The NANOGrav 12.5 yr Data Set: Search for an Isotropic Stochastic Gravitational-wave Background," Astrophys. J. Lett. **905** (2020) no.2, L34 [arXiv:2009.04496 [astro-ph.HE]].

[20] https://www.elisascience.org.

[21] P. Amaro-Seoane *et al.* [LISA], "Laser Interferometer Space Antenna," [arXiv:1702.00786 [astro-ph.IM]].

[22] E. Barausse, E. Berti, T. Hertog, S. A. Hughes, P. Jetzer, P. Pani, T. P. Sotiriou, N. Tamanini, H. Witek and K. Yagi, *et al.* "Prospects

for Fundamental Physics with LISA," Gen. Rel. Grav. **52** (2020) no.8, 81 [arXiv:2001.09793 [gr-qc]].

[23] S. Kawamura, M. Ando, N. Seto, S. Sato, M. Musha, I. Kawano, J. Yokoyama, T. Tanaka, K. Ioka and T. Akutsu, *et al.* "Current status of space gravitational wave antenna DECIGO and B-DECIGO," PTEP **2021** (2021) no.5, 05A105 [arXiv:2006.13545 [gr-qc]].

[24] W. H. Ruan, Z. K. Guo, R. G. Cai and Y. Z. Zhang, "Taiji program: Gravitational-wave sources," Int. J. Mod. Phys. A **35** (2020) no.17, 2050075 [arXiv:1807.09495 [gr-qc]].

[25] J. Luo *et al.* [TianQin], "TianQin: a space-borne gravitational wave detector," Class. Quant. Grav. **33** (2016) no.3, 035010 [arXiv:1512.02076 [astro-ph.IM]].

[26] L. Badurina, E. Bentine, D. Blas, K. Bongs, D. Bortoletto, T. Bowcock, K. Bridges, W. Bowden, O. Buchmueller and C. Burrage, *et al.* "AION: An Atom Interferometer Observatory and Network," JCAP **05** (2020), 011 [arXiv:1911.11755 [astro-ph.CO]].

[27] R. Abbott *et al.* [KAGRA, Virgo and LIGO Scientific], "Upper limits on the isotropic gravitational-wave background from Advanced LIGO and Advanced Virgo's third observing run," Phys. Rev. D **104** (2021) no.2, 022004 [arXiv:2101.12130 [gr-qc]].

[28] M. Maggiore, C. Van Den Broeck, N. Bartolo, E. Belgacem, D. Bertacca, M. A. Bizouard, M. Branchesi, S. Clesse, S. Foffa and J. García-Bellido, *et al.* "Science Case for the Einstein Telescope," JCAP **03** (2020), 050 [arXiv:1912.02622 [astro-ph.CO]].

[29] P. Ivanov, P. Naselsky and I. Novikov, "Inflation and primordial black holes as dark matter," Phys. Rev. D **50** (1994), 7173-7178.

[30] J. Yokoyama, "Chaotic new inflation and formation of primordial black holes," Phys. Rev. D **58** (1998), 083510 [arXiv:astro-ph/9802357 [astro-ph]].

[31] S. L. Cheng, W. Lee and K. W. Ng, "Production of high stellar-mass primordial black holes in trapped inflation," JHEP **02** (2017), 008 [arXiv:1606.00206 [astro-ph.CO]].

[32] J. Garcia-Bellido and E. Ruiz Morales, "Primordial black holes from single field models of inflation," Phys. Dark Univ. **18** (2017), 47-54 [arXiv:1702.03901 [astro-ph.CO]].

[33] J. M. Ezquiaga, J. Garcia-Bellido and E. Ruiz Morales, "Primordial Black Hole production in Critical Higgs Inflation," Phys. Lett. B **776** (2018), 345-349 [arXiv:1705.04861 [astro-ph.CO]].

[34] C. Germani and T. Prokopec, "On primordial black holes from an inflection point," Phys. Dark Univ. **18** (2017), 6-10 [arXiv:1706.04226 [astro-ph.CO]].

[35] H. Motohashi and W. Hu, "Primordial Black Holes and Slow-Roll Violation," Phys. Rev. D **96** (2017) no.6, 063503 [arXiv:1706.06784 [astro-ph.CO]].

[36] J. Garcia-Bellido, A. D. Linde and D. Wands, "Density perturbations and black hole formation in hybrid inflation," Phys. Rev. D **54** (1996), 6040-6058 [arXiv:astro-ph/9605094 [astro-ph]].

[37] M. Kawasaki, N. Sugiyama and T. Yanagida, "Primordial black hole formation in a double inflation model in supergravity," Phys. Rev. D **57** (1998), 6050-6056 [arXiv:hep-ph/9710259 [hep-ph]].

[38] P. H. Frampton, M. Kawasaki, F. Takahashi and T. T. Yanagida, "Primordial Black Holes as All Dark Matter," JCAP **04** (2010), 023 [arXiv:1001.2308 [hep-ph]].

[39] S. Clesse and J. García-Bellido, "Massive Primordial Black Holes from Hybrid Inflation as Dark Matter and the seeds of Galaxies," Phys. Rev. D **92** (2015) no.2, 023524 [arXiv:1501.07565 [astro-ph.CO]].

[40] M. Kawasaki, A. Kusenko, Y. Tada and T. T. Yanagida, "Primordial black holes as dark matter in supergravity inflation models," Phys. Rev. D **94** (2016) no.8, 083523 [arXiv:1606.07631 [astro-ph.CO]].

[41] K. Inomata, M. Kawasaki, K. Mukaida, Y. Tada and T. T. Yanagida, "Inflationary Primordial Black Holes as All Dark Matter," Phys. Rev. D **96** (2017) no.4, 043504 [arXiv:1701.02544 [astro-ph.CO]].

[42] J. R. Espinosa, D. Racco and A. Riotto, "Cosmological Signature of the Standard Model Higgs Vacuum Instability: Primordial Black Holes as Dark Matter," Phys. Rev. Lett. **120** (2018) no.12, 121301 [arXiv:1710.11196 [hep-ph]].

[43] K. Inomata, M. Kawasaki, K. Mukaida and T. T. Yanagida, "Double inflation as a single origin of primordial black holes for all dark matter and LIGO observations," Phys. Rev. D **97** (2018) no.4, 043514 [arXiv:1711.06129 [astro-ph.CO]].

[44] M. Kawasaki, H. Nakatsuka and I. Obata, "Generation of Primordial Black Holes and Gravitational Waves from Dilaton-Gauge Field Dynamics," JCAP **05** (2020), 007 [arXiv:1912.09111 [astro-ph.CO]].

[45] G. A. Palma, S. Sypsas and C. Zenteno, "Seeding primordial black holes in multifield inflation," Phys. Rev. Lett. **125** (2020) no.12, 121301 [arXiv:2004.06106 [astro-ph.CO]].

[46] H. Di and Y. Gong, "Primordial black holes and second order gravitational waves from ultra-slow-roll inflation," JCAP **07** (2018), 007 [arXiv:1707.09578 [astro-ph.CO]].

[47] G. Ballesteros and M. Taoso, "Primordial black hole dark matter from single field inflation," Phys. Rev. D **97** (2018) no.2, 023501 [arXiv:1709.05565 [hep-ph]].

[48] M. P. Hertzberg and M. Yamada, "Primordial Black Holes from Polynomial Potentials in Single Field Inflation," Phys. Rev. D **97** (2018) no.8, 083509 [arXiv:1712.09750 [astro-ph.CO]].

[49] S. L. Cheng, W. Lee and K. W. Ng, "Primordial black holes and associated gravitational waves in axion monodromy inflation," JCAP **07** (2018), 001 [arXiv:1801.09050 [astro-ph.CO]].

[50] M. Cicoli, V. A. Diaz and F. G. Pedro, "Primordial Black Holes from String Inflation," JCAP **06** (2018), 034 [arXiv:1803.02837 [hep-th]].

[51] O. Özsoy, S. Parameswaran, G. Tasinato and I. Zavala, "Mechanisms for Primordial Black Hole Production in String Theory," JCAP **07** (2018), 005 [arXiv:1803.07626 [hep-th]].

[52] M. Biagetti, G. Franciolini, A. Kehagias and A. Riotto, "Primordial Black Holes from Inflation and Quantum Diffusion," JCAP **07** (2018), 032 [arXiv:1804.07124 [astro-ph.CO]].

[53] I. Dalianis, A. Kehagias and G. Tringas, "Primordial black holes from $\alpha$-attractors," JCAP **01** (2019), 037 [arXiv:1805.09483 [astro-ph.CO]].

[54] T. J. Gao and Z. K. Guo, "Primordial Black Hole Production in Inflationary Models of Supergravity with a Single Chiral Superfield," Phys. Rev. D **98** (2018) no.6, 063526 [arXiv:1806.09320 [hep-ph]].

[55] Y. Tada and S. Yokoyama, "Primordial black hole tower: Dark matter, earth-mass, and LIGO black holes," Phys. Rev. D **100** (2019) no.2, 023537 [arXiv:1904.10298 [astro-ph.CO]].

[56] I. Dalianis and G. Tringas, "Primordial black hole remnants as dark matter produced in thermal, matter, and runaway-quintessence postinflationary scenarios," Phys. Rev. D **100** (2019) no.8, 083512 [arXiv:1905.01741 [astro-ph.CO]].

[57] V. Atal, J. Cid, A. Escrivà and J. Garriga, "PBH in single field inflation: the effect of shape dispersion and non-Gaussianities," JCAP **05** (2020), 022 [arXiv:1908.11357 [astro-ph.CO]].

[58] R. Mahbub, "Primordial black hole formation in inflationary $\alpha$-attractor models," Phys. Rev. D **101** (2020) no.2, 023533 [arXiv:1910.10602 [astro-ph.CO]].

[59] S. S. Mishra and V. Sahni, "Primordial Black Holes from a tiny bump/dip in the Inflaton potential," JCAP **04** (2020), 007 [arXiv:1911.00057 [gr-qc]].

[60] G. Ballesteros, J. Rey and F. Rompineve, "Detuning primordial black hole dark matter with early matter domination and axion monodromy," JCAP **06** (2020), 014 [arXiv:1912.01638 [astro-ph.CO]].

[61] D. V. Nanopoulos, V. C. Spanos and I. D. Stamou, "Primordial Black Holes from No-Scale Supergravity," Phys. Rev. D **102** (2020) no.8, 083536 [arXiv:2008.01457 [astro-ph.CO]].

[62] I. D. Stamou, "Mechanisms of producing primordial black holes by breaking the $SU(2,1)/SU(2) \times U(1)$ symmetry," Phys. Rev. D **103** (2021) no.8, 083512 [arXiv:2104.08654 [hep-ph]].

[63] J. Liu, Z. K. Guo and R. G. Cai, "Analytical approximation of the scalar spectrum in the ultraslow-roll inflationary models," Phys. Rev. D **101** (2020) no.8, 083535 [arXiv:2003.02075 [astro-ph.CO]].

[64] A. A. Starobinsky, "Spectrum of adiabatic perturbations in the universe when there are singularities in the inflation potential," JETP Lett. **55** (1992), 489-494.

[65] J. A. Adams, B. Cresswell and R. Easther, "Inflationary perturbations from a potential with a step," Phys. Rev. D **64** (2001), 123514 [arXiv:astro-ph/0102236 [astro-ph]].

[66] S. M. Leach and A. R. Liddle, "Inflationary perturbations near horizon crossing," Phys. Rev. D **63** (2001), 043508 [arXiv:astro-ph/0010082 [astro-ph]].

[67] S. M. Leach, M. Sasaki, D. Wands and A. R. Liddle, "Enhancement of superhorizon scale inflationary curvature perturbations," Phys. Rev. D **64** (2001), 023512 [arXiv:astro-ph/0101406 [astro-ph]].

[68] D. K. Hazra, M. Aich, R. K. Jain, L. Sriramkumar and T. Souradeep, "Primordial features due to a step in the inflaton potential," JCAP **10** (2010), 008 [arXiv:1005.2175 [astro-ph.CO]].

[69] K. Kannike, L. Marzola, M. Raidal and H. Veermäe, "Single Field Double Inflation and Primordial Black Holes," JCAP **09** (2017), 020 [arXiv:1705.06225 [astro-ph.CO]].

[70] S. Pi, Y. l. Zhang, Q. G. Huang and M. Sasaki, "Scalaron from $R^2$-gravity as a heavy field," JCAP **05** (2018), 042 [arXiv:1712.09896 [astro-ph.CO]].

[71] C. Fu, P. Wu and H. Yu, "Primordial Black Holes from Inflation with Nonminimal Derivative Coupling," Phys. Rev. D **100** (2019) no.6, 063532 [arXiv:1907.05042 [astro-ph.CO]].

[72] I. Dalianis, S. Karydas and E. Papantonopoulos, "Generalized Non-Minimal Derivative Coupling: Application to Inflation and Primordial Black Hole Production," JCAP **06** (2020), 040 [arXiv[1910.00622 [astro-ph.CO]].

[73] D. Y. Cheong, S. M. Lee and S. C. Park, "Primordial black holes in Higgs-$R^2$ inflation as the whole of dark matter," JCAP **01** (2021), 032 [arXiv:1912.12032 [hep-ph]].

[74] J. Lin, Q. Gao, Y. Gong, Y. Lu, C. Zhang and F. Zhang, "Primordial black holes and secondary gravitational waves from $k$ and $G$ inflation," Phys. Rev. D **101** (2020) no.10, 103515 [arXiv:2001.05909 [gr-qc]].

[75] M. Kawasaki, N. Kitajima and T. T. Yanagida, "Primordial black hole formation from an axionlike curvaton model," Phys. Rev. D **87** (2013) no.6, 063519 [arXiv:1207.2550 [hep-ph]].

[76] K. Kohri, C. M. Lin and T. Matsuda, "Primordial black holes from the inflating curvaton," Phys. Rev. D **87** (2013) no.10, 103527 [arXiv:1211.2371 [hep-ph]].

[77] K. Ando, K. Inomata, M. Kawasaki, K. Mukaida and T. T. Yanagida, "Primordial black holes for the LIGO events in the axionlike curvaton model," Phys. Rev. D **97** (2018) no.12, 123512 [arXiv:1711.08956 [astro-ph.CO]].

[78] K. Ando, M. Kawasaki and H. Nakatsuka, "Formation of primordial black holes in an axionlike curvaton model," Phys. Rev. D **98** (2018) no.8, 083508 [arXiv:1805.07757 [astro-ph.CO]].

[79] R. G. Cai, Z. K. Guo, J. Liu, L. Liu and X. Y. Yang, "Primordial black holes and gravitational waves from parametric amplification of curvature perturbations," JCAP **06** (2020), 013 [arXiv:1912.10437 [astro-ph.CO]].

[80] Y. F. Cai, X. Tong, D. G. Wang and S. F. Yan, "Primordial Black Holes from Sound Speed Resonance during Inflation," Phys. Rev. Lett. **121** (2018) no.8, 081306 [arXiv:1805.03639 [astro-ph.CO]].

[81] Y. F. Cai, C. Chen, X. Tong, D. G. Wang and S. F. Yan, "When Primordial Black Holes from Sound Speed Resonance Meet a Stochastic Background of Gravitational Waves," Phys. Rev. D **100** (2019) no.4, 043518 [arXiv:1902.08187[astro-ph.CO]].

[82] C. Chen and Y. F. Cai, "Primordial black holes from sound speed resonance in the inflaton-curvaton mixed scenario," JCAP **10** (2019), 068 [arXiv:1908.03942 [astro-ph.CO].

[83] C. Chen, X. H. Ma and Y. F. Cai, "Dirac-Born-Infeld realization of sound speed resonance mechanism for primordial black holes," Phys. Rev. D **102** (2020) no.6, 063526 [arXiv:2003.03821 [astro-ph.CO]].

[84] Z. Zhou, J. Jiang, Y. F. Cai, M. Sasaki and S. Pi, "Primordial black holes and gravitational waves from resonant amplification during inflation," Phys. Rev. D **102** (2020) no.10, 103527 [arXiv:2010.03537 [astro-ph.CO]].

[85] G. Ballesteros, J. Beltran Jimenez and M. Pieroni, "Black hole formation from a general quadratic action for inflationary primordial fluctuations," JCAP **06**, 016 (2019) [arXiv:1811.03065 [astro-ph.CO]].

[86] X. Chen, "Primordial Non-Gaussianities from Inflation Models," Adv. Astron. **2010** (2010), 638979 [arXiv:1002.1416 [astro-ph.CO]].

[87] J. Chluba, J. Hamann and S. P. Patil, "Features and New Physical Scales in Primordial Observables: Theory and Observation," Int. J. Mod. Phys. D **24** (2015) no.10, 1530023 [arXiv:1505.01834 [astro-ph.CO]].

[88] A. Slosar, K. N. Abazajian, M. Abidi, P. Adshead, Z. Ahmed, D. Alonso, M. A. Amin, B. Ansarinejad, R. Armstrong and C. Baccigalupi, *et al.* "Scratches from the Past: Inflationary Archaeology through Features

in the Power Spectrum of Primordial Fluctuations," Bull. Am. Astron. Soc. **51** (2019) no.3, 98 [arXiv:1903.09883 [astro-ph.CO]].

[89] J. A. Adams, G. G. Ross and S. Sarkar, "Multiple inflation," Nucl. Phys. B **503** (1997), 405-425 [arXiv:hep-ph/9704286 [hep-ph]].

[90] L. Covi, J. Hamann, A. Melchiorri, A. Slosar and I. Sorbera, "Inflation and WMAP three year data: Features have a Future!," Phys. Rev. D **74** (2006), 083509 [arXiv:astro-ph/0606452 [astro-ph]].

[91] J. Hamann, L. Covi, A. Melchiorri and A. Slosar, "New Constraints on Oscillations in the Primordial Spectrum of Inflationary Perturbations," Phys. Rev. D **76** (2007), 023503 [arXiv:astro-ph/0701380 [astro-ph]].

[92] Z. G. Liu, J. Zhang and Y. S. Piao, "Phantom Inflation with A Steplike Potential," Phys. Lett. B **697** (2011), 407-411 [arXiv:1012.0673 [gr-qc]].

[93] A. Gallego Cadavid, A. E. Romano and S. Gariazzo, "Effects of local features of the inflaton potential on the spectrum and bispectrum of primordial perturbations," Eur. Phys. J. C **76** (2016) no.7, 385 [arXiv:1508.05687 [astro-ph.CO]].

[94] A. Gallego Cadavid, A. E. Romano and S. Gariazzo, "CMB anomalies and the effects of local features of the inflaton potential," Eur. Phys. J. C **77** (2017) no.4, 242 [arXiv:1612.03490 [astro-ph.CO]].

[95] M. A. Fard and S. Baghram, "Late time sky as a probe of steps and oscillations in primordial Universe," JCAP **01** (2018), 051 [arXiv:1709.05323 [astro-ph.CO]].

[96] N. Kaloper and M. Kaplinghat, "Primeval corrections to the CMB anisotropies," Phys. Rev. D **68** (2003), 123522 [arXiv:hep-th/0307016 [hep-th]].

[97] G. D'Amico and N. Kaloper, "Rollercoaster cosmology," JCAP **08** (2021), 058 [arXiv:2011.09489 [hep-th]].

[98] G. D'Amico, N. Kaloper and A. Westphal, "Double Monodromy Inflation: A Gravity Waves Factory for CMB-S4, LiteBIRD and LISA," Phys. Rev. D **104**, no.8, L081302 (2021) [arXiv:2101.05861 [hep-th]].

[99] A. A. Starobinsky and J. Yokoyama, "Density fluctuations in Brans-Dicke inflation," [arXiv:gr-qc/9502002 [gr-qc]].

[100] M. Sasaki and E. D. Stewart, "A General analytic formula for the spectral index of the density perturbations produced during inflation," Prog. Theor. Phys. **95**, 71-78 (1996) doi:10.1143/PTP.95.71 [arXiv:astro-ph/9507001 [astro-ph]].

[101] J. Garcia-Bellido and D. Wands, "Metric perturbations in two field inflation," Phys. Rev. D **53** (1996), 5437-5445 [arXiv:astro-ph/9511029 [astro-ph]].

[102] A. D. Linde and V. F. Mukhanov, "Nongaussian isocurvature perturbations from inflation," Phys. Rev. D **56** (1997), R535-R539 [arXiv:astro-ph/9610219 [astro-ph]].

[103] D. Langlois, "Correlated adiabatic and isocurvature perturbations from double inflation," Phys. Rev. D **59** (1999), 123512 [arXiv:astro-ph/9906080 [astro-ph]].

[104] C. Gordon, D. Wands, B. A. Bassett and R. Maartens, "Adiabatic and entropy perturbations from inflation," Phys. Rev. D **63** (2000), 023506 [arXiv:astro-ph/0009131 [astro-ph]].

[105] S. Tsujikawa and H. Yajima, "'New constraints on multifield inflation with nonminimal coupling," Phys. Rev. D **62** (2000), 123512 [arXiv:hep-ph/0007351 [hep-ph]].

[106] A. D. Linde, "Generation of Isothermal Density Perturbations in the Inflationary Universe," Phys. Lett. B **158** (1985), 375-380

[107] L. A. Kofman, "What Initial Perturbations May Be Generated in Inflationary Cosmological Models," Phys. Lett. B **173** (1986), 400-404

[108] D. Polarski and A. A. Starobinsky, "Isocurvature perturbations in multiple inflationary models," Phys. Rev. D **50** (1994), 6123-6129 [arXiv:astro-ph/9404061 [astro-ph]].

[109] V. F. Mukhanov and P. J. Steinhardt, "Density perturbations in multifield inflationary models," Phys. Lett. B **422** (1998), 52-60 [arXiv:astro-ph/9710038 [astro-ph]].

[110] J. Fumagalli, S. Renaux-Petel and L. T. Witkowski, "Oscillations in the stochastic gravitational wave background from sharp features and particle production during inflation," JCAP **08** (2021), 030 [arXiv:2012.02761 [astro-ph.CO]].

[111] M. Braglia, X. Chen and D. K. Hazra, "Probing Primordial Features with the Stochastic Gravitational Wave Background," JCAP **03** (2021), 005 [arXiv:2012.05821 [astro-ph.CO]].

[112] A. Achucarro, J. O. Gong, S. Hardeman, G. A. Palma and S. P. Patil, "Features of heavy physics in the CMB power spectrum," JCAP **01** (2011), 030 [arXiv:1010.3693 [hep-ph]].

[113] A. Achucarro, J. O. Gong, S. Hardeman, G. A. Palma and S. P. Patil, "Mass hierarchies and non-decoupling in multi-scalar field dynamics," Phys. Rev. D **84** (2011), 043502 [arXiv:1005.3848 [hep-th]].

[114] X. Chen, "Primordial Features as Evidence for Inflation," JCAP **01** (2012), 038 [arXiv:1104.1323 [hep-th]].

[115] G. Shiu and J. Xu, "Effective Field Theory and Decoupling in Multi-field Inflation: An Illustrative Case Study," Phys. Rev. D **84** (2011), 103509 [arXiv:1108.0981 [hep-th]].

[116] S. Cespedes, V. Atal and G. A. Palma, "On the importance of heavy fields during inflation," JCAP **05** (2012), 008 [arXiv:1201.4848 [hep-th]].

[117] A. Avgoustidis, S. Cremonini, A. C. Davis, R. H. Ribeiro, K. Turzynski and S. Watson, "Decoupling Survives Inflation: A Critical Look at Effective Field Theory Violations During Inflation," JCAP **06** (2012), 025 [arXiv:1203.0016 [hep-th]].

[118] X. Gao, D. Langlois and S. Mizuno, "Influence of heavy modes on perturbations in multiple field inflation," JCAP **10** (2012), 040 [arXiv:1205.5275 [hep-th]].

[119] A. Achúcarro, J. O. Gong, G. A. Palma and S. P. Patil, "Correlating features in the primordial spectra," Phys. Rev. D **87** (2013) no.12, 121301 [arXiv:1211.5619 [astro-ph.CO]].

[120] M. Konieczka, R. H. Ribeiro and K. Turzynski, "The effects of a fast-turning trajectory in multiple-field inflation," JCAP **07** (2014), 030 [arXiv:1401.6163 [astro-ph.CO]].

[121] A. R. Brown, "Hyperbolic Inflation," Phys. Rev. Lett. **121** (2018) no.25, 251601 [arXiv:1705.03023 [hep-th]].

[122] A. Achúcarro, E. J. Copeland, O. Iarygina, G. A. Palma, D. G. Wang and Y. Welling, "Shift-symmetric orbital inflation: Single field or multi-field?," Phys. Rev. D **102** (2020) no.2, 021302 [arXiv:1901.03657 [astro-ph.CO]].

[123] J. Fumagalli, S. Garcia-Saenz, L. Pinol, S. Renaux-Petel and J. Ronayne, "Hyper-Non-Gaussianities in Inflation with Strongly Nongeodesic Motion," Phys. Rev. Lett. **123** (2019) no.20, 201302 [arXiv:1902.03221 [hep-th]].

[124] T. Bjorkmo, "Rapid-Turn Inflationary Attractors," Phys. Rev. Lett. **122** (2019) no.25, 251301 [arXiv:1902.10529 [hep-th]].

[125] P. Christodoulidis, D. Roest and E. I. Sfakianakis, "Scaling attractors in multi-field inflation," JCAP **12** (2019), 059 [arXiv:1903.06116 [hep-th]].

[126] M. Braglia, D. K. Hazra, F. Finelli, G. F. Smoot, L. Sriramkumar and A. A. Starobinsky, "Generating PBHs and small-scale GWs in two-field models of inflation," JCAP **08** (2020), 001 [arXiv:2005.02895 [astro-ph.CO]].

[127] Y. Aldabergenov, A. Addazi and S. V. Ketov, "Primordial black holes from modified supergravity," Eur. Phys. J. C **80** (2020) no.10, 917 [arXiv:2006.16641 [hep-th]].

[128] J. Fumagalli, S. Renaux-Petel, J. W. Ronayne and L. T. Witkowski, "Turning in the landscape: a new mechanism for generating Primordial Black Holes," [arXiv:2004.08369 [hep-th]].

[129] L. Iacconi, H. Assadullahi, M. Fasiello and D. Wands, "Revisiting small-scale fluctuations in $\alpha$-attractor models of inflation," JCAP **06**, no.06, 007 (2022) [arXiv:2112.05092 [astro-ph.CO]].

[130] A. J. Tolley and M. Wyman, "The Gelaton Scenario: Equilateral non-Gaussianity from multi-field dynamics," Phys. Rev. D **81** (2010), 043502 [arXiv:0910.1853 [hep-th]].

[131] S. Cremonini, Z. Lalak and K. Turzynski, "Strongly Coupled Perturbations in Two-Field Inflationary Models," JCAP **03** (2011), 016 [arXiv:1010.3021 [hep-th]].

[132] A. Achucarro, J. O. Gong, S. Hardeman, G. A. Palma and S. P. Patil, "Effective theories of single field inflation when heavy fields matter," JHEP **05** (2012), 066 [arXiv:1201.6342 [hep-th]].

[133] S. Pi and M. Sasaki, "Curvature Perturbation Spectrum in Two-field Inflation with a Turning Trajectory," JCAP **10** (2012), 051 [arXiv:1205.0161 [hep-th]].

[134] A. Achucarro, V. Atal, S. Cespedes, J. O. Gong, G. A. Palma and S. P. Patil, "Heavy fields, reduced speeds of sound and decoupling during inflation," Phys. Rev. D **86** (2012), 121301 [arXiv:1205.0710 [hep-th]].

[135] J. Fumagalli, G. A. Palma, S. Renaux-Petel, S. Sypsas, L. T. Witkowski and C. Zenteno, "Primordial gravitational waves from excited states," JHEP **03**, 196 (2022) [arXiv:2111.14664 [astro-ph.CO]].

[136] V. C. Spanos and I. D. Stamou, "Gravitational waves and primordial black holes from supersymmetric hybrid inflation," Phys. Rev. D **104** (2021) no.12, 123537 [arXiv:2108.05671 [astro-ph.CO]].

[137] S. Weinberg, "Gravitation and Cosmology: Principles and Applications of the General Theory of Relativity,"

[138] S. M. Carroll, "Spacetime and Geometry,"

[139] N. Aghanim *et al.* [Planck], "Planck 2018 results. VI. Cosmological parameters," Astron. Astrophys. **641**, A6 (2020) [erratum: Astron. Astrophys. **652**, C4 (2021)] [arXiv:1807.06209 [astro-ph.CO]].

[140] A. H. Guth, "The Inflationary Universe: A Possible Solution to the Horizon and Flatness Problems," Phys. Rev. D **23**, 347-356 (1981)

[141] D. Baumann, "Inflation," [arXiv:0907.5424 [hep-th]].

[142] P. A. R. Ade *et al.* [Planck], "Planck 2013 results. XXII. Constraints on inflation," Astron. Astrophys. **571**, A22 (2014) [arXiv:1303.5082 [astro-ph.CO]].

[143] B. A. Bassett, S. Tsujikawa and D. Wands, "Inflation dynamics and reheating," Rev. Mod. Phys. **78**, 537-589 (2006) [arXiv:astro-ph/0507632 [astro-ph]].

[144] V. F. Mukhanov, H. A. Feldman and R. H. Brandenberger, "Theory of cosmological perturbations. Part 1. Classical perturbations. Part 2. Quantum theory of perturbations. Part 3. Extensions," Phys. Rept. **215**, 203-333 (1992)

[145] Hannu Kurki-Suonio, *"Cosmological Perturbation Theory I,II"*, University of Helsinki (2020).

[146] V. F. Mukhanov, "Quantum Theory of Gauge Invariant Cosmological Perturbations," Sov. Phys. JETP **67** (1988), 1297-1302.

[147] M. Sasaki, "Large Scale Quantum Fluctuations in the Inflationary Universe," Prog. Theor. Phys. **76** (1986), 1036.

[148] K. Kefala, G. P. Kodaxis, I. D. Stamou and N. Tetradis, "Features of the inflaton potential and the power spectrum of cosmological perturbations," Phys. Rev. D **104**, no.2, 023506 (2021) [arXiv:2010.12483 [astro-ph.CO]].

[149] O. Özsoy and G. Tasinato, "On the slope of the curvature power spectrum in non-attractor inflation," JCAP **04**, 048 (2020) [arXiv:1912.01061 [astro-ph.CO]].

[150] A. A. Starobinsky, "A New Type of Isotropic Cosmological Models Without Singularity," Phys. Lett. B **91** (1980), 99-102.

[151] I. Dalianis, G. P. Kodaxis, I. D. Stamou, N. Tetradis and A. Tsigkas-Kouvelis, "Spectrum oscillations from features in the potential of single-field inflation," Phys. Rev. D **104**, no.10, 103510 (2021) [arXiv:2106.02467 [astro-ph.CO]].

[152] K. Boutivas, I. Dalianis, G. P. Kodaxis and N. Tetradis, "The effect of multiple features on the power spectrum in two-field inflation," JCAP **08**, no.08, 021 (2022) [arXiv:2203.15605 [astro-ph.CO]].

[153] C. T. Byrnes, P. S. Cole and S. P. Patil, "Steepest growth of the power spectrum and primordial black holes," JCAP **06** (2019), 028 [arXiv:1811.11158 [astro-ph.CO]].

[154] P. Carrilho, K. A. Malik and D. J. Mulryne, "Dissecting the growth of the power spectrum for primordial black holes," Phys. Rev. D **100** (2019) no.10, 103529 [arXiv:1907.05237 [astro-ph.CO]].

[155] K. Inomata, E. McDonough and W. Hu, "Amplification of primordial perturbations from the rise or fall of the inflaton," JCAP **02**, no.02, 031 (2022) [arXiv:2110.14641 [astro-ph.CO]].

[156] G. Tasinato, "An analytic approach to non-slow-roll inflation," Phys. Rev. D **103**, no.2, 023535 (2021) [arXiv:2012.02518 [hep-th]].

[157] R. Kallosh and A. Linde, "Universality Class in Conformal Inflation," JCAP **07** (2013), 002 [arXiv:1306.5220 [hep-th]].

[158] S. Ferrara, R. Kallosh, A. Linde and M. Porrati, "Minimal Supergravity Models of Inflation," Phys. Rev. D **88** (2013) no.8, 085038 [arXiv:1307.7696 [hep-th]].

[159] R. Kallosh, A. Linde and D. Roest, "Large field inflation and double $\alpha$-attractors," JHEP **08** (2014), 052 [arXiv:1405.3646 [hep-th]].

[160] Y. Akrami *et al.* [Planck], "Planck 2018 results. X. Constraints on inflation," Astron. Astrophys. **641** (2020), A10 [arXiv:1807.06211 [astro-ph.CO]].

[161] I. Dalianis and K. Kritos, "Exploring the Spectral Shape of Gravitational Waves Induced by Primordial Scalar Perturbations and Connection with the Primordial Black Hole Scenarios," Phys. Rev. D **103** (2021) no.2, 023505 [arXiv:2007.07915 [astro-ph.CO]].

[162] B. Carr, K. Kohri, Y. Sendouda and J. Yokoyama, "Constraints on primordial black holes," Rept. Prog. Phys. **84** (2021) no.11, 116902 [arXiv:2002.12778 [astro-ph.CO]].

[163] W. H. Press and P. Schechter, "Formation of galaxies and clusters of galaxies by selfsimilar gravitational condensation," Astrophys. J. **187** (1974), 425-438.

[164] J. C. Niemeyer and K. Jedamzik, "Near-critical gravitational collapse and the initial mass function of primordial black holes," Phys. Rev. Lett. **80** (1998), 5481-5484 [arXiv:astro-ph/9709072 [astro-ph]].

[165] M. Shibata and M. Sasaki, "Black hole formation in the Friedmann universe: Formulation and computation in numerical relativity," Phys. Rev. D **60** (1999), 084002 [arXiv:gr-qc/9905064 [gr-qc]].

[166] I. Musco, J. C. Miller and A. G. Polnarev, "Primordial black hole formation in the radiative era: Investigation of the critical nature of the collapse," Class. Quant. Grav. **26**, 235001 (2009) [arXiv:0811.1452 [gr-qc]].

[167] I. Musco and J. C. Miller, "Primordial black hole formation in the early universe: critical behaviour and self-similarity," Class. Quant. Grav. **30** (2013) 145009 [arXiv:1201.2379 [gr-qc]].

[168] T. Harada, C. M. Yoo and K. Kohri, "Threshold of primordial black hole formation," Phys. Rev. D **88** (2013) no.8, 084051 [erratum: Phys. Rev. D **89** (2014) no.2, 029903] [arXiv:1309.4201 [astro-ph.CO]].

[169] C. Germani and I. Musco, "Abundance of Primordial Black Holes Depends on the Shape of the Inflationary Power Spectrum," Phys. Rev. Lett. **122**, no.14, 141302 (2019) [arXiv:1805.04087 [astro-ph.CO]].

[170] C. T. Byrnes, M. Hindmarsh, S. Young and M. R. S. Hawkins, "Primordial black holes with an accurate QCD equation of state," JCAP **08** (2018), 041 [arXiv:1801.06138 [astro-ph.CO]].

[171] S. Young, C. T. Byrnes and M. Sasaki, "Calculating the mass fraction of primordial black holes," JCAP **1407**, 045 (2014) [arXiv:1405.7023 [gr-qc]].

[172] M. Y. Khlopov and A. G. Polnarev, "Primordial Black Holes As A Cosmological Test Of Grand Unification," Phys. Lett. **97B** (1980) 383.

[173] A. G. Polnarev and M. Y. Khlopov, "Cosmology, Primordial Black Holes, And Supermassive Particles," Sov. Phys. Usp. **28** (1985) 213 [Usp. Fiz. Nauk **145** (1985) 369].

[174] T. Harada, C. M. Yoo, K. Kohri, K. i. Nakao and S. Jhingan, "Primordial black hole formation in the matter-dominated phase of the Universe," Astrophys. J. **833** (2016) no.1, 61 [arXiv:1609.01588 [astro-ph.CO]].

[175] T. Harada, C. M. Yoo, K. Kohri and K. I. Nakao, "Spins of primordial black holes formed in the matter-dominated phase of the Universe," Phys. Rev. D **96** (2017) no.8, 083517 Erratum: [Phys. Rev. D **99** (2019) no.6, 069904] [arXiv:1707.03595 [gr-qc]].

[176] S. Matarrese, O. Pantano and D. Saez, "A General relativistic approach to the nonlinear evolution of collisionless matter," Phys. Rev. D **47** (1993), 1311-1323.

[177] S. Matarrese, O. Pantano and D. Saez, "General relativistic dynamics of irrotational dust: Cosmological implications," Phys. Rev. Lett. **72** (1994), 320-323 [arXiv:astro-ph/9310036 [astro-ph]].

[178] S. Matarrese, S. Mollerach and M. Bruni, "Second order perturbations of the Einstein-de Sitter universe," Phys. Rev. D **58** (1998), 043504 [arXiv:astro-ph/9707278 [astro-ph]].

[179] S. Mollerach, D. Harari and S. Matarrese, "CMB polarization from secondary vector and tensor modes," Phys. Rev. D **69** (2004), 063002 [arXiv:astro-ph/0310711 [astro-ph]].

[180] H. Noh and J. c. Hwang, "Second-order perturbations of the Friedmann world model," Phys. Rev. D **69** (2004), 104011.

[181] C. Carbone and S. Matarrese, "A Unified treatment of cosmological perturbations from super-horizon to small scales," Phys. Rev. D **71** (2005), 043508 [arXiv:astro-ph/0310711 [astro-ph]].

[182] K. Nakamura, "Second-order gauge invariant cosmological perturbation theory: Einstein equations in terms of gauge invariant variables," Prog. Theor. Phys. **117** (2007), 17-74 [arXiv:gr-qc/0605108 [gr-qc]].

[183] D. Baumann, P. J. Steinhardt, K. Takahashi and K. Ichiki, "Gravitational Wave Spectrum Induced by Primordial Scalar Perturbations," Phys. Rev. D **76** (2007), 084019 [arXiv:hep-th/0703290 [hep-th]].

[184] K. N. Ananda, C. Clarkson and D. Wands, "The Cosmological gravitational wave background from primordial density perturbations," Phys. Rev. D **75** (2007), 123518 [arXiv:gr-qc/0612013 [gr-qc]].

[185] H. Assadullahi and D. Wands, "Gravitational waves from an early matter era," Phys. Rev. D **79** (2009), 083511 [arXiv:0901.0989 [astro-ph.CO]].

[186] K. Jedamzik, M. Lemoine and J. Martin, "Generation of gravitational waves during early structure formation between cosmic inflation and reheating," JCAP **04** (2010), 021 [arXiv:1002.3278 [astro-ph.CO]].

[187] I. Dalianis and C. Kouvaris, "Gravitational waves from density perturbations in an early matter domination era," JCAP **07** (2021), 046 [arXiv:2012.09255 [astro-ph.CO]].

[188] R. g. Cai, S. Pi and M. Sasaki, "Gravitational Waves Induced by non-Gaussian Scalar Perturbations," Phys. Rev. Lett. **122** (2019) no.20, 201101 [arXiv:1810.11000 [astro-ph.CO]].

[189] P. Amaro-Seoane *et al.* [LISA], "Laser Interferometer Space Antenna," [arXiv:1702.00786 [astro-ph.IM]].

[190] K. Kohri and T. Terada, "Semianalytic calculation of gravitational wave spectrum nonlinearly induced from primordial curvature perturbations," Phys. Rev. D **97** (2018) no.12, 123532 [arXiv:1804.08577 [gr-qc]].

[191] R. Saito and J. Yokoyama, "Gravitational wave background as a probe of the primordial black hole abundance," Phys. Rev. Lett. **102** (2009),

161101 [erratum: Phys. Rev. Lett. **107** (2011), 069901] [arXiv:0812.4339 [astro-ph]].

[192] S. Pi and M. Sasaki, "Gravitational Waves Induced by Scalar Perturbations with a Lognormal Peak," JCAP **09** (2020), 037 [arXiv:2005.12306 [gr-qc]].

[193] R. G. Cai, S. Pi, S. J. Wang and X. Y. Yang, "Resonant multiple peaks in the induced gravitational waves," JCAP **05** (2019), 013 [arXiv:1901.10152 [astro-ph.CO]].

[194] G. Domènech, "Scalar Induced Gravitational Waves Review," Universe **7** (2021) no.11, 398 [arXiv:2109.01398 [gr-qc]].

[195] K. Jedamzik, "Primordial black hole formation during the QCD epoch," Phys. Rev. D **55** (1997), 5871-5875 [arXiv:astro-ph/9605152 [astro-ph]].

[196] E. Thrane and J. D. Romano, "Sensitivity curves for searches for gravitational-wave backgrounds," Phys. Rev. D **88** (2013) no.12, 124032 [arXiv:1310.5300 [astro-ph.IM]].